Modulation of hepatic *abcb4* and *cyp3a65* gene expression and multidrug/multixenobiotic resistance (MDR/MXR) functional activity in the model teleost, *Danio rerio* (zebrafish)

by

Jeremy Scott Jackson

B.Sc. (Hons.), Simon Fraser University, 2010

Thesis Submitted In Partial Fulfillment of the
Requirements for the Degree of
Master of Environmental Toxicology

in the
Department of Biological Sciences
Faculty of Science

SIMON FRASER UNIVERSITY

Summer 2014

Approval

Name: **Jeremy S. Jackson**

Degree: **Master of Environmental Toxicology**

Title of Thesis: **Modulation of hepatic *abcb4* and *cyp3a65* gene expression and multidrug/multixenobiotic resistance (MDR/MXR) functional activity in the model teleost, *Danio rerio* (zebrafish)**

Examining Committee: Chair: Dr. Julian Christians
Associate Professor

Dr. Chris Kennedy
Senior Supervisor
Professor

Dr. Fiona Brinkman
Supervisor
Professor
Department of Molecular Biology and Biochemistry

Dr. Margo Moore
Supervisor
Professor

Dr. Carl Lowenberger
Internal Examiner
Professor

Date Defended: August 28, 2014

Partial Copyright Licence

Ethics Statement

The author, whose name appears on the title page of this work, has obtained, for the research described in this work, either:

a. human research ethics approval from the Simon Fraser University Office of Research Ethics,

or

b. advance approval of the animal care protocol from the University Animal Care Committee of Simon Fraser University;

or has conducted the research

c. as a co-investigator, collaborator or research assistant in a research project approved in advance,

or

d. as a member of a course approved in advance for minimal risk human research, by the Office of Research Ethics.

A copy of the approval letter has been filed at the Theses Office of the University Library at the time of submission of this thesis or project.

The original application for approval and letter of approval are filed with the relevant offices. Inquiries may be directed to those authorities.

Simon Fraser University Library
Burnaby, British Columbia, Canada

update Spring 2010

Abstract

The multidrug/multixenobiotic resistance (MDR/MXR) mechanism is a cellular response involving the induction and coordinated action of the ATP-binding cassette (ABC) transporter, P-glycoprotein (P-gp), and the phase I metabolizing enzyme, cytochrome P450 3A (CYP3A), which confers protection against potentially cytotoxic exposures of various drugs and environmental contaminants. In mammals, ligand-mediated pregnane X receptor (PXR) transcriptional activity regulates the induction of P-gp and CYP3A but this mechanism is not well characterized in fish species. In this study, zebrafish treated with the Pxr (PXR) agonist PCN co-modulated P-gp (Abcb4) and CYP3A (Cyp3a65) mRNA expression and this co-modulation was associated with increased hepatic MDR/MXR functional activity *in vivo*. Consistent with a mammalian-like MDR/MXR mechanism regulated by PXR, zebrafish co-treated with PCN and the mammalian PXR antagonist, ketoconazole (KTC) attenuated the PCN-mediated modulation of hepatic *abcb4* and *cyp3a* mRNA levels, as well as attenuated the PCN-mediated modulation of MDR/MXR functional activity. These results suggest *abcb4* may be involved with the MDR/MXR response in the adult zebrafish liver, and that Pxr (PXR) may regulate this dynamic process. Finally, the lack of Cyp3c1 mRNA modulation by PCN suggests that Cyp3c1 and Cyp3a65 may be regulated by separate transcriptional pathways.

Keywords: P-glycoprotein; pregnane X receptor; cytochrome P450, pregnenolone 16α-carbonitrile; ketoconazole; zebrafish

Dedication

I dedicate this thesis to my mom and dad.

Acknowledgements

I would like to express my sincere thanks to my senior supervisor, Dr. Chris Kennedy, who provided great support and guidance throughout my thesis at Simon Fraser University (SFU). Special thanks to my other supervisors, Dr. Margo Moore and Dr. Fiona Brinkman, for their time and help in guiding me throughout my thesis.

My genuine gratitude goes to Raymond Lo, who helped me get started on PCR and DNA gels in the Brinkman lab at SFU. I owe thanks to Dr. Heather Osachoff who shared her knowledge of qPCR analysis with me early on in my thesis. I thank Dr. William Davidson for sharing his qPCR thermocycler, and Krzysztof Lubienieki for coordinating his busy schedule to ensure I could use the thermocycler. I would also like to extend my sincere thanks to Bruce Leighton for taking great care of the zebrafish during my work with the *in vivo* rhodamine exposures.

Finally, I owe my sincerest thanks to my girlfriend Julienne for her ongoing support and encouragement throughout my time at SFU.

Table of Contents

Approval ii
Partial Copyright Licence iii
Ethics Statement iv
Abstract v
Dedication vi
Acknowledgements vii
Table of Contents viii
List of Tables x
List of Figures xi
List of Acronyms xii
Gene and protein symbol nomenclature xiii

1. Introduction 1
1.1. Cellular defense mechanisms against xenobiotics 1
1.2. Investigating the MDR/MXR mechanism in zebrafish 4
1.3. P-glycoprotein (P-gp) 5
1.3.1. Zebrafish P-glycoproteins 11
1.4. Nuclear receptor 'xenosensors' 12
1.5. PXR-mediated regulation of P-gp and CYP3A 14
1.5.1. Zebrafish Pxr 16
1.5.2. Zebrafish Cyp3a 17
1.6. Summary and objectives 18

2. Materials and Methods 21
2.1. Fish 21
2.2. Chemicals 21
2.3. Chemical administration and exposures 21
2.4. Rhodamine 123 kinetics 22
2.4.1. Determination of R123 loading exposure 23
2.4.2. R123 clearance assay 24
2.4.3. R123 accumulation assay 25
2.4.4. Statistical analyses for R123 assays 25
2.4.5. Area under curve (AUC) analyses of MDR/MXR functional activity 26
2.5. Evaluation of gene expression 27
2.5.1. RNA extraction and cDNA preparation 27
2.5.2. Gene expression analysis 29
2.5.3. Restriction digest of target amplicons 29
2.5.4. Statistical analysis for gene expression 29

3. Results 31
3.1. R123 exposure trials 31
3.1.1. Effect of R123 exposure concentration on hepatic R123 uptake 31
3.1.1. Effect of R123 exposure duration on hepatic R123 uptake 32
3.2. Effect of drug treatment on hepatic R123 concentration 33
3.2.1. Effect of drug treatment on hepatic clearance of R123 33

3.2.2. Area under curve (AUC) analysis of hepatic R123 clearance 34
3.3. Effect of drug treatment on hepatic R123 uptake 36
Area under curve (AUC) analysis of hepatic R123 uptake 37
3.4. Effect of drug treatment on liver gene expression 39

4. Discussion 41
4.1. The use of zebrafish to study hepatic rhodamine 123 kinetics *in vivo* 41
4.2. Effect of PCN and KTC on P-glycoprotein functional activity 45
4.3. Effect of PCN and KTC on gene expression 50

5. Conclusion and future directions 55

References: 57

Appendices 69
Appendix A. 70
Appendix B. 72
Appendix C. 73
Appendix D. 77
Appendix E. 84
Appendix F. 91
Appendix G. 100
Appendix H. 104
Appendix I. 111
Appendix J. 115
Appendix K. 122
Appendix L. 124
Appendix M. 127
Appendix N. 128
Appendix O. 129
Appendix P. 131
Appendix Q. 134
Appendix R. 136
Appendix S. 138

List of Tables

Table 1.1 Zebrafish Abcb4 and Abcb5 amino acid similarity across vertebrates 12

Table 3.1. Summary of AUC estimates: Hepatic clearance of R123 35

Table 3.2: Summary of AUC contrasts and statistical analyses 35

Table 3.3: Summary of AUC estimates: Rhodamine 123 uptake assay 38

Table 3.4: Summary of AUC contrasts and statistical analyses 38

List of Figures

Figure 1.1: Mechanism of a phase I oxidation reaction 2

Figure 1.2: Multidrug/multixenobiotic resistance (MDR/MXR) activity 4

Figure 1.3 Examples of xenobiotic substrates transported by P-glycoprotein 9

Figure 1.4 Known inhibitors of P-gp activity 10

Figure 1.5 PXR-mediated induction of ABCB1 and CYP3A in mammals 15

Figure 3.1: Effect of R123 exposure concentration on hepatic R123 uptake 32

Figure 3.2: Effect of R123 exposure duration on hepatic R123 uptake 33

Figure 3.3: Effect of drug treatment on overall hepatic clearance of R123 34

Figure 3.4: Differences between mean AUCs of hepatic R123 clearance assay 36

Figure 3.5: Effect of drug treatment on hepatic R123 uptake 37

Figure 3.6: Differences between mean AUCs of R123 uptake assay 39

Figure 3.7: Effect of drug treatment on hepatic gene expression 40

List of Acronyms

a.a.	Amino acid
ABC	ATP binding cassette
ABCB1	ATP binding cassette subfamily B, member 1 (protein)
ATP	Adenosine triphosphate
BCRP	Breast cancer resistance protein
cDNA	Complementary DNA
CYP450	Cytochrome P450
DBD	DNA binding domain
DNA	Deoxyribonucleic acid
i.p.	Intraperitoneal
KTC	Ketoconazole
LBD	Ligand binding domain
MDR	Multidrug resistance
MDR/MXR	Multidrug/multixenobiotic resistance
MDR1	Multidrug resistance 1 (protein)
mRNA	Messenger RNA
MRP1	Multridrug resistance–associated protein 1
MXR	Multixenobiotic resistance
NADPH	Nicotinamide adenine dinucleotide phosphate
NR	Nuclear receptor
PAH	Polycyclic aryl hydrocarbon
PCB	Polychlorinated biphenyl
PCN	Pregnenolone 16α-carbonitrile
P-gp	Permeability glycoprotein
PXR	Pregnane X receptor
R123	Rhodamine 123
RNA	Ribonucleic acid

Gene and protein symbol nomenclature

Organism	Gene	Protein
Human	*ABCDE*	ABCDE
Rodents (e.g.,mouse and rat)	*Abcde*	ABCDE
Fish and other non-mammalian vertebrates	*abcde*	Abcde

The conventional nomenclature used in this thesis is exemplified by the hypothetical '*ABCDE'* gene, with the corresponding gene and protein symbology used for different organisms.

1. Introduction

1.1. Cellular defense mechanisms against xenobiotics

Fish species are both ecologically and economically-relevant organisms, due to their importance to marine and freshwater food webs as well as to commercial fishing. Fish are often acutely or chronically exposed to harmful xenobiotics such as natural toxins (e.g., cyanobacterial toxins) as well as pollutants from human activities (e.g., personal care and industrial chemicals). These anthropogenic contaminants can enter water systems through stormwater runoff, direct inputs as effluents, atmospheric deposition, and ground water pathways (Ritter et al, 2002; Richards and Shieh, 1986). They can include a variety of different contaminants including agricultural pesticides, metals, dioxins, polychlorinated biphenols (PCBs), pharmaceuticals /personal care products, and industrial polycyclic aromatic hydrocarbons (PAHs).

Long before *Homo sapiens* and the widespread release of anthropogenic contaminants into the environment, all organisms were exposed to a variety of potentially toxic chemicals from natural sources. These organisms required protection against microbial and animal toxins, as well as protection against allelochemical toxins produced by plants (Snyder and Glendinning, 1996). At the cellular level, this protection came in the form of two major processes: (1) biotransformation enzymes and (2) transporter systems (Pascussi et al, 2008). These cellular defense mechanisms were early evolutionary adaptations to both endogenous and exogenous chemical accumulations and are found ubiquitously in every biological kingdom (Higgins, 1992; Gotoh, 2012).

Lipophilic xenobiotics that can passively diffuse into cells are often substrates for biotransformation enzymes that catalyze their modification to metabolites with altered structural and chemical properties (Brodie et al, 1958). Biotransformation reactions are classified as Phase I or Phase II biotransformation reactions, which can decrease the toxicity of the compound and facilitate its clearance from the organism. Phase I reactions

largely involve the cytochrome P450 (CYP450) monooxygenases, which comprise a highly conserved superfamily of enzymes localized in the membrane of the endoplasmic reticulum (Nelson et al, 2013). In vertebrates, the CYP450s are highly expressed in the liver and small intestine, consistent with their key role in first-pass metabolism (Pelkonen et al, 1998; Bard, 2000; Gelatin et al, 2006). CYP450-mediated oxidation reactions result in the insertion of an oxygen atom into the substrate, increasing its water-solubility and facilitating clearance from the organism (Meunier et al, 2004). This biotransformation is achieved through the action of nicotinamide adenine dinucleotide phosphate (NADPH)-cytochrome P450 reductase, which can reduce the CYP450 molecule to drive catalysis (Enoch and Strittmatter, 1979) (Figure 1.1). Members of the cytochrome P450 subfamily 1A (CYP1A), and subfamily 3A (CYP3A) are of particular interest to toxicology, as they are known to biotransform numerous drugs and environmental pollutants such as polycyclic and polyhalogenated aromatic hydrocarbons as well as carbamate (CYP1A), and organophosphorous (CYP3A) pesticides (Guengrich, 1999).

Figure 1.1: Mechanism of a phase I oxidation reaction

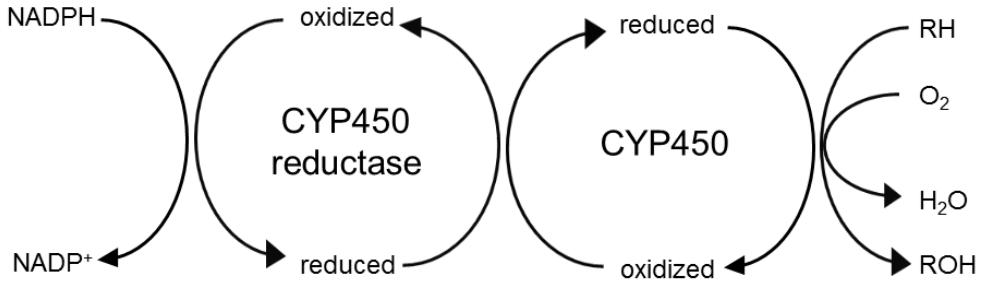

Reduction of CYP450 by NADPH-CYP450 reductase drives the phase I oxidation of a parent molecule (RH) to a more water-soluble metabolite (ROH).

Phase II biotransformation involves several enzymes that modify parent xenobiotic substrates or Phase I metabolites though conjugation mechanisms and include the acetylation of amino groups, amino acid conjugation to carboxylic acids, glucuronic acid transfer to aglycones, sulfate transfer to amino or carboxyl groups, and conjugation of a peptide to an electrophilic O-, N-, S-, or C- atom (Jancova, 2010). Phase II reactions further increase the water-solubility of xenobiotic substrates, which can be reactive

metabolites of phase I reactions (Xu et al, 2005). In this sense, phase II biotransformation can be considered a second line of defence against xenobiotics. Common enzymes involved with phase II detoxification include glutathione S-transferase, UDP-glucuronosyltransferases, sulfotransferases, N-acetyltransferases, and methyltransferases (Iyanagi, 2007). Similar to the CYP450 enzymes, the phase II enzymes are ubiquitous in organisms ranging from bacteria to mammals (Nebert, 1989).

In addition to xenobiotic metabolism through phase I and II biotransformation mechanisms, membrane-bound transporter proteins also play a key role in cellular defense mechanisms against xenobiotic accumulation (Leslie et al, 2005). A highly conserved superfamily of transmembrane proteins known as the adenosine triphosphate (ATP)-binding cassette transporters (ABC transporters) is involved with actively shuttling substrates across cellular membranes in all organisms studied to date, including prokaryotes, fungi, plants, and animals (Higgins, 1992). Substrates for ABC-transporters include metabolites of phase I and phase II biotransformation, as well as their unchanged parent molecules (Epel et al, 2008). ABC-transporters which have demonstrated a role in xenobiotic defense include multidrug resistance protein 1 (MDR1), also known as Permeability-glycoprotein (P-gp); the breast cancer resistance protein (BCRP), and MDR-associated proteins 1 and 2 (MRP1 and MRP2) (Chang, 2003; Leslie et al, 2005). Of these transporters, the most well-characterized is P-gp (see Section 1.2), a transmembrane efflux “pump” involved with limiting the cellular accumulation of endogenous substrates, as well as a wide range of drugs, xenobiotics and their metabolites (Seelig, 1998). The transport activity of P-gp, in effect, modulates the toxic effects of xenobiotics by manipulating their disposition and bioavailability within organisms (Fromm, 2000; Kurata et al, 2002).

A common feature of these xenobiotic defense mechanisms is their responsiveness to xenobiotic challenges by gene induction and/or increases in the functional activity of proteins associated with phase I and II biotransformation and xenobiotic transport (Schuetz et al, 1996; Tran et al, 2002). This modulation from basal activity shares a feature of the adaptive immune response whereby xenobiotics can elicit the up-regulation of specific proteins to confer a tailored cellular response (Sarkadi et al, 2006). Although this system does not have memory, unlike the adaptive immune response, this inductive property of cellular defense mechanisms is highly regulated and

can provide a specific and appropriate level of defense activity (Sarkadi et al, 2006). The co-operative action of phase I and phase II biotransformation as well as ABC-transporter-mediated efflux, encompass the mechanism of multidrug/multixenobiotic resistance (MDR/MXR), which confers protection to cells and tissues against the accumulation of cytotoxic substances (Figure 1.2).

Figure 1.2: Multidrug/multixenobiotic resistance (MDR/MXR) activity

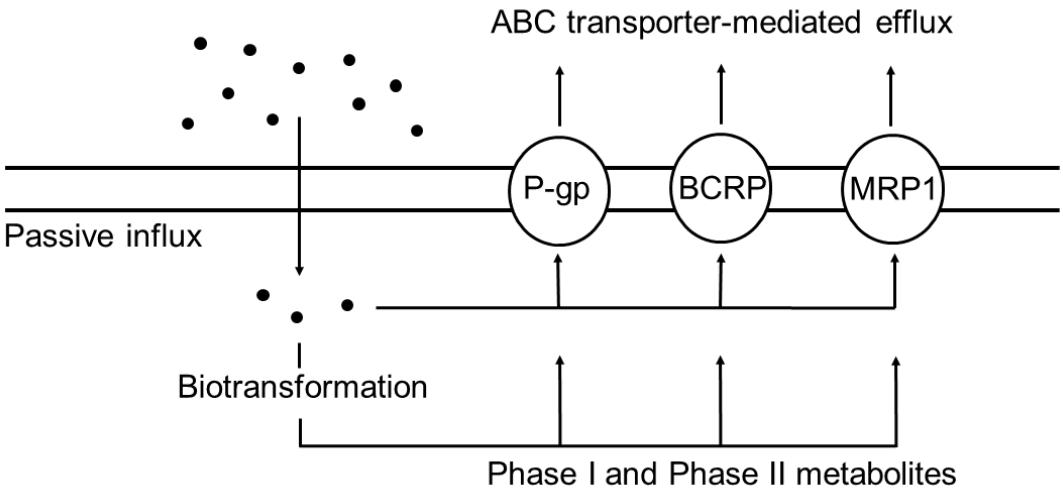

Xenobiotics entering the cell by passive diffusion are directly cleared by ABC-transporters such as P-glycoprotein (P-gp), the breast cancer resistance protein (BCRP), or the Multidrug resistance protein 1 (MRP1). Xenobiotics can also be metabolized by phase I /II biotransformation enzymes prior to cellular efflux by ABC-transporters.

1.2. Investigating the MDR/MXR mechanism in zebrafish

The zebrafish (*Danio rerio*) is perhaps best known for its role as a model organism to study developmental processes in vertebrate species. Over the last twenty years, this teleost fish has also emerged to play a prominent role in pharmacological and toxicological investigations (Dai et al, 2014). It is therefore beneficial to understand the underlying regulatory mechanisms involved with the cellular and physiological responses to xenobiotic challenges in this species. Due to the clinical significance of cellular defense mechanisms, there is a wealth of data describing the multidrug/multixenobiotic resistance (MDR/MXR) mechanism in mammalian models. However, emerging evidence suggests teleost fish may share overlapping MDR/MXR-associated processes with distantly related

vertebrate species, including humans. The majority of these investigations have used *in vitro* methods to help characterize MDR/MXR mechanisms in fish; however, further *in vivo* data is required to represent accurately these biological processes in the context of the living organism. While studying cellular mechanisms *in vitro* has several key advantages (e.g., low variability and ease of maintenance), *in vivo* data is critical for the development of 'real-world' applications directly involving cellular defense mechanisms, such as pharmaceutical therapies, or the use of molecular biomarkers for ecological biomonitoring and exposure assessments.

The zebrafish is a particularly useful organism in the laboratory setting due to its small size, relative hardiness, short reproductive cycle, and transparent *ex utero* embryonic development. In addition, the latest zebrafish reference genome (Zv9 assembly) has been completely sequenced and annotated, and up to 69% of zebrafish genes have at least one obvious human orthologue (Howe et al, 2013). Furthermore, the sensitivity of zebrafish to various aquatic contaminants, including heavy metals, endocrine disrupting chemicals (EDCs), and organic pollutants, makes this fish a suitable model organism for aquatic toxicology applications (Dai et al, 2014). A variety of molecular biomarkers of chemical exposure have been identified and used in zebrafish, including Cyp1a induction as a marker for waterborne aryl hydrocarbon receptor (AhR) agonists (Kennedy and Jones, 1994) metallothionein (*Mt*) mRNA induction as a marker for mercury (Hg^{2+}) and cadmium (Cd^{2+}) in water (Chan et al, 2006), as well as vitellogenin 1 (*vtg1*) mRNA induction as a marker of EDCs such as polybrominated diphenyl ethers (PBDEs), dioxins, and bisphenol A (BPA) (Muncke and Eggen, 2006). Despite these and various other biomarkers of exposure to specific classes of waterborne contaminants, less is known about the MDR/MXR mechanism in zebrafish.

1.3. P-glycoprotein (P-gp)

In humans, P-gp is a 170 kilodalton (kDa) dimer with both domains consisting of 6 transmembrane α-helices, including a single intracellular nucleotide binding site on one domain (Chin et al, 1989). P-gp is encoded by the ABCB1 (MDR1) gene, which is constitutively expressed in multiple organs such as the liver, brain, intestines, pancreas, adrenal cortex and kidneys (Thiebaut et al, 1987). ABCB1 gene expression can be

induced by a variety of structurally-unrelated substrates, which are often substrates for or metabolites of detoxifying enzymes such as the CYP450 monooxygenase, CYP3A (Wacher et al, 1995). These substrates are both endogenous and exogenous in origin and are often moderately hydrophobic or amphipathic molecules ranging in size from 250 to 1250 kDa (Seelig, 1998). Indeed, P-gp's broad tissue expression, inducibility, and diversity of substrates underscore how P-gp mediated transport plays a key role in protecting the body from potentially cytotoxic substances.

Overexpression of P-gp is a well-known response involved in the mechanism of multidrug/multixenobiotic resistance (MDR/MXR), which prevents the bioaccumulation of various drugs and environmental toxicants in cells (Gottesman and Pastan, 1993; Bard, 2000). For example, the P-gp-mediated MDR/MXR phenotype in malignant tumour cells is a major barrier to achieving therapeutic concentrations of anti-cancer drugs and hence, successful treatment of disease (Wacher et al, 1995). Functional P-gp limits the cellular accumulation of cytotoxic substances through selective transport of chemicals out of the cytosol. While the identification of P-gp substrates has primarily focused on pharmaceuticals, environmental chemicals such as arsenite, industrial nonylphenol ethoxylates, and the organophosphate pesticides phosalon and diazinon have been reported as substrates for P-gp in fish (Loo and Cark, 1998). With a vast and growing number of anthropogenic pollutants in the environment, additional ecotoxicologically-relevant substrates for P-gp are likely to be identified (Georganzopoulou et al, 2014). P-gp is also known to mediate the transport of endogenous molecules including lipids, bile salts, and steroid hormones, suggesting P-gp plays an important role in multiple cellular processes (vanHelvoort et al, 1996; Wang et al, 2009; Lee et al, 2013). The role of P-gp in glucocorticoid transport has been studied in various cell and animal models, which indicated that P-gp activity can also influence endocrine signaling in the hypothalamus-pituitary-adrenal cortex (HPA) axis (Karssen et al, 2001).

Numerous *in vitro* and *in vivo* assays have demonstrated chemical inhibition or gene knock down of P-gp can result in the reduced clearance of various P-gp substrates (Choi et al, 2011; Rumpold et al, 2005). Environmental contaminants such as organophosphorous and organochlorine pesticides strongly inhibit P-gp functional activity, which may lead to increased cellular accumulation and sensitivity to cytotoxic P-gp substrates in wild populations (Bain and LeBlanc, 1996). In contrast, induction of P-gp

expression by rifampicin, dexamethasone, and St. John's wort has been shown to increase the cellular clearance of the P-gp substrate and tracer dye for P-gp-mediated transport, rhodamine 123 (R123) (Kageyama, 2006). Transport kinetics of other P-gp substrates, such as digoxin, also correspond to P-gp expression levels (Pinto et al, 2005). Furthermore, single nucleotide polymorphisms (SNPs) of the *ABCB1* gene, which result in altered protein structure, have been shown to influence the pharmacokinetics of various drugs, including anti-cancer therapies (Kroetz et al, 2003; Han et al, 2007; Johnatty et al, 2008). Thus it appears P-gp activity plays a key role in the toxicokinetic -toxicodynamic (TK-TD) fate of xenobiotics, and altering P-gp expression, structure, and function can significantly affect the efficiency of the MDR/MXR mechanism.

P-gp-like proteins have been described in a variety of aquatic organisms including sponges, mussels, oysters, and various fish species such as guppy, killifish, flounder, prickleback, and zebrafish (Bard et al, 2002; Bard, 2005; Chan et al, 1992; Fischer et al, 2013; Keppler et al, 2001; Kurelec et al, 1992; Smital et al, 2003). The immunohistochemical detection of P-gp in fish has been performed with the monoclonal antibody C219, which recognizes a highly conserved epitope common to all known P-gps and their isoforms. In the teleost fish guppy (*Poecilia reticulate*), P-gp expression has been detected in the gills, intestines, kidney, pancreas, brain, and liver (Hemmer et al, 1995). In addition, elevated levels of P-gp have been observed in liver or liver tumours of killifish, European flounder, and winter flounder living in contaminated waters (Cooper et al, 1999; Kohler et al, 1998).

Several P-gp activity assays have been performed with aquatic species that demonstrate similar functional activity to mammalian P-gp. Using competitive inhibition substrate binding assays, Kurulec and Pivcevic (1991) and Kurelec (1996) showed that the mammalian P-gp substrates acetylaminofluorene and vincristine bind to P-gp in the marine mussel, *Mytilus galloprovincialis*, and that the established P-gp inhibitor, verapamil, suppresses the transport of these substrates by mussel P-gp. Furthermore, decreased cellular clearance of the P-gp substrate and fluorescent dye calcein-AM was observed in sponge cells treated with verapamil (Muller et al, 1996). Recently, zebrafish embryos either knocked down for P-gp or treated with the P-gp inhibitors verapamil, cyclosporin A or valspodar (PSC 833), showed an increased accumulation of the P-gp substrate and fluorescent dye, rhodamine B, in several tissues. These same treatments resulted in

elevated sensitivity and mortality to the known human P-gp substrates vinblastine, vincristine, doxorubicin, and the ecotoxicologically-relevant PAH pollutant, phenanthrene (Fischer et al, 2013). Thus, zebrafish appear to have an MDR/MXR mechanism that is dependent on P-gp expression and functional activity, and that substrates of mammalian P-gp are shared to some degree by aquatic species.

Figure 1.3 Examples of xenobiotic substrates transported by P-glycoprotein

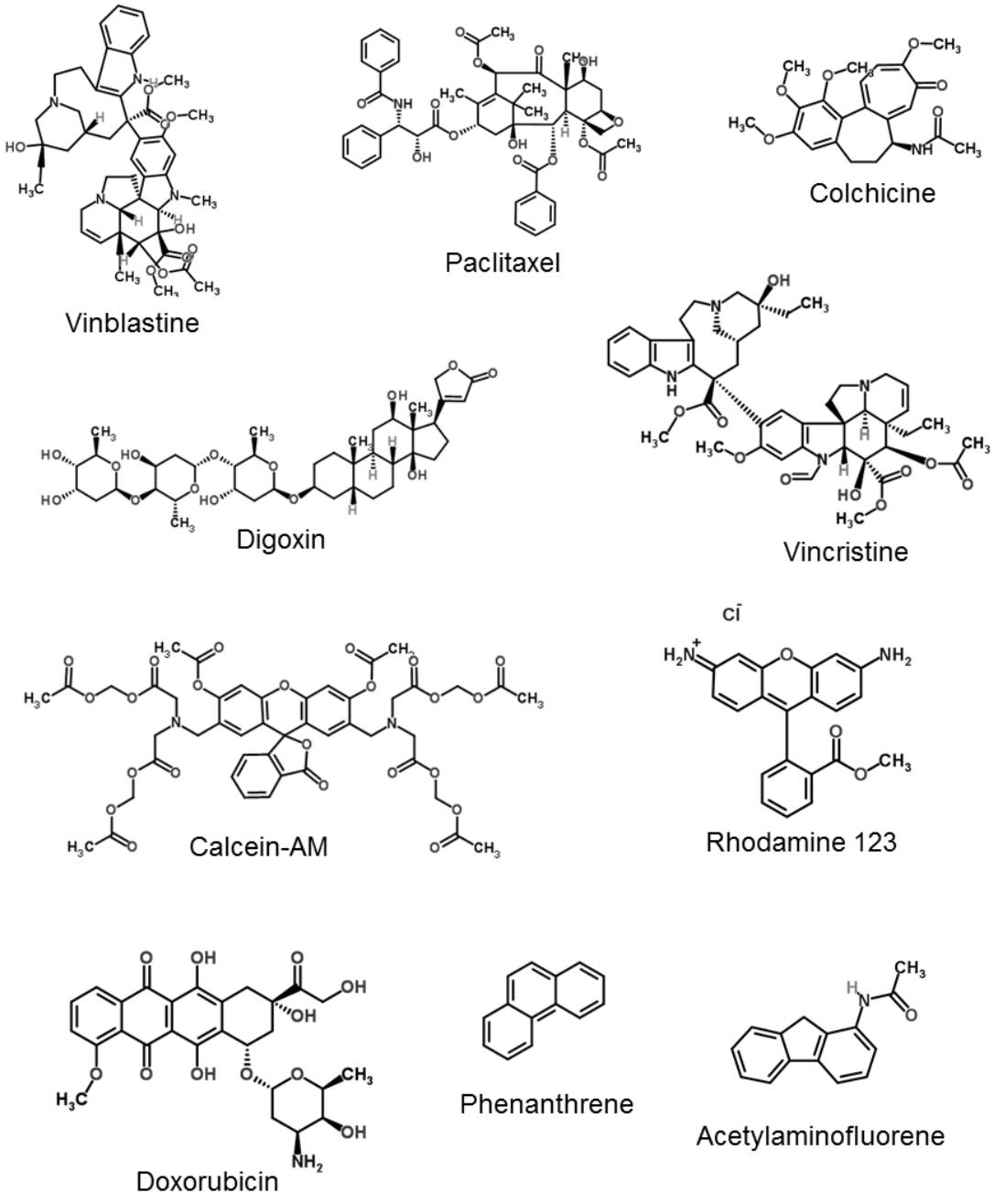

Images obtained from ChemSpider (www.chemspider.com)

Figure 1.4 Known inhibitors of P-gp activity

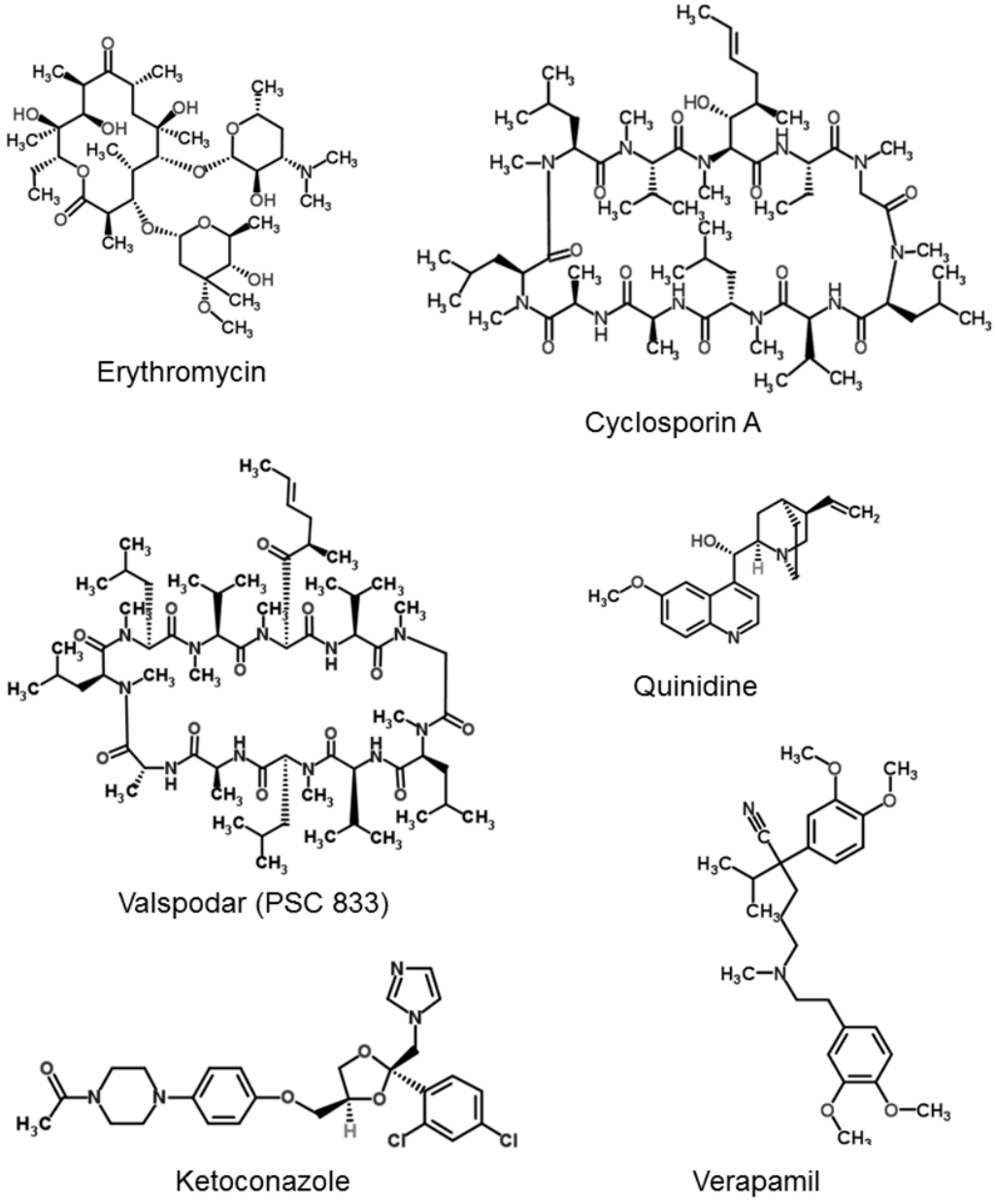

Images obtained from ChemSpider (www.chemspider.com)

1.3.1. Zebrafish P-glycoproteins

Zebrafish lack a direct orthologue of mammalian ABCB1 (MDR1), but possess two gene paralogues, ATP-binding cassette subfamily B members 4 and 5 (*abcb4* and *abcb5*), with common ancestry to the human p-glycoproteins *ABCB4* and *ABCB5*. Although the zebrafish *abcb4* and *abcb5* paralogues share 59% cDNA identity and 56% amino acid (a.a.) sequence similarity, how closely these gene products share cellular function with each other is still an open question (Joshi and Xu, 2007). Based on sequence alignment and substrate activity assays, both zebrafish P-gp transporters are assumed to be functionally similar to mammalian MDR1 (ABCB1) which is involved in multi-xenobiotic resistance (Fischer et al, 2013). Although limited gene expression and functional activity data indicate that both zebrafish genes may behave, to some degree, as xenobiotic transporters, the expression patterns of *abcb4* and *abcb5* in specific tissues during different life stages and under various physiological conditions are not well understood (Bresolin et al, 2005; Reschly et al, 2007; Fischer et al, 2013).

Gene sequence alignments reveal that the zebrafish *abcb4* gene shares 65% cDNA identity with human *ABCB4* and *ABCB1* (*MDR1)*, and 64% a.a. similarity with the corresponding P-glycoproteins, ABCB4 and ABCB1 (MDR1). Synteny analysis by Fischer et al (2013) indicates that the zebrafish *abcb4* and human *ABCB4* genes are evolutionary orthologues, based on chromosomal co-localization of *abcb4* /*ABCB4* and the gene that encodes carnitine O-octanoyltransferase, *crot* /*CROT*. Orthologues to zebrafish *abcb4* and its protein, Abcb4, are also observed in several other vertebrate species, such as rainbow trout [*Oncorhynchus mykiss*; 74% identity with *abcb1* (*mdr1*) cDNA, 77% a.a. similarity with trout Abcb1 (Mdr1)], and the western clawed frog [*Xenopus tropilcalus*; 61% identity with *abcb1* (*mdr1*) cDNA, 60% a.a. similarity with Abcb1 (Mdr1)]. Morpholino knockdown of *abcb4* in zebrafish embryos resulted in increased cellular accumulation of rhodamine B, as well as an increased sensitivity of fish to cytotoxic P-gp substrates (Fischer et al, 2013). Thus, the zebrafish Abcb4 protein appears to function as an ABCB1 (MDR1)-like multixenobiotic efflux pump. In contrast, the human ABCB4 orthologue is thought to function primarily in fatty acid transport and lacks a clear role in multixenobiotic resistance (Elferink and Paulusma, 2007).

Zebrafish Abcb5 shows 55% cDNA identity and 50% a.a. similarity with human ABCB5, and 57% cDNA identity and 55% a.a. similarity to human ABCB4. Based on gene annotations in the Ensembl data base, the zebrafish *abcb5* gene shows high synteny with human *ABCB5*, as both loci are co-localized with a cluster of genes indicating common ancestral origin (Fischer et al, 2013). Orthologues to zebrafish *abcb5* are found in other vertebrates, including rainbow trout [*Oncorynchus mykiss*; 58% identity with *abcb1* (*mdr1*) cDNA, 53% a.a. similarity with Abcb1 (Mdr1)], and in western clawed frog [*Xenopus tropilcalus*; 61% identity with *abcb1* (*mdr1*) cDNA, 60% a.a. similarity with Abcb1 (Mdr1)] (Fischer et al, 2013). In contrast to the human ABCB4 transporter, human ABCB5 plays a role in multidrug resistance, showing increased gene expression and transport activity of therapeutic drugs in malignant melanomas (Frank et al, 2005; Frank et al, 2009; Kawanobe et al, 2012). However, direct evidence of a similar xenobiotic transport function for zebrafish Abcb5 is currently lacking.

Table 1.1 Zebrafish Abcb4 and Abcb5 amino acid similarity across vertebrates

	H. sapiens ABCB1	H. sapiens ABCB4	H. sapiens ABCB5	O. mykiss Abcb1	O. mykiss Abcb11	O. latipes Abcb4	X. tropicalis Abcb1	X. tropicalis Abcb5	T. nigrovindis Abcb4	G. gallus Abcb1	G. gallus Abcb4	G. gallus Abcb5
D. rerio Abcb4	64	64	56	77	51	69	60	59	71	64	65	58
D. rerio Abcb5	59	58	50	58	48	55	57	67	59	59	57	67

Zebrafish (*D. rerio*) Abcb4 and Abcb5 share amino acid similarity with several ABCB/Abcb (P-glycoprotein) orthologues, suggesting possible evolutionarily-conserved functions between Zebrafish and other vertebrate P-gps. *Homo sapiens = H. sapiens; Oncorhynchus mykiss = O. mykiss* (Trout); *Oryzias latipes = O. latipes* (Medaka)*; Xenopus tropicalis = X. tropicalis (*Western clawed frog*); Tetraodon nigrovindis = T. nigrovindis* (Green spotted pufferfish); *Gallus = G. gallus* (Chicken). Sequence alignment was performed by Fisher et al (2013) with Clustal X.

1.4. Nuclear receptor 'xenosensors'

Nuclear receptors (NRs) are a family of highly conserved transcription factors found in all animals studied to date (Sladek, 2011). All NRs share common structural features which include a ligand binding domain (LBD) responsible for recognizing specific lipophilic ligands, and a DNA binding domain (DBD) responsible for targeting the NR to specific response element sequences in DNA to initiate gene transcription (Olefsky, 2001).

Ligands of NRs range from endogenous compounds (e.g., retinoids, bile salts, fatty acids, hormones and vitamins) to xenobiotic ligands such as antibiotics, synthetic drugs, and environmental contaminants (Blumberg and Evans, 1998; Parks et al; 1999; Janosek et al, 2006). The physiological role of NRs is far-reaching, covering critical aspects of endocrine signalling, development, disease, energy metabolism, and cellular defense. Although discovery of the 'classical' nuclear hormone receptors (e.g., vitamin D (VDR), estrogen (ER), glucocorticoid (GR), thyroid (TR), progesterone (PR), and retinoic acid (RAR) receptors) established and defined the NR superfamily, the evolutionary history of NRs is thought to predate the endocrine system itself. Indeed, emerging evidence suggests the original role of NRs may have been to function as xenobiotic sensors (xenosensors) prior to the evolution of NRs capable of responding to ligands originating from the host organism (Sladek, 2011).

The three most established xenosensors include the aryl hydrocarbon receptor (AhR), the constitutive androstane receptor (CAR), and the pregnane X receptor (PXR). These xenosensors are involved in detecting potentially harmful xenobiotics within the cell and coordinating the transcription of genes involved with biotransformation and elimination in response to chemical stress. AhR is an evolutionarily conserved ligand-activated transcription factor found in a broad range of distantly related species. As a xenosensor, AhR is known to bind many environmental toxicants, including polychlorinated dibenzodioxins (PCDDs), polycyclic aromatic hydrocarbons (PAHs), and various other synthetic and natural chemicals. Upon ligand activation, the AhR receptor complex (AhRC) dissociates, allowing AhR to dimerize with the AhR nuclear translocator (ARNT). The AhR/ARNT dimer then migrates to the nucleus and initiates the induction of the cytochrome P450 mixed function oxidase CYP1A, as well as a battery of other phase I and phase II metabolizing enzymes. Knowledge of this xenobiotic response pathway has led to the development of CYP1A as a molecular biomarker for ecological contamination (Goksoyr, 1995).

In contrast to AhR, the constitutive androstane receptor (CAR) has been described in only mammals to date, and is thought to have arisen from a duplication of an ancestral gene coding for the pregnane X receptor (PXR) (Reschly and Krasowski, 2006). Members of the NR1i subfamily of nuclear receptors, CAR and PXR are closely related "sister receptors" which overlap in several target genes and xenobiotic activators (Yang and

Wang, 2014). Unlike PXR, CAR is constitutively expressed in a ligand-independent manner; however, several prototypical agonists (phenobarbitol and 1,4-*Bis*(3,5-Dichloro-2-pyridinyloxy)benzene) and inverse agonists (iandrostanol and androstenol) are known to induce or decrease baseline CAR activity, respectively (Wagner et al, 2005; Forman et al, 1998). Genes under the transcriptional control of CAR include phase I metabolising enzymes of the cytochrome P450 subfamilies CYP3A and CYP2B, and several phase II transferases (UGT isoforms, GSTs, and sulfotransferases) (Maglich et al, 2002).

1.5. PXR-mediated regulation of P-gp and CYP3A

It is well established that P-glycoprotein is under the transcriptional control of the pregnane X receptor (PXR) in humans and other mammals. Unlike the constitutive androstane receptor (CAR), which has only been described in mammals, PXR has been identified in various distantly-related vertebrate species including zebrafish, chicken, rodents, dog, rhesus monkey, and humans (Reschly and Krasowski, 2006). The promiscuity of PXR is the result of a C-terminus ligand binding domain (LBD) that forms a relatively large, hydrophobic, and expandable binding pocket with low agonist specificity (Watkins et al, 2003).

Upon ligand binding, PXR simultaneously mediates the transcriptional induction of phase I and phase II metabolising enzymes as well as cellular efflux pumps. In mammals, the ligand-mediated activation of PXR involves heterodimerization with the retinoid X receptor alpha (RXRα) followed by nuclear translocation to initiate transcription of target genes (Kliewer et, 1998; Gu et al, 2006). The combined DNA binding domains (DBDs) of the PXR-RXRα complex bind to AGGTTC repeats in the xenobiotic response elements (XREs) of various detoxification enzymes, including the phase I biotransformation enzyme, CYP3A (Handschin and Meyer, 2003; Kliewer et al, 2002). In addition, PXR-RXRα binds to the XRE of *ABCB1* to induce expression of P-gp and mediates the cellular clearance of xenobiotics (Masuyama et al, 2005; Geick et al, 2001) (Figure 1.5). However, it remains to be established whether the Pxr-mediated induction of P-gp and Cyp3a also occurs in fish.

In mammalian systems, PXR is thought to interact with several co-activators (SRC-1, SRC-2, NRIP-1, PGC-1, and FKHR) and corepressors (SHP and SMRT) to control the

expression of genes involved with xenobiotic metabolism and transport (Wang et al, 2008; Ourlin et al, 2003; Pascussi et al, 2008). Phosphorylation of PXR by protein kinases such as PKA, PKC, CDK2, and p70S6K also appears to contribute to the post-translational regulation of PXR activity (Johnson et al, 2006; Pondugula et al 2009).

Studies of the PXR-mediated induction of P-gp in fish are limited. Zebrafish has shown to up-regulate Pxr (*nr1i2*), P-gp (*abcb5*) and Cyp3a (*cyp3c1*) expression following exposure to the synthetic steroid pregnenolone 16α-carbonitril (PCN), a model PXR activator in mammals (Bresolin et al, 2005). P-gp

Figure 1.5 PXR-mediated induction of *ABCB1* and *CYP3A* in mammals

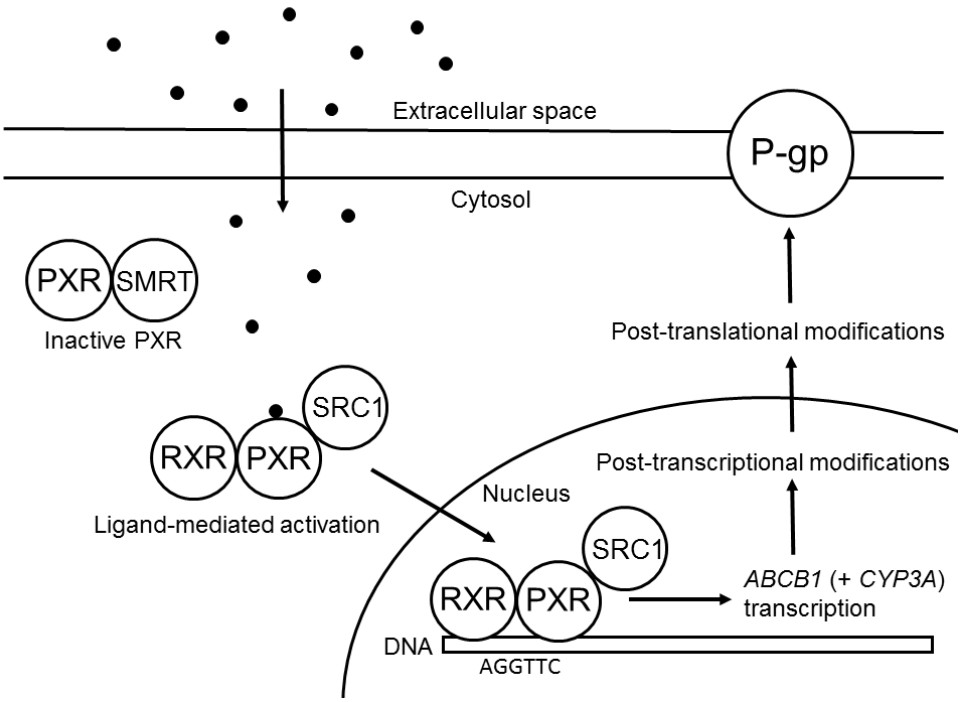

Inactivated cytosolic PXR is bound to the co-repressor SMRT. Upon ligand binding, the co-activator SRC-1 is recruited to PXR, while the PXR-SMRT interaction is disrupted. Activated PXR induces target gene expression by forming a heterodimer with the retinoid X receptor alpha (RXRα), and is imported to the nucleus. To initiate gene transcription, the combined DNA binding domains (DBDs) of the PXR-RXRα complex bind to AGGTTC repeats in the xenobiotic response elements (XREs) of *ABCB1* and *CYP3A*.

messenger RNA (mRNA) levels also increased in zebrafish treated with the endogenous bile salt and PXR activator, 5α-cyprinol 27-sulfate (Reschly et al, 2007). Furthermore, *nr1i2* (*pxr*), *abcb1* (*mdr1*), and *cyp3a27* mRNA were up-regulated in cultured

Oncorhynchus mykiss (rainbow trout) hepatocytes treated with PCN (Wassmur et al, 2010). Thus, it appears Pxr may play a role in mediating xenobiotic transport mechanisms in teleost fish.

1.5.1. Zebrafish Pxr

The zebrafish '*pxr*' gene, nuclear receptor subfamily 1 group I member 2 (*nr1i2*), is highly expressed in the intestine and liver, with considerably lower levels expressed in the testis, ovary, heart, kidney, brain, and eye (Bainy et al, 2013). Recently, the full-length zebrafish *nr1i2* (*pxr*) cDNA was sequenced and found to contain 1290 nucleotides, sharing 46% sequence identity to human, monkey, mouse, and rat *PXR*. The highest degree of similarity within the ray-finned fishes is to the *nr1i2* gene in Cave Fish (*Astyanax mexicanus*), with 67% sequence identity. Based on gene annotations within the Ensembl genome browser, zebrafish *nr1i2* (*pxr*) shows synteny with mammalian, frog and teleost fish *pxr*, indicating common ancestral origin (Bainy et al, 2013).

The DNA binding domain (DBD) of zebrafish Pxr is highly similar to the human PXR-DBD, sharing 74% sequence identity. Interestingly, the zebrafish Pxr ligand binding domain (LBD) shares only 44-46% identity with the human, monkey, rodent and rabbit PXR-LBD (Bainy et al, 2013). This lack of PXR-LBD similarity between zebrafish and mammalian species may reflect the contrasting habitats and subsequent shift in xenobiotic challenges that have accompanied speciation over time. In fact, compared to other nuclear receptor LBDs, the PXR-LBD shows significantly higher inter-species divergence as well as marked differences in ligand-specificity between species (Krawsowski et al, 2008). Limited evidence suggests that zebrafish Pxr may be activated by known mammalian PXR agonists such as nifedipine, clotrimazole and pregnenolone-16-α-carbonitrile; however, inconsistent results have been observed between in vitro and in vivo exposures (Bresolin et al, 2005; Fischer et al, 2013; Bainy et al, 2013). As with the mammalian PXR pathway, a zebrafish 'CYP3A' gene (cyp3a65) appears to be under the transcriptional regulation of zebrafish Pxr, indicating this nuclear receptor is a potential key regulator of multixenobiotic defense mechanisms in zebrafish (Tseng et al, 2004; Li et al, 2013; Bainy et al, 2013).

1.5.2. Zebrafish Cyp3a

Within the cytochrome P450 family, the CYP3A enzymes comprise the most abundant subfamily and play a major role in the phase I metabolism of a variety of endogenous and exogenous (xenobiotic) molecules. Unique to vertebrates, fish in the class *Actinopterygii* (ray-finned fishes, including zebrafish) possess multiple subfamilies of the *cyp3* gene family, namely the *cyp3a*, *cyp3b*, *cyp3c*, and *cyp3d* subfamilies. The emergence of the *cyp3b/c* subfamilies from a *cyp3* ancestor is thought to be the result of a fish-specific whole-genome duplication event prior to the emergence of *Actinopterygii*. Subsequent tandem repeat duplications of *cyp3b/c* genes later in *Actinopterygii* evolution ultimately resulted in the establishment of the *cyp3a/b/c/d* subfamilies in this class of bony fishes (Yon and Cai, 2010).

According to the Ensembl genome browser (*www.ensembl.org*), zebrafish possesses two Cyp3 paralogues, Cyp3a65 and Cyp3c1, which share 52-56% and 43-48% a.a. identity to human CYP3A, respectively. Based on the maximum likelihood gene tree method in Ensembl, these two genes are predicted to represent vertebrate CYP3A homologues in zebrafish (Villela et al, 2009). In adult zebrafish, *cyp3a65* mRNA is highly expressed in intestines and liver, with lower levels found in the eye, heart, gills, and skin (Corley-Smith et al, 2006). This expression pattern is reminiscent of that found for zebrafish Pxr, which has been implicated in regulating *cyp3a65* gene transcription following *in vivo* and *in vitro* exposures to established mammalian PXR agonists (Tseng et al, 2004; Li et al, 2013; Bainy et al, 2013). However, the precise regulatory mechanisms for *cyp3a65* expression remain unclear in zebrafish. For example, the canonical AhR agonist, TCDD, has triggered the induction of *cyp3a65* in zebrafish larvae, indicating possible crosstalk between the Pxr and AhR/ARNT pathways in regulating *cyp3a65* gene expression (Corley-Smith, 2009; Chang et al, 2013).

Similar to *cyp3a65*, the zebrafish *cyp3c1* gene is also highly expressed in the intestines and liver of adult fish, with lower mRNA levels detected in the gills, heart, brain and eyes (Tseng et al, 2005). However, treatment of zebrafish larva with known mammalian PXR agonists such as rifampicin and dexamethasone has resulted in cyp3a65 induction with no concomitant changes to *cyp3c1* mRNA levels suggesting that *cyp3a65* and *cyp3c1* may be regulated by separate mechanisms (Tseng et al, 2005; Corley-Smith,

2009). Complicating the issue is the observed increase of cyp3c1 mRNA following an in vivo exposure to the PXR agonist pregnenolone-16α-carbonitrile (PCN) in adult zebrafish (Bresolin et al, 2005). These observations may represent a tissue and/or age-specific response in cyp3c1 gene induction to xenobiotic /cytotoxic challenges.

1.6. Summary and objectives

The precise regulatory mechanisms by which fish protect their cells from the accumulation of xenobiotic chemicals remain only partially characterized. Numerous studies have contributed to our understanding of the multidrug/multixenobiotic resistance (MDR/MXR) mechanism in mammals, which is regulated by the nuclear receptor and xenosensor, PXR. The ligand-mediated activation of PXR results in the co-induction of several xenobiotic response genes, including *CYP3A* and *ABCB1* (*MDR1*), to help coordinate the metabolism and elimination of cytotoxic substances absorbed by cells.

Emerging evidence suggests that zebrafish possess an MDR/MXR mechanism with similar characteristics to those in mammals yet many details remain to be uncovered. Recent work by Fischer et al (2013) has demonstrated that zebrafish utilize a P-gp xenobiotic transporter, Abcb4, with functional activity similar to mammalian MDR1 (ABCB1). Zebrafish larvae knocked down for *abcb4* show increased tissue accumulation of the P-gp substrate rhodamine B, and increased sensitivity to known cytotoxic substrates for mammalian ABCB1 (MDR1) (Fischer et al, 2013). Several studies have demonstrated that mammalian PXR agonists can also activate zebrafish Pxr and trigger the induction of *cyp3a65*, the zebrafish ortholog of the MDR/MXR – associated *CYP3A* gene in mammals (Tseng et al, 2004; Li et al, 2013; Bainy et al, 2013). Similarly, the rodent PXR agonist pregnenolone 16α-carbonitrile (PCN) triggered the co-induction of *abcb5* and a *CYP3A* ortholog, *cyp3c1*, in adult zebrafish liver (Bresolin et al, 2005). Together, these observations point to a xenobiotic defense strategy in zebrafish which is functionally consistent with the classic MDR/MXR mechanism.

Despite our progress in unraveling how zebrafish confer resistance to xenobiotic challenges at the cellular level, the regulation of the MDR/MXR-like mechanism in this species requires further characterization. Reports describing gene expression patterns of

the two zebrafish P-gp paralogues, Abcb4 and Abcb5, are limited and inconsistent. For example, Abcb4, but not Abcb5, played a key role in xenobiotic clearance from zebrafish larvae (Fischer et al, 2013). In contrast, induction of the *abcb5* gene was observed in adult zebrafish liver following exposure to the PXR agonist, PCN (Bresolin et al, 2005). Similar inconsistencies in gene expression patterns have been observed between *cyp3a65* and *cyp3c1* following various xenobiotic exposures (Tseng et al, 2004; Li et al, 2013; Bainy et al, 2013). Thus, the question of whether these xenobiotic response genes are regulated by multiple pathways, or in a tissue and age-dependent manner has not been resolved.

The aim of this research is to further characterize the MDR/MXR mechanism in the model teleost, zebrafish. Because zebrafish have emerged as a model organism in pharmacological /toxicological investigations, it is critical to characterize the underlying regulatory mechanisms involved in the response to xenobiotic challenges in this species. Despite the zebrafish liver being a major site of xenobiotic transformation, detoxification, and clearance, there are no reports describing the regulation of zebrafish P-gp functional activity *in vivo*. Furthermore, no previous studies have investigated the possible involvement of Pxr in the transcriptional regulation of the zebrafish P-gp gene, *abcb4*. In addition, the potential mammalian-like co-induction of *cyp3a65* and *abcb4* during the zebrafish MDR/MXR response has previously not been investigated. To help fill these gaps in our knowledge of the MDR/MXR response in zebrafish, the following two objectives were explored:

Objective 1: To investigate the functional activity of zebrafish P-glycoprotein following treatment with Pxr modulators in vivo. The rationale for this approach is to help uncover the possible involvement of Pxr in regulating MDR/MXR functional responses in zebrafish liver

This study used an established zebrafish Pxr agonist, pregnenolone 16α-carbonitrile (PCN), to activate hepatic Pxr *in vivo*. In addition, a co-exposure of PCN and the Pxr inhibitor, ketoconazole (KTC), was used to antagonize the activation of Pxr by PCN. The objective was to determine whether measurable changes in P-gp functional activity occur following exposure to PCN or PCN + KTC. The transport activity of P-gp was evaluated using hepatic clearance and uptake assays with the fluorescent dye and P-gp substrate, rhodamine 123 (R123).

Objective 2: To examine the hepatic transcriptional responses of MDR/MXR-associated genes following treatment with Pxr modulators in vivo. The rationale for this approach is to help characterize the mechanism(s) regulating MDR/MXR-associated gene transcription

This study investigated the *in vivo* mRNA levels of MDR/MXR-associated genes following exposure to PCN and PCN + KTC. The objective was to determine whether drug treatment targeting Pxr caused alterations in hepatic *abcb4*, *abcb5*, *cyp3a65*, *cyp3c1*, and *nr1i2* (*pxr*) gene expression. Gene expression was analyzed by the real-time quantitative polymerase chain reaction (RT-qPCR) technique.

These objectives represent the first investigations of both the functional activity of zebrafish P-gp in the liver (*Objective 1*) and the modulation of MDR/MXR-associated genes (*Objective 2*) following exposure to modulators of Pxr activity *in vivo*. The information gained from this study will further characterize the role of zebrafish Pxr, Abcb4, Abcb5, Cyp3a65, and Cyp3c1 in conferring protection against the toxic effects associated with xenobiotic accumulation in cells.

2. Materials and Methods

2.1. Fish

Adult male and female zebrafish weighing approximately 400 to 700 mg were obtained from Aquatic Research Organisms (Hampton, NH, USA) and a local retail supplier in Vancouver, BC, Canada. Fish were housed in tanks on a zebrafish housing rack with 10-12 fish in each individual 6 L tank. Tanks were supplied with dechlorinated water maintained at 28°C at a constant pH of 7.0 using an automated flow-through water filtering system. Fish were fed with ground Omega One™ Freshwater Flakes twice daily. A regular photoperiod of 14 h light and 10 h dark was maintained for the duration of care. Fish were acclimated for a minimum of 2 weeks prior to any experiment. All experimental procedures were performed under an Animal Care Permit issued by the Simon Fraser University Animal Care Committee and were in accordance with the Canadian Council on Animal Care guidelines.

2.2. Chemicals

Rhodamine 123 (R123) was purchased from Cedarlane (Westbury, NY, USA). Pregnenolone 16α-carbonitrile (PCN) and Ketoconazole (KTC) were purchased from Sigma-Aldrich (Oakville, ON, Canada). Ethidium bromide (EtBR) was obtained by donation from Dr. Fiona Brinkman's laboratory, Department of Molecular Biology and Biochemistry, Simon Fraser University, BC, Canada.

2.3. Chemical administration and exposures

Fish were fasted for 48 h prior to any treatment and were randomly selected and placed in several treatment groups. There were three treatment groups: PCN only, a

combined equimolar dose of PCN and KTC, and a control group (vehicle only). To administer chemicals, individual zebrafish were anesthetized with 100 mg/L sodium bicarbonate-buffered MS-222 (pH 7.4), and then weighed. Following weighing, fish were placed on a wetted sponge in the supine position, and injected intraperitoneally (i.p.) with either: 20 mg /kg PCN alone, a combined equimolar dose of PCN and KTC (20 mg/kg and 31 mg /kg, respectively), or vehicle only (corn oil with 5% v/v dimethyl sulfoxide [DMSO]). These doses were used for all experiments. To help achieve sterile and homogenous mixtures for each dosing solution, PCN and KTC (with ACD/log*P* octanol-water partition coefficients of 3.49 and 4.04, respectively) were dissolved in DMSO then heated in syringe-filtered (pore size of 0.2 µm) corn oil at 90°C for 10 min. Corn oil is a common vehicle for chemical delivery and was used as a non-polar vehicle to dissolve the chemicals and facilitate absorption. A 26s-gauge Hamilton© syringe (2" needle, 10 µl volume) was used for all i.p. injections. The route of absorption following i.p. injection is likely via the mesenteric vessels that distribute the drug to the portal vein and the liver before it enters the systemic circulation (Turner et al, 2011).

The doses of PCN and KTC were based on previous work by Bresolin (2005), Hasselberg et al (2008), and Hontoria et al (2013). Injection volumes were based on the nearest 50 mg wet body mass and ranged from 5.7 to 10.0 µl (corresponding fish weights from 0.4 to 0.7 g). To reduce stress associated with injections, chemical solutions were maintained at the tank water temperature of 28°C, and were injected gradually over 10 sec. Following injections, fish were returned to tanks and quickly recovered from sedation with no signs of abnormal behaviour, bleeding, or other visible complications. Treated fish remained in flow-through tanks for a period of 48 h prior to any further experimental procedures. Following all experimental exposures, euthanasia of the fish was carried out in 500 mg/L sodium bicarbonate buffered MS-222 (pH 7.4). To block for potential tank effects, each experimental group was separated into 3 tanks (9 tanks total).

2.4. Rhodamine 123 kinetics

Rhodamine 123 (R123) is a fluorescent probe and P-gp substrate that is actively cleared from cells via P-gp-mediated efflux. Intracellular R123 accumulation is inversely proportional to P-gp activity: relatively high levels of intracellular R123 indicate reduced P-

gp activity, while low intracellular R123 levels indicate increased relative P-gp activity (Forster et al, 2012). R123 and other rhodamine dyes (e.g., rhodamines B, 6G, and 110) have been used extensively to study the pharmacokinetics of multidrug resistance in various animal cell lines (Chaudhary and Roninson, 1991; Lee et al, 1994; Doyle et al, 1998; Forster et al 2012). Furthermore, several studies have used intravenous injection of rhodamine to investigate P-gp activity *in vivo* (Liu et al, 2006; Jin et al 2012). However, reports involving the use of rhodamine dyes in live fish models are limited (Damare, 2009; Fischer et al, 2013).

2.4.1. Determination of R123 loading exposure

To validate the use of zebrafish for in vivo R123 liver accumulation assays, it was critical to show that: 1) R123 is absorbed to measurable levels in zebrafish liver, and 2) the amount of R123 detected in liver is related to the R123 exposure concentration. To test these basic criteria, two preliminary R123 loading trials were performed. The first trial measured the accumulation of liver R123 in zebrafish exposed to various R123 concentrations (0, 1.25, 2.5, 5, 10, and 20 µM R123) for a 2 h loading period, while the second trial measured R123 accumulation in fish exposed to 5 µM R123 over several loading periods (0, 0.5, 1, 2, and 4 h). To perform these preliminary trials, fish were placed individually in glass vessels containing 200 ml dechlorinated water spiked with R123 (or no R123). Each vessel was continuously aerated. Fish remained in the R123-spiked water for the designated loading period to allow for accumulation of R123 in the liver. Following R123 loading, fish were removed, rinsed, and then sacrificed in a solution with 500 mg/L sodium bicarbonate buffered MS-222 (pH 7.4). Fish were immediately rinsed again, then decapitated to facilitate the drainage of blood from the body. Livers were excised, rinsed with Hank's balanced salt solution (HBSS) (Gibco®, Life Technologies, Burlington, ON, Canada), then placed in 500 µl of homogenization buffer (HBSS containing 0.05% Triton X-100), and homogenized using a bead mixer mill. Samples were centrifuged at 18,000 *x g* for 15 min. The supernatant was then loaded into black 96-well plates (100 µl per well, in triplicate) and measured for R123 fluorescence in a SpectraMax® M2e fluorometer (Molecular Devices, LLC; Sunnyvale, CA, USA). The samples were fluorometrically measured according to R123 product specifications (Sigma Aldrich, Oakville, ON, Canada) using excitation and emission wavelengths of 510 nm and 535 nm, respectively. Sample

R123 concentration was calculated using a R123 standard curve constructed from a two-fold serial dilution of R123 (2.5 to 0 µM) in homogenization buffer (Figure A1, **Appendix A**). To account for inter-individual variations in liver size, R123 measurements were normalized to total protein content of livers. To quantify total liver protein content, 5 µl of supernatant from the homogenized liver samples was loaded in triplicate in a clear 96-well plate, and 250 µl of Quick Start™ Bradford dye (Bio-Rad®, Mississauga, ON, Canada) was added to each well. Absorbance at 595 nm was measured using a BioTek® PowerWave™ 340 microplate reader (BioTek®, Winooski, VT, USA). Total protein concentration was determined from a standard curve constructed from a two-fold serial dilution (1 mg/ml to 0 mg/ml) of bovine serum albumin, BSA (Sigma Aldrich, Oakville, ON, Canada) in homogenization buffer (Figure 2, **Appendix A**). Triton X-100 was experimentally determined to not interfere with the Bradford assay at 0.05% v/v (data not shown). R123 accumulation is presented as R123 (nmol)/mg protein (Figures 1 - 4, Results).

2.4.2. R123 clearance assay

To observe the effects of chemical (PCN and KTC) treatment on R123 clearance from liver, zebrafish were treated with PCN, an equimolar co-treatment of PCN and KTC, or vehicle control as previously described. At 48 h following intraperitoneal (i.p.) injection, fish were loaded with R123 by water exposure in the experimentally-determined exposure of 5 µM R123 for 2 h. Fish were then removed from the exposure water, rinsed with clean water and individually placed in new vessels containing 200 ml fresh, clean and continuously aerated water. The water in each vessel was replaced every 2 h (up to 8 h) to remove excreted R123 or its metabolites. At six time points (0, 1, 2, 4, 8, and 24 h), 6 fish from each treatment (108 fish in total) were serially sacrificed and samples processed as previously described. Briefly, livers were rinsed with HBSS and stored at -80 °C overnight. To measure sample fluorescence, livers were thawed to 4 °C and placed in 500 µl of homogenization buffer (HBSS + 0.05% Triton X-100), and homogenized using a bead mixer mill. Samples were centrifuged at 18,000 *x g* for 15 min. The supernatant was loaded in black 96-well plates (100 µl per well in triplicate) and measured for R123 fluorescence. The 0 h time point was comprised of fish never exposed to R123, and was

used as a background measurement for fluorometric analysis of liver R123. Liver R123 is presented as nmol R123/mg protein.

2.4.3. R123 accumulation assay

To observe the effects of chemical (PCN or PCN and KTC) exposure on the accumulation of R123 in zebrafish liver, fish were i.p. treated with PCN, an equimolar co-treatment of PCN and KTC, or vehicle control as previously described. At 48 h post i.p. injection, a serial sacrifice design was used to compare rhodamine 123 (R123) accumulation in liver across all treatment groups at 0, 1.5, and 3 h of R123 exposure. At the 0 h time point, 9 fish per treatment were sacrificed to isolate livers without exposure to R123. These fish served as a measure of background fluorescence in each experimental group. The remaining fish were individually placed in glass vessels containing 100 ml of fresh dechlorinated water spiked with 5 µM R123. Each vessel contained an air supply for continuous water aeration. At 0, 1.5 and 3 h, fish from each treatment group were sacrificed for liver excision. Livers were rinsed with HBSS and stored at -80 °C overnight. To measure sample fluorescence, livers were removed from storage buffer, and processed as previously described. In contrast to the R123 clearance assay, the R123 accumulation assay had a larger sample size (n = 9 at 0 h, 11 at 1.5 h, and 12 at 3 h). The basis for increasing the sample size from the previous clearance experiment was to account for the high inter-individual variation of sample fluorescence observed in the R123 clearance assay.

2.4.4. Statistical analyses for R123 assays

All R123 assays were based on a completely randomized design (CRD) and were analyzed for significant differences in mean R123 concentrations using appropriate statistical tests that fit the characteristics of the data. Diagnostics of the residuals, or fitted errors ($\hat{E} = Y_i - \bar{Y}$), from each assay were performed to check the analysis of variance (ANOVA) assumptions, which follow the same underlying principles of linear regression models. Briefly, the validity of these statistical models relies on the residuals of the data to show independence of errors, equal variance (homoscedasticity), and approximately normal (Guassian) distribution. These model assumptions were analyzed in JMP statistical software by visual inspection of the residual *vs.* predicted response plot (to

assess the variance of errors), inspection of the residual vs. residual lag plot (to assess independence of errors), and inspection of the normal probability plot to assess the normal distribution of errors (JMP® Software, version 10, SAS Institute Inc., Cary, NC, 1989-2007).

In addition to visual inspection of the residual error terms, the Brown-Forsythe method was used to formally test the null-hypothesis that all experimental groups have equal variance, while the Shapiro-Wilk goodness-of-fit test was used to formally test the null-hypothesis the data are from a normal distribution. Single extreme values were considered for removal from the statistical analysis if variables were flagged by Grubb's test for outliers ($\alpha = 0.05$), or if residual analysis found an influential data point by visual inspection of the residual vs. predicted response and Cook's Distance (D) plots (see **Appendix E**). If data were suspected of violating the above model assumptions, a Box-Cox transformation (see **Appendix B**) of the original data was attempted in JMP software to improve the fit of the data (Box and Cox, 1964).

The R123 exposure assessments (effect of R123 concentration or R123 exposure duration on liver R123 concentrations) were analyzed by one-way ANOVA followed by Tukey's honest significant differences (HSD) post-hoc. The two-factor R123 clearance and accumulation assays (i.e., effect of chemical (PCN, PCN and KTC) treatment on liver R123 levels over time) were analyzed by two-way ANOVA followed by Tukey's multiple comparison post-hoc test. Mean R123 concentrations were compared across chemical treatment groups at specific time points. In all cases, mean R123 concentrations were considered statistically different at a significance level of $\alpha = 0.05$. A complete report of each ANOVA and post-hoc test is found in **Appendices C – J**.

2.4.5. Area under curve (AUC) analyses of MDR/MXR functional activity

To assess the effect of drug treatment on overall MDR/MXR functional activity, an additional statistical analysis using the area under the curve (AUC) method was performed on the R123 clearance and R123 accumulation data. In contrast to statistical analyses comparing liver R123 concentration at individual time points (Figure 3, results), analyses using the mean AUCs of each treatment group allow for comparisons of *total* liver R123

exposure over a period of time. Thus, analyses of AUCs help describe the general trend of treatment effects on MDR/MXR activity that may not be apparent in more discrete analyses. The AUC analysis for serial sacrifice designs is described in detail by Bailer (1987), and outlined in **Appendix K**. Bonferroni's adjustment to account for the family-wise error rate was incorporated into the statistical analysis of AUCs, whereby AUC contrasts were considered statistically significant when $|Z_{obs}|$ was greater than the Bonferroni-adjusted Z_{crit} value of 2.394 ($\alpha = 0.05$) or 2.93 ($\alpha = 0.01$).

2.5. Evaluation of gene expression

2.5.1. RNA extraction and cDNA preparation

At 48 hours post i.p. injection of PCN and KTC (using the same doses as previously described in the R123 accumulation and clearance assays), 12 fish per treatment group (n = 36 total) were euthanized in 500 mg/L sodium bicarbonate buffered MS222 (pH 7.0), washed, and briefly stored on ice water prior to excision of livers. Isolated whole livers were submerged in 300 µl RNA*later*® solution (Life Technologies, Burlington, ON, Canada) and stored at -80°C. Total RNA extraction was performed using RNeasy Micro Spin kits (Qiagen®, Toronto, ON, Canada). Individual livers (1-2 mg) were thawed, placed in 2 ml microcentrifuge tubes, and homogenized in 350 µl of Buffer RLT (Qiagen) containing 10% v/v β-mercaptoethanol. Samples were centrifuged at 15,000 x *g* and the supernatant was transferred to a new microcentrifuge tube to which an equal volume of 70% ethanol was added. Samples were loaded onto spin columns and washed as per the manufacturer's protocol (Qiagen), including an on-column DNase treatment (Qiagen). Following RNA extraction, 1 µl of each sample was loaded into individual wells of an RNA microfluidic chip (Agilent Technologies, Mississauga, ON, Canada) and analyzed for total RNA concentration, integrity, and purity with the Agilent 2100 Bioanalyzer (**Appendix L**). Samples were stored at -80°C until needed.

Complementary DNA (cDNA) was synthesized from total RNA (1 µg) using the Quantitect Reverse Transcription kit (Qiagen). All steps were followed according to the manufacturer's protocol (Qiagen), which includes a preliminary treatment with genomic DNA Wipeout Buffer (Qiagen) at 42°C for 2 min. Reverse transcription of template RNA

was carried out at 42°C for 30 minutes in a 20 µl reaction mix containing Quantiscript Reverse Transcriptase (containing RNase inhibitor), Quantiscript RT Buffer, and RT Primer Mix (containing a combination of oligo-dT and random hexamer primers) (Qiagen). The reaction was terminated by raising the incubation temperature to 95°C for 3 min. The resulting cDNA was stored at -20°C in nuclease-free water. Control samples containing no reverse transcriptase were used to verify that no detectable amount of genomic DNA contamination occurred during the reverse transcription step (see **Appendix N**).

Liver mRNA expression levels of all genes were analyzed at 48 hours post i.p. injection, and compared between control, PCN-treated, and PCN + KTC treated fish using the quantitative polymerase chain reaction (qPCR) technique. All primers were synthesized by Integrated DNA Technologies (Coralville, IA, USA), and are listed in Table M1, **Appendix M**. Primer sequences for *abcb4* (ATP-binding casette, subfamily B, member 4) were obtained from Fisher et al. (2013). Sequences for *cyp3a65* (cytochrome P450, family 3, subfamily A, polypeptide 65) were obtained from Lister et al. (2009). Primer sequences for *nr1l2* (nuclear receptor subfamily 1, group I, member 2), and *cyp3c1* (cytochrome P450, family 3, subfamily C, polypeptide 1) were designed in PrimerQuest online software developed by Integrated DNA Technologies (*www.idtdna.com*). The sequences for the endogenous control genes, ***ef1α*** (also known as *eef1a1l1*: eukaryotic translation elongation factor 1, alpha 1, like 1) and *bactin2* (actin, beta 2), were obtained from Casadei et al. (2011). The primer sequences for each gene targeted all corresponding mRNA splice variants listed in Ensembl. To determine the optimal annealing temperature (T_a) for each primer pair, end-point PCR was carried out using a T_a gradient (**Appendix O**). .

Individual samples and no template controls (NTCs) were run in triplicate using optically clear 384-well qPCR plates (Applied BioSciences) in the Applied BioSciences® 7900HT Real-Time qPCR System (Life Technologies, Burlington, ON, Canada). Total reaction volumes were 10 µl, which contained 5 µl PerfeCTa SYBR Green with ROX (Quanta BioSciences, Gaithesberg, MD, USA), 1.25 µl of forward primer (500nM), 1.25 µl of reverse primer (500nM), and 2.5 µl of template cDNA diluted in nuclease-free water. The qPCR conditions for all target genes were as follows: initial denaturing at 95°C for 10 min followed by 40 cycles of 95°C for 30 s (denaturing step), 55°C for 30 s (annealing

step), and 72°C for 30 s (elongation step). qPCR specificity was verified by melting curve analysis following qPCR (**Appendix Q**).

2.5.2. Gene expression analysis

Gene expression was analyzed using the relative standard curve method as described in "Guide to Performing Relative Quantification of Gene Expression Using Real-Time Quantitative PCR" by Applied Biosystems (2004). For each target and endogenous control gene, a two-fold serial dilution of pooled template cDNA (1:5 – 1:320) was included on each qPCR plate, in triplicate (**Appendix P**). The mRNA level for each target gene (*abcb4, abcb5, cyp3a65, cyp3c1, nr1i2*) was normalized to the geometric mean of the mRNA levels for *bactin2* and *ef1a,* which are commonly-used endogenous control genes in zebrafish studies (McCurley and Callard, 2008). To validate stable expression of the endogenous control genes, the raw quantification cycle (Cq) values for *bactin2* and *ef1α* were analyzed with the BestKeeper© version 1 (Pfaffl et al, 2004) applet in Microsoft Excel (**Appendix R**). All gene expression experiments were performed according to the MIQE (Minimum Information for Publication of Quantitative Real-Time PCR Experiments) guidelines recommended by Bustin et al (2009).

2.5.3. Restriction digest of target amplicons

To verify the identity of a target amplicon, sample cDNA was amplified by PCR (using the primer pairs listed in appendix D) then incubated with a restriction endonuclease (Table 2, **Appendix S**) as outlined in the manufacturer's protocol (New England Biolabs, Whitby, ON, Canada). The no-template control (NTC), target cDNA, and restriction digest products were loaded into separate wells on a 4% agarose gel. A low-molecular weight DNA ladder was used to help estimate the size of the small digest fragments (Figure 1, **Appendix S**).

2.5.4. Statistical analysis for gene expression

The gene expression assay was based on a completely randomized design (CRD). The statistical analysis of mean mRNA expression levels across experimental groups was run independently for each target gene, and was tailored to each set of data. Extreme

data points were identified using Grubb's test for outliers (α = 0.05). Gene expression data was diagnosed by visual inspection of the residuals for homoscedasticity, independence of the error terms, and normality. In addition, formal tests for normality (Shapiro-Wilk, α = 0.05) and equal variance (Brown-Forsythe, α = 0.05) were conducted for further diagnostics of the data. Data assumed to have approximate normal distribution and equal variance were analyzed by one-way analysis of variance (ANOVA) and Tukey's honestly significant difference (HSD) post hoc test. When normality or equal variance could not be assumed, a Box-Cox power transformation was applied to the original data (anchored at 1) prior to running the statistical test. If a Box-Cox transformation (**Appendix B**) did not improve the assumption of normality, but sufficient homoscedasticity of the residuals was indicated in non-transformed data, the non-parametric Wilcoxon Rank Sums and Steel-Dwass multiple-comparison post-hoc tests (when applicable) were performed on the non-transformed data. Mean differences between experimental groups were considered statistically significant if $p < 0.05$. All statistical procedures were carried out in JMP (JMP® Software, version 10, SAS Institute Inc., Cary, NC, 1989-2007), and GraphPad Prism (Prism version 6.00 for Windows, GraphPad Software, La Jolla California USA, www.graphpad.com).

3. Results

3.1. R123 exposure trials

3.1.1. Effect of R123 exposure concentration on hepatic R123 uptake

To validate an *in vivo* R123 assay for zebrafish and to establish an R123 loading exposure concentration, fish were exposed to water containing R123 at several concentrations (0, 1.25, 2.5, 5, 10, and 20 µM R123) for 2 h. Overall, mean liver R123 accumulation (nmol R123 /mg protein) was significantly affected by the R123 exposure concentration (µM R123) in water (F [5, 24] = 9.7561, $p < 0.0001$). Fish exposed to test concentrations less than 5 µM R123 did not accumulate hepatic R123 to levels significantly above background (0 µM R123) (Figure 1). In contrast, the accumulation of R123 in the livers of fish exposed to 5 µM R123 reached 8.0 ± 1.0 nmol R123 /mg protein, which is significantly greater than the background control (p = 0.0004). No further increases in hepatic R123 were observed with exposures of 10 or 20 µM R123. Given these results, 5 µM R123 was chosen as a suitable exposure (R123 loading) concentration to measure R123 kinetics in zebrafish.

Figure 3.1: Effect of R123 exposure concentration on hepatic R123 uptake

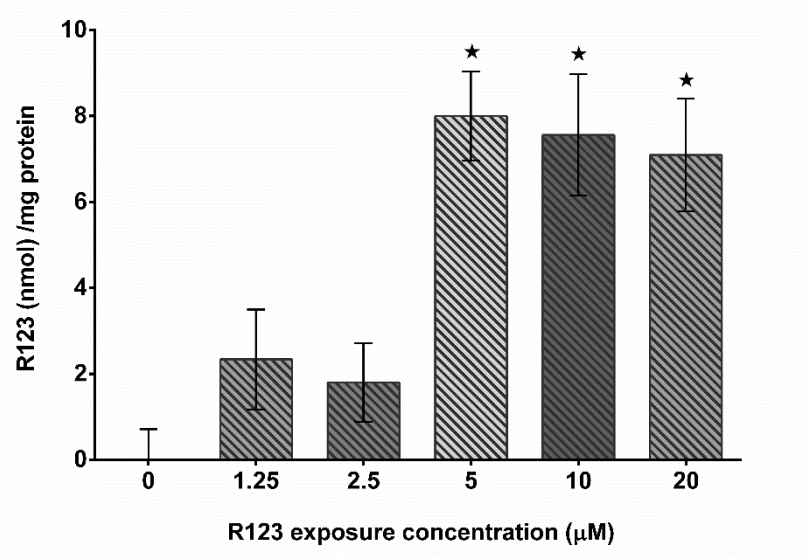

Mean hepatic R123 accumulation in zebrafish exposed to several concentrations of R123 for 2 h (n = 5). Error bars are the standard error (SE) about the mean. Differences in means were analyzed by one-way ANOVA followed by Tukey's HSD multiple comparison test. Means significantly different from background (0 μM R123) are denoted by * ($p < 0.001$).

3.1.2. Effect of R123 exposure duration on hepatic R123 uptake

To validate the *in vivo* R123 assay for zebrafish and to establish a R123 loading exposure time, fish were exposed to water containing 5 μM R123 for several exposure durations (0, 0.5, 1, 2, and 4 h). Overall, hepatic R123 accumulation (nmol R123 /mg protein) was significantly affected by the exposure duration (F [4, 15] = 29.81, $p < 0.0001$). Of the exposure times tested, those less than 2 h resulted in no significant hepatic R123 accumulation above the background control (0 h) (Figure 3.2). In contrast, the accumulation of R123 in the livers of fish exposed to R123 for 2 h reached 9.6 ± 1.3 nmol R123 /mg protein, which is significantly greater than the background control ($p = 0.0001$). No further increase in hepatic R123 was observed after 4 h. Given these results, 2 h was chosen as a suitable exposure (R123 loading) duration to measure R123 kinetics in zebrafish.

Figure 3.2: Effect of R123 exposure duration on hepatic R123 uptake

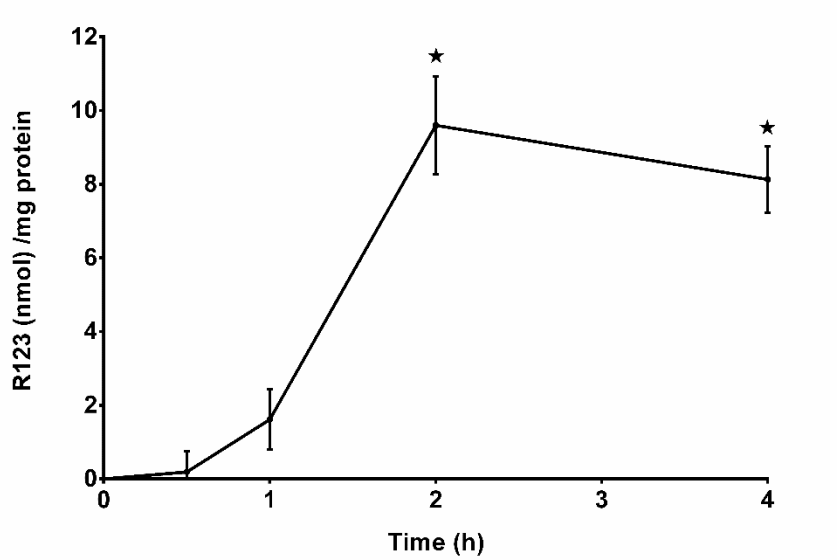

Time course of hepatic R123 uptake in zebrafish (mean ± SE, n = 5) exposed to 5 µM R123. Differences in means were analyzed by a one-way ANOVA followed by Tukey's HSD multiple comparison test. Means significantly different from background (0 h exposure) are denoted by * ($p < 0.0001$).

3.2. Effect of drug treatment on hepatic R123 concentration

3.2.1. Effect of drug treatment on hepatic clearance of R123

Fish treated with PCN, PCN + KTC, and the vehicle control for 48 h were compared for their ability to clear accumulated R123 from livers following an initial water exposure of 5 µM R123 for 2 h. Hepatic R123 concentrations in each experimental group were measured at 0, 1, 2, 4, 8, and 24 h following R123 loading (Figure 3). After fish were removed from the R123 exposure, mean hepatic R123 levels continued to rise in all experimental groups for at least 2 h, although none of these increases were statistically significant. Of all experimental groups, the control group accumulated the highest maximum concentration of liver R123 (C_{max} = 16.1 nmol /mg; T_{max} = 4 h), followed by PCN + KTC-treated fish (C_{max} = 11.5 nmol /mg; T_{max} = 2 h). The lowest C_{max} occurred in PCN-treated fish (C_{max} = 3.9 nmol R123 /mg; T_{max} = 8 h). Following this initial period of R123 accumulation, R123 was completely cleared from the livers of control and PCN + KTC-treated fish, with the majority of clearance occurring between 2 and 4 h (PCN + KTC)

and between 4 and 8 h (control). In contrast, R123 was only partially cleared from PCN-treated fish, and remained at detectable levels even after 24 h. The control group cleared R123 with a maximum hepatic clearance rate (CR_{max}) of 3.8 nmol/mg/h, compared to PCN-treated fish (CR_{max} = 0.31 nmol/mg/h) and PCN + KTC-treated fish (CR_{max} = 5.2 nmol/mg/h). In all cases, the maximum clearance rate was achieved directly after reaching C_{max}. Refer to **Appendix E** for statistical diagnostics and summary statistics.

Figure 3.3: Effect of drug treatment on overall hepatic clearance of R123

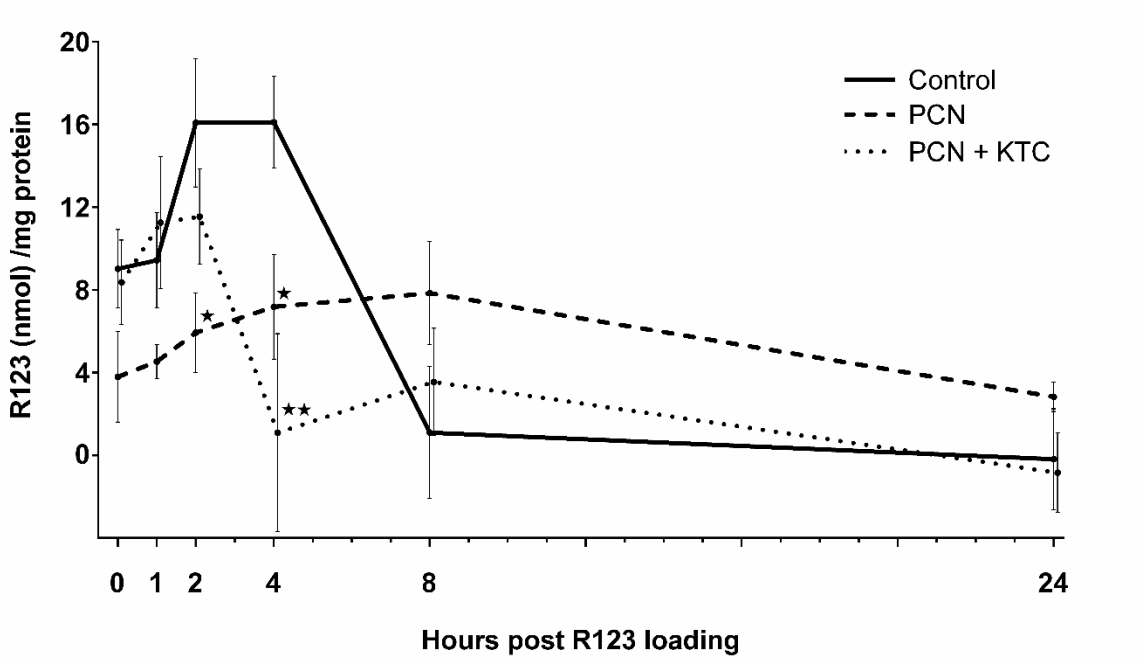

R123 clearance following a R123 water exposure of 5 µM R123 for 2 h. For each treatment group, mean R123 concentrations were normalized to background fluorescence measured from the livers of fish unexposed to R123. Error bars are one standard error (SE) about the mean. Differences in means were analyzed by a two-way ANOVA followed by Tukey's HSD multiple comparison test. Means significantly different from the vehicle control are denoted by * ($p < 0.05$) and ** ($p < 0.001$).

3.2.2. Area under curve (AUC) analysis of hepatic R123 clearance

The area under the curve (AUC) method was used to further analyze the effect of drug treatment on MDR/MXR functional activity in the liver. Here, the mean AUC is an estimation of the area under the R123 concentration *vs.* time curve and represents total liver R123 exposure over the duration of the clearance assay. Vehicle control fish had an estimated *AUC* of 95.9 ± 38.4 (mean ± SD), while PCN and PCN + KTC-treated fish had estimated *AUCs* of 138.0 ± 27.0 and 77.7 ± 31.1, respectively (Table 1). The AUC of the

PCN-treated fish was not significantly different from the AUC of the vehicle control (Z_{obs} = -0.90) or the PCN + KTC fish (Z_{obs} = 1.47). No statistically significant difference was observed between the mean AUC of vehicle control and the mean AUC of PCN + KTC-treated fish (Z_{obs} = -0.37) (Table 2). The 95% confidence intervals (C.I.'s) for the mean AUC contrasts appear in Table 2 and Figure 4. The procedures for calculating the AUCs, AUC contrasts, and 95% C.I.'s are explained in **Appendix K**.

Table 3.1. Summary of AUC estimates: Hepatic clearance of R123

Drug treatment	Mean AUC (R123 uptake time)	SD (AUC)
Control	95.9	38.4
PCN	138.0	27.0
PCN + KTC	77.7	31.1

Summary statistics for the area under curve (AUC) calculations of each experimental group in the R123 clearance assay. SD (AUC) = the standard deviation of the area under the curve estimation.

Table 3.2: Summary of AUC contrasts and statistical analyses

Contrast	Mean contrast (AUC_1 - AUC_2)	Z_{obs}	Bonferroni's Z_{crit} (α = 0.05)	$\lvert Z_{obs} \rvert > Z_{crit}$?	95% C.I.
Control vs. PCN	-42.1	-0.90	2.394	No	[-154, 70]
Control vs. PCN + KTC	-18.2	-0.37	2.394	No	[-137, 100]
PCN vs. PCN + KTC	60.3	1.47	2.394	No	[-38, 159]

Summary statistics of the AUC contrasts between each experimental group in the R123 uptake assay. $\lvert Z_{obs} \rvert$ is the observed Z value of an AUC contrast; Z_{crit} is the critical Z value of the two-tailed hypothesis test. Differences in AUCs were considered statistically significant if the absolute value of Z_{obs} was greater than a Bonferroni-adjusted Z_{crit} (to account for the family-wise error rate of multiple comparisons). The 95% C.I. is the confidence interval of the AUC contrast.

Figure 3.4: Differences between mean AUCs of hepatic R123 clearance assay

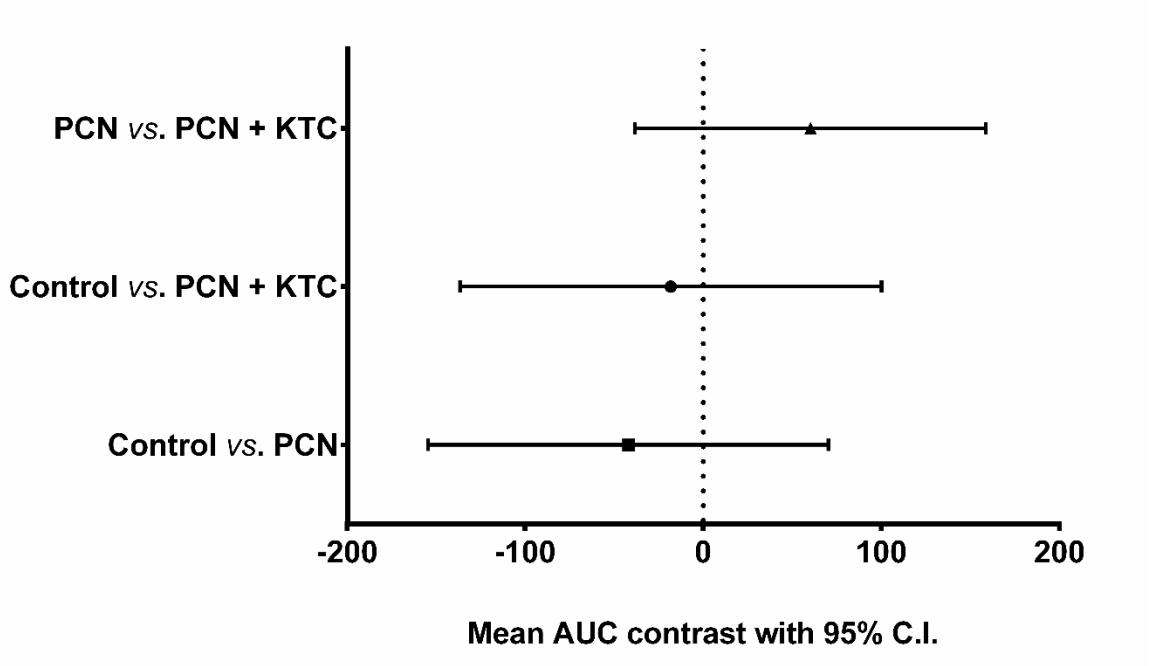

Contrasts of mean AUCs between each experimental group of the R123 clearance assay. Error bars represent the 95% confidence intervals (error bars). An AUC contrast (e.g., "Control *vs.* PCN") is the mean difference between AUCs of two treatment groups (see Appendix J). Intervals crossing x = 0 belong to a pair of AUCs which do not significantly differ (α = 0.05).

3.3. Effect of drug treatment on hepatic R123 uptake

Fish treated with PCN, PCN + KTC, and the vehicle control for 48 h were compared for hepatic R123 accumulation at 0, 1.5, and 3 h of exposure to 5 µM R123 (Figure 4). Overall, drug treatment was found by two-way ANOVA to have a significant effect on hepatic R123 accumulation, F (2, 4) = 7.33, p = 0.0012. Maximum R123 accumulation rates (AR_{max}) were achieved between 0 and 1.5 h, where control fish accumulated hepatic R123 at a rate of 5.2 nmol/mg/h, compared to 3.8 nmol/mg/h in fish treated to PCN, and 5.5 nmol/mg/h (PCN + KTC). Between 1.5 and 3 h, the rate of R123 accumulation decreased to 1.1 nmol/mg/h (control), 0.75 nmol/mg/h (PCN + KTC), and 1.2 nmol/mg/h (PCN). Based on measurements at 1.5 and 3 h, vehicle control and PCN + KTC-treated fish accumulated nearly identical levels of R123 in the liver, while mean hepatic R123 accumulation in PCN-treated fish was lower than both of these groups. Statistically significant differences in R123 accumulation are observed at 1.5 h, where

PCN-treated fish accumulated, on average, 26.9 ± 8.3% less R123 than the vehicle-only control group (p = 0.0038), and 31.8 ± 7.4% less R123 than the PCN + KTC group (p = 0.0006). Maximum R123 accumulation in all treatment groups occurred at 3 h of exposure, where PCN-treated fish accumulated, on average, 14.9 ± 6.7% less R123 than the vehicle-only control group. However, this difference was not determined to be statistically significant (p = 0.0503). In contrast, PCN-treated fish accumulated, on average, 17.0 ± 6.6% (SE) less R123 relative to the PCN + KTC-treated fish at 3 h (p = 0.0303). Refer to **Appendix F** for statistical diagnostics and summary statistics.

Figure 3.5: Effect of drug treatment on hepatic R123 uptake

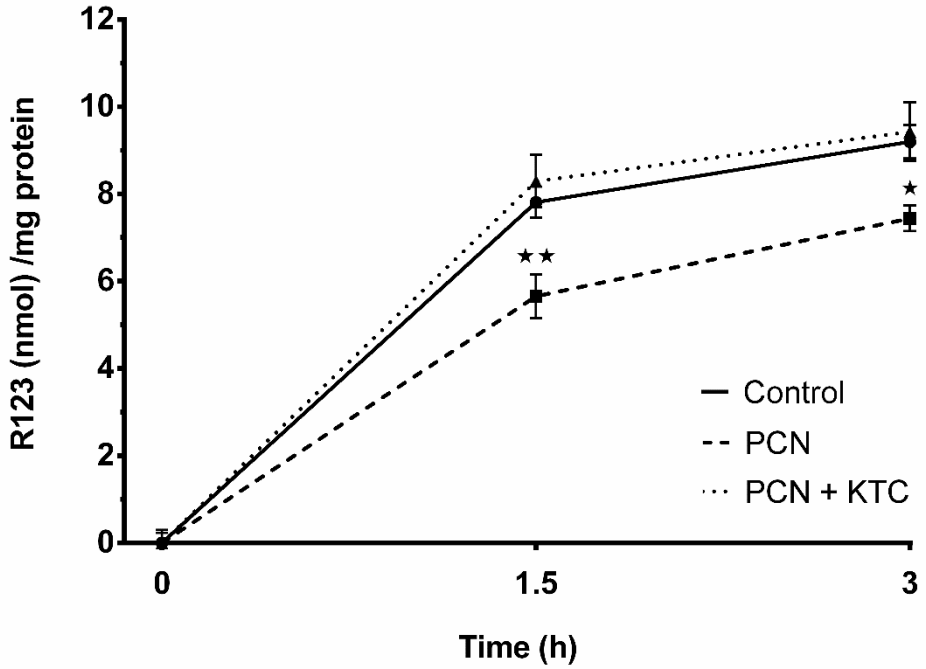

Hepatic R123 uptake in zebrafish during a water exposure of 5 µM R123 for 3 h. Error bars are one standard error (SE) about the mean. For each treatment group, mean R123 concentrations were normalized to background fluorescence measured from the livers of fish unexposed to R123 (0 h). Differences in means were analyzed by a two-way ANOVA followed by Tukey's HSD multiple comparison test. Means significantly different from vehicle control and PCN + KTC are denoted by ** (p < 0.01) and means significantly different from PCN + KTC only are denoted by * (p < 0.05).

Area under curve (AUC) analysis of hepatic R123 uptake

R123 accumulation in vehicle control fish had an AUC of 18.6 ± 0.5 (mean ± SD), while PCN and PCN and KTC-treated fish had AUCs of 14.7 ± 0.8 and 19.5 ± 1.2,

respectively. The AUC of the PCN-treated fish differed significantly from the AUC of the vehicle control (Z_{obs} = 3.36) and the PCN + KTC fish (Z_{obs} = 3.36). No statistically significant differences were seen between AUC values from the vehicle control and the PCN and KTC-treated fish (Z_{obs} = 0.68). AUC summary statistics and the 95% confidence intervals (C.I.) for the AUC contrasts appear in tables 1 and 2, and figure 6. The procedure for calculating the AUCs, AUC contrasts, and 95% C.I.'s is explained in **Appendix J**.

Table 3.3: Summary of AUC estimates: Rhodamine 123 uptake assay

Drug treatment	Mean AUC (R123 uptake time)	s^2 (AUC)
Control	18.6	0.5
PCN	14.7	0.8
PCN + KTC	19.5	1.2

Summary statistics for the area under curve (AUC) calculations of each experimental group in the R123 uptake assay

Table 3.4: Summary of AUC contrasts and statistical analyses

Contrast	Mean contrast (AUC_1 - AUC_2)	$\|Z_{obs}\|$	Bonferroni's Z_{crit} (α = 0.05)	$\|Z_{obs}\| > Z_{crit}$?	95% C.I.
Control vs. PCN	3.9	3.36	2.394	Yes	[6.73, 1.12]
Control vs. PCN + KTC	-0.9	0.68	2.394	No	[2.3, -4.1]
PCN vs. PCN + KTC	-4.8	3.36	2.394	Yes	[-4.1, -8.3]

Summary statistics of the AUC contrasts between each experimental group in the R123 accumulation assay. $|Z_{obs}|$ is the observed Z value of an AUC contrast; Z_{crit} is the critical Z value of the two-tailed hypothesis test. Differences in AUCs were considered statistically significant if the absolute value of Z_{obs} was greater than a Bonferroni-adjusted Z_{crit} (to account for the family-wise error rate of multiple comparisons). The 95% C.I. is the confidence interval of the AUC contrast.

Figure 3.6: Differences between mean AUCs of R123 uptake assay

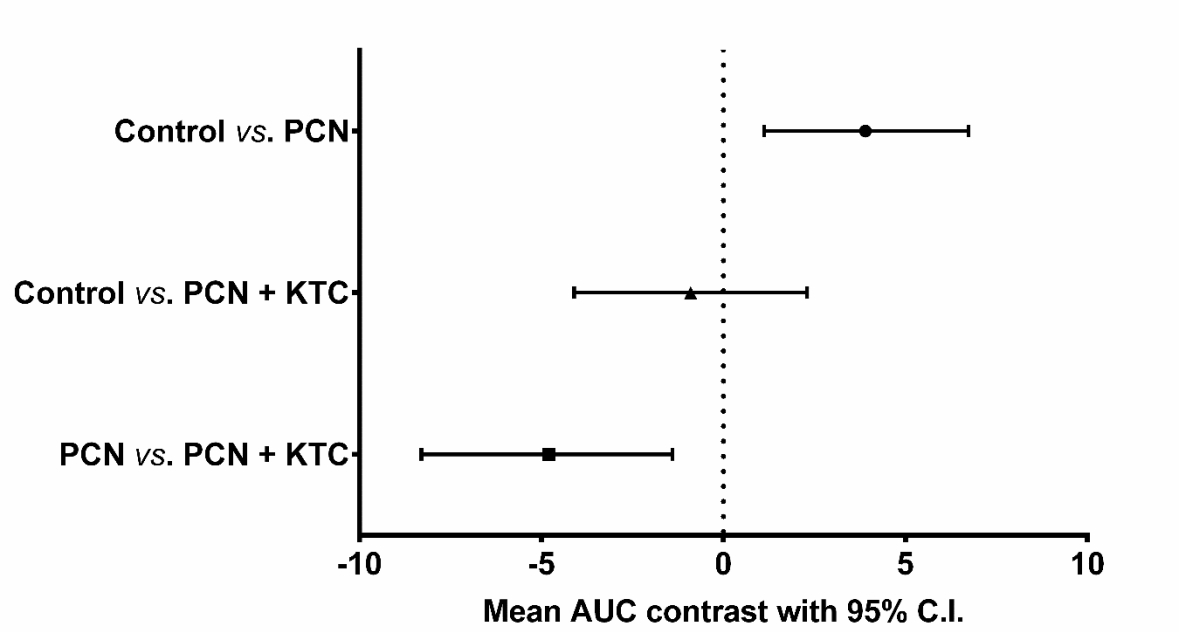

Contrasts of mean AUCs between each experimental group of the R123 uptake assay. Error bars represent the 95% confidence intervals (error bars). An AUC contrast (e.g., "Control *vs.* PCN") is the mean difference between the AUCs of two treatment groups (see Appendix J). Intervals that do not cross x = 0 belong to contrasts which are significantly different (α = 0.05).

3.4. Effect of drug treatment on liver gene expression

To observe the effects of PCN as well as PCN + KTC on gene expression, RT-qPCR was used to quantify hepatic *abcb4*, *cyp3a65*, *nr1i2*, and *cyp3c1* mRNA levels after 48 h of exposure. For *abcb4*, the Wilcoxon Rank Sums test indicated significant differences in *abcb4* mRNA levels between experimental groups, X^2 (2, N = 33) = 6.301, p = 0.0428. Relative to vehicle control, mean hepatic *abcb4* mRNA was reduced by 39% in PCN-treated fish. Similarly, PCN + KTC-treated fish showed that mean *abcb4* mRNA was reduced by 29% relative to the vehicle control, although mean mRNA levels did not significantly differ (Figure 7). For *cyp3a65*, one-way ANOVA indicated significant differences in *cyp3a65* mRNA levels between experimental groups F (2, 33) = 4.641, p = 0.0173. Consistent with *abcb4* expression, *cyp3a65* mRNA was reduced by 68% in PCN-treated fish relative to the vehicle control. Similarly, PCN and KTC-treated fish showed that *cyp3a65* mRNA was reduced by 32% relative to the vehicle control, although this difference was not statistically significant. The gene coding for PXR (*nr1i2*) did not show

any changes in transcript abundance, as the Wilcoxon Rank Sums test indicated no significant differences in mean mRNA between experimental groups, X^2 (2, N = 35) = 0.924, p = 0.6300. Similarly, *cyp3c1* mRNA was not found to be significantly altered in any experimental group by one-way ANOVA, F (2, 33) = 2.134, p = 0.1354. High Cqs and loss of linearity in the standard curve made the relative quantification of *abcb5* mRNA a significant challenge (Figure 1, **Appendix O**). In addition, qPCR melting curves for *abcb5* routinely showed substantial primer-dimer formation (Figure 1, **Appendix P**). Numerous attempts with various primer pair sequences and reaction conditions (e.g., varying primer concentrations) generated no improvement in the qPCR results. For these reasons, no analysis for *abcb5* was achieved in this study.

Figure 3.7: Effect of drug treatment on hepatic gene expression

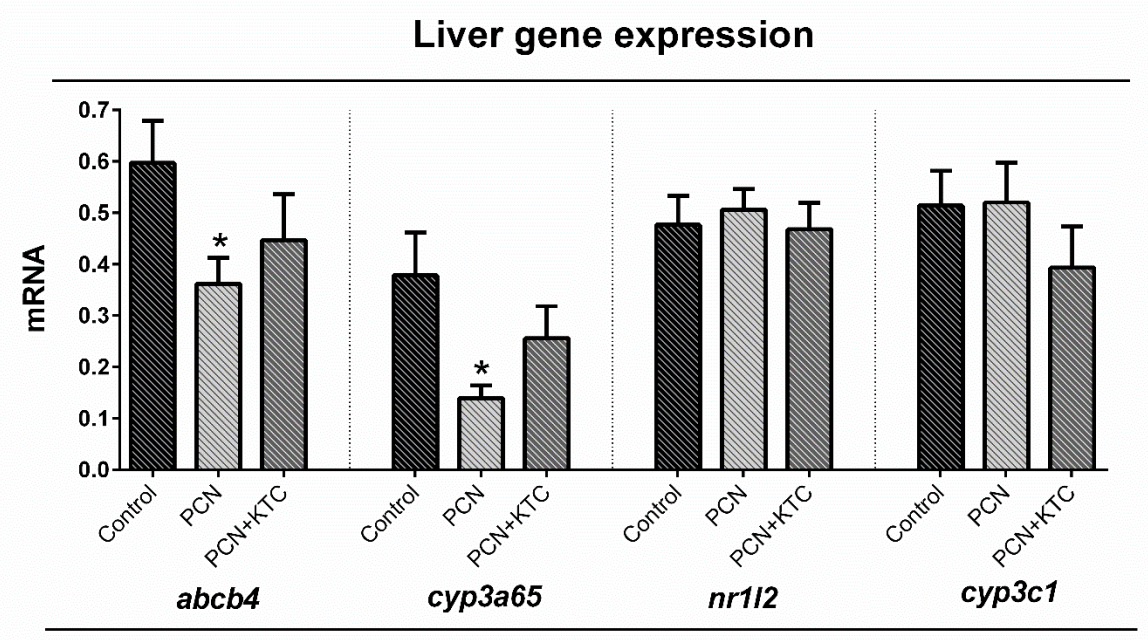

Hepatic gene expression of *abcb4*, *cyp3a65*, *nr1i2 (pxr)*, and *cyp3c1* presented as mean mRNA level (in arbitrary units). Means significantly different from the control group are denoted with * ($p < 0.05$).

4. Discussion

Fish species have cellular defenses that are comparable to the multidrug/multixenobiotic resistance (MDR/MXR) mechanism in mammals and other vertebrates. Similarities between vertebrate species include the coordinated induction and action of ABC-transporters such as P-glycoprotein (P-gp), as well as phase I and phase II biotransformation enzymes to reduce the potential cytotoxic effects of xenobiotics. However, little is known regarding the levels, performance, and regulation of these cellular defense mechanisms in response to xenobiotic exposure. To further characterize the MDR/MXR mechanism in the model teleost, zebrafish (*Danio rerio*), hepatic P-gp activity and gene expression was investigated following exposure to the PXR agonist, pregnenolone 16α-carbonitrile (PCN), as well as following co-exposure to PCN and the PXR antagonist, ketoconazole (KTC) *in vivo*.

4.1. The use of zebrafish to study hepatic rhodamine 123 kinetics *in vivo*

Zebrafish have emerged to play a prominent role in pharmacological and toxicological investigations; therefore, it is critical to characterize underlying regulatory mechanisms involved with the response to xenobiotic challenges in this species. Little to no information exists regarding MDR/MXR processes in whole zebrafish liver despite its importance as a major site of xenobiotic transformation, detoxification, and clearance. Due to their relatively low cytotoxicity, the fluorescent P-gp substrate, rhodamine 123 (R123), and other rhodamine dyes (e.g., rhodamines B, 6G, and 110) have been used extensively to study MDR and ABC-transporter activity in various animal cell lines (Chaudhary and Roninson, 1991; Lee et al, 1994; Doyle et al, 1998; Forster et al 2012). Furthermore, several mammalian studies have used intravenous injections of rhodamines to investigate P-gp activity *in vivo* (Liu et al, 2006; Jin et al 2012). However, there have been only two studies to date using rhodamine dyes in live fish models (Damare, 2009; Fischer et al 2014).

To my knowledge, this is the first study to use an *in vivo* R123 assay to investigate MDR/MXR functional activity in zebrafish liver. Therefore, it was necessary to describe the relationship between R123 exposure and hepatic R123 accumulation to confirm that fish accumulate R123 in a predictable, exposure-dependent manner (i.e., , increased R123 exposure results in increased hepatic R123 accumulation). Furthermore, these data help establish an exposure of R123 that is high enough to produce a detectable fluorescent signal in liver homogenates. The concentration and time-dependent increases of hepatic R123 observed in zebrafish indicate that 5 µM R123 for 2 h is an optimal exposure for loading R123 in the liver as lower exposures failed to produce R123 fluorescence significantly higher than background levels in non-R123-exposed fish (Figures 1 and 2, Results). In addition, R123 exposures higher than 5 µM for 2 h produced no further increases in liver R123 levels. This concentration and time-dependent accumulation (and subsequent plateau) of R123 concentrations in fish liver appears consistent with nonlinear R123 kinetics observed in cell models from various species, including fish (Forster, 2012; Hirsch-Ernst et al, 2001). An *in vitro* assay using rainbow trout epidermal cells showed that R123 accumulation during an exposure to 5 µM R123 reached saturation after 2 h (Shuilleabhain et al, 2005). Likewise, intracellular R123 accumulation was shown to increase in a dose-dependent manner in trout hepatocytes, with intracellular R123 saturation occurring between approximately 1.5 and 2 h (Bains and Kennedy, 2004). While R123 is not a substrate for CYP3A (Yumoto et al, 2001), the metabolism of R123 into the deacylated R110 metabolite by hepatic esterases (which results in a weaker fluorescence signal) is a possible reason for hepatic R123 reaching a plateau at higher exposures (Forster, 2012). Altered transport activity at high intracellular R123 concentrations may also contribute to limiting the accumulation of R123.

Importantly, the above *in vitro* models do not completely reproduce the physiological conditions that exist in whole fish and may display different R123 pharmacokinetics relative to observations *in vivo*. For example, the accumulation of unbound R123 in the liver is influenced by its bioavailability, the interaction of R123 with blood components, as well as physiological and genetic factors which contribute to inter-individual variability in the rate of hepatic R123 metabolism and transport across membranes (Ando et al, 2001; Forster et al, 2012; Pelkonen and Turpeinen, 2007). Despite differences in pharmacokinetic parameters between cell and whole fish models,

the liver R123 kinetics observed in this study are consistent with data resulting from comparable R123 exposures on both mammalian and teleost primary hepatocyte cultures (Hirsch-Ernst et al, 2001; Bains and Kennedy, 2005). Thus, the optimal R123 exposure of 5 µM for 2 h experimentally determined herein is further supported by *in vitro* data as a suitable exposure to load R123 in whole zebrafish liver.

As previously reported, R123 is a relatively nontoxic tracer dye widely used in numerous cell-based assays. While there is a lack of robust R123 toxicity data in the literature for live fish or fish cell lines, exposure concentrations of 5 - 10 µM R123 have been used for *in vitro* fish studies with no reported cytotoxicity following 2 – 4 h of exposure. Using membrane permeability as an indicator of cell viability, these studies evaluated R123 cytotoxicity with the trypan blue exclusion assay and extracellular lactate dehydrogenase (LDH) activity (Bains and Kennedy, 2005; Gourley and Kennedy 2009). It is well known that R123 can accumulate in the mitochondria of living cells, and may inhibit oxidative phosphorylation at high doses (Johnson et al, 1980; Lampidis et al, 1984). A previous study using rainbow trout hepatocytes demonstrated that cells exposed to 5 and 10 µM R123 increased respiration rates by up to 26% relative to baseline activity (Bains and Kennedy, 2005). However, mitochondrial oxygen consumption was unaffected by R123 at all concentrations tested (0, 1, 5, and 10 µM), suggesting R123 does not significantly impair mitochondrial function at these concentrations.

Overt symptoms indicative of stress in whole fish, such as increased opercular movement, gasping for air at the surface, loss of equilibrium, or dispigmentation (Bhavani and Karuppasamy, 2014), were not observed in zebrafish at any point during all R123 exposures tested in the current study. While the absence of behavioural responses to R123 exposure does not in itself imply a lack of physiologically-relevant effects, the lack of stress behaviour displayed by zebrafish during R123 loading is consistent with data indicating R123 is a relatively nontoxic fluorescent tracer dye. Based on the results of the *in vivo* R123 exposures, a loading exposure of 5 µM for 2 to 4 h satisfies the criteria of producing a measurable quantity of R123 in the liver while not causing overt symptoms of toxicity in fish. However, more investigation into the *in vivo* pharmacokinetics and physiological effects associated with R123 exposure is warranted to further develop *in vivo* R123 assays involving aquatic organisms such as zebrafish.

While R123 is a well-established substrate and marker for P-gp activity, it is also potentially transported to a lesser extent by members of the ABCC (MRP) subfamily of ABC-transporters implicated in the MDR/MXR mechanism (Twentyman et al, 1994; Long et al, 2011). The P-gp-mediated transport of R123 has been extensively used to study MDR/MXR activity in numerous *in vitro* vertebrate models, but reports on the degree of R123 efflux contributed by MRP transporters are limited. Feller et al (1995) observed that cell lines underexpressing P-gp which possess the MRP-mediated MDR phenotype failed to alter R123 clearance following chemical inhibition of MRP activity. In a different study, there was no observed correlation between MRP1 expression and R123 transport kinetics in MRP-mediated MDR cell lines separately treated to three known MRP1 inhibitors. The authors of this study concluded that R123 is not a suitable tracer dye for investigating MRP-mediated drug transport (Dogan et al, 2004). Interestingly, the ABCG2 (BCRP) transporter does not show R123 transport activity, but human carcinoma cell lines with acquired mutations at amino acid residue 482 of BCRP have shown marked R123 efflux activity relative to parental ('wild type') cell lines, suggesting a crucial role of this residue in facilitating substrate specificity (Honjo et al, 2001). Despite the apparent specificity of R123 for P-gp, future assays aiming to investigate the functional role of candidate MDR/MXR-associated zebrafish P-gps (e.g., Abcb4 and Abcb5) would benefit from targeted *in vivo* knock-down approaches to accurately describe the functional activity of specific ABC-transporters.

The PCN-mediated decreases in hepatic R123 accumulation observed in this study are considered more likely the result of altered P-gp functional activity rather than changes to MRP-mediated clearance, as genes encoding P-gp and ABCC1 (MRP1) appear to be under the transcriptional control of separate regulatory mechanisms which are differentially responsive to PCN (Cho et al, 2011; Lee and Piquette-Miller, 2001; Martin et al, 2008 and 2010). While unreported in fish models, PCN has been shown to have no effect on *ABCC1* (*MRP1*) gene expression in the human HepG2 and Caco-2 cell lines (Martin et al 2008), as well as in rat intestinal cells and primary hepatocytes (Martin et al, 2010). In adult zebrafish, *abcc1* mRNA was observed to be only weakly expressed in the liver relative to various tissues such as the testes, ovaries, and eyes, raising some doubt in its contribution to MDR/MXR activity in the liver (Long et al, 2010). Nevertheless, the

potential role of other ABC transporters in R123 efflux should be considered when interpreting the results of R123-based assays for P-gp activity.

4.2. Effect of PCN and KTC on P-glycoprotein functional activity

P-gp functions as a barrier against the cellular accumulation of xenobiotics by mediating the efflux of substrates out of the cell. To investigate if the functional activity of P-gp is altered following exposure to PXR modulators in zebrafish, the hepatic clearance and uptake of the fluorescent P-gp substrate, rhodamine 123 (R123), were compared in fish following treatment with PCN, PCN + KTC, or a vehicle control. Previous studies have provided strong evidence that R123 is a substrate for P-gp in fish species, including trout and zebrafish. These reports investigated MDR/MXR functional activity using P-gp substrates (e.g., verapamil and vinblastine) to competitively inhibit the P-gp-mediated transport of R123 (Sturm, Cravedi et al, 2001), or by altering P-gp expression *in vivo* by sterically blocking translation of zebrafish P-gp mRNAs encoded by *abcb5* and *abcb4* (using morpholino antisense oligonucleotides to knockdown specific transcripts) (Fischer et al, 2013).

To my knowledge, the work presented herein is the first study to use R123 as a probe to investigate the effects of PCN and KTC on the regulation of P-gp functional activity in fish. Based on the results of the R123 clearance assay, PCN appears to have a measurable stimulatory effect on R123 clearance in zebrafish. Fish treated with PCN showed significantly reduced levels of hepatic R123 relative to control fish, which may be due to increased P-gp activity mediating a 'protective' mechanism against R123 accumulation in the liver. While R123 is not metabolized by the PCN-inducible CYP3A enzyme in mammalian systems (Yutomo et al, 2001), the potential for PCN to modulate the expression and activity of enzymes capable of metabolizing R123 is not well characterized. Thus, the observed effects of PCN on R123 clearance may be the result of a combined PCN-induced change in P-gp and R123-metabolizing enzyme activity in zebrafish liver. PCN did not significantly effect R123 clearance at each time point of the clearance assay, bringing into question the efficacy of the PCN exposure used to elicit a physiologically-relevant and predictable change of R123 clearance in the liver. This

uncertainty is related to the high inter-individual variability of hepatic R123 levels observed in the clearance assay. Sources of this variability may include inter-individual differences in biological parameters, such as genetics, sex, and fish health (i.e., stress, organ dysfunction, energy stores, etc.) which may affect the pharmacokinetics of drugs and other xenobiotics (Boucher et al, 2006; Gourley and Kennedy, 2008; Waxman et al, 2009).

Due to the high variability of hepatic R123 concentrations in all treatment groups, the results of the R123 clearance assay failed to provide evidence for antagonistic effects of KTC on the potential induction of MDR/MXR activity by PCN. This variability also limited the statistical power of the 'area under the curve' (AUC) analysis to detect significant effects of drug treatment on R123 clearance. Nevertheless, observations that PCN alone caused a significant reduction of hepatic R123 concentrations at 2 of the 6 time points (2 and 4 h) support the possibility that PCN may be interacting with a mechanism at the molecular level that regulates P-gp activity in zebrafish, even if this response wasn't detected as a change in overall R123 exposure using AUC analyses.

Because P-gp is known to limit the accumulation of R123 in cells through its activity as an efflux pump, studies using R123 as a tracer dye often investigate P-gp functional activity through measuring cellular R123 clearance following a pre-loading period, and/or measuring cellular R123 uptake (influx) during R123 loading. In addition to studying zebrafish MDR/MXR activity using an R123 clearance assay, this study also investigated the effects of PCN and the co-treatment of PCN + KTC on R123 accumulation during a water exposure to R123. Two features of the R123 clearance assay results prompted this additional investigation of MDR/MXR functional activity. First, PCN-treated fish in the clearance assay displayed hepatic R123 concentrations 52 – 58 % lower than control fish between 0 and 4 h (during which mean hepatic R123 concentrations rose in both groups). Although reduced R123 accumulation in PCN-treated fish was not determined to be statistically different from control fish until 2 and 4 h, it is possible zebrafish treated to PCN initially accumulated less R123 due to elevated P-gp functional activity during the R123 water exposure. Indeed, observations that cellular R123 accumulation is inversely proportional to P-gp activity have been reported in various cell lines (Davey et al, 1996; Colabufo et al, 2008; Forster et al, 2012). For example, trout hepatocytes treated with the P-gp inhibitors verapamil and cyclosporin A showed increased cellular accumulation of R123 relative to control (Sturm, Zeimann et al, 2001). In a multidrug-resistant mouse

tumour cell line overexpressing P-gp, R123 accumulation was shown to be significantly reduced relative to the non-resistant parental cell line (Twentyman et al, 1994).

The second feature of the R123 clearance assay prompting further investigation into the effects of PCN and the co-treatment of PCN + KTC on MDR/MXR activity was the high inter-individual variability of hepatic R123 concentrations observed in all treatment groups. To improve on the variability observed in the R123 clearance assay, the sample size at each time point of the R123 uptake (influx) assay was increased by up to two-fold (see Materials and Methods). This adjustment in sample size increased the precision of the statistical analysis of R123 accumulation across experimental treatments. In the R123 uptake assay, significantly decreased hepatic R123 concentrations were observed in fish treated with PCN relative to control and PCN + KTC-treated fish. These observations suggest that PCN can stimulate P-gp functional activity in zebrafish and that KTC antagonizes the effect of PCN. This apparent induction of MDR/MXR functional activity in zebrafish is consistent with the stimulatory effects of PCN on P-gp activity in mammals, suggesting overlapping regulatory MDR/MXR mechanisms between zebrafish and other vertebrate species (LeCluyse, 2001; Martin et al, 2010).

The observed antagonism of KTC on PCN-induced R123 clearance in zebrafish is consistent with KTC's known inhibitory interaction with PXR and the subsequent attenuation of P-gp activity in mammalian cell lines (Ward et al, 2004; Huang et al, 2007). KTC antagonizes the ligand-mediated activation of PXR through non-competitive binding to the activation function 2 (AF-2) domain of PXR, which disrupts the interaction of PXR with the co-activator SRC-1 (Li et al, 2013). The antagonism of KTC on the PCN-mediated activation of murine PXR has also been reported *in vivo* (Huang et al, 2007), although this inhibitory mechanism of KTC has not yet been demonstrated in fish. Elevated accumulation of R123 in the livers of zebrafish treated to PCN + KTC (relative to fish treated to PCN alone) suggests zebrafish respond to MDR/MXR modulators in a similar way to mammalian systems; however, further investigation is warranted to characterize the interactions of PCN and KTC with zebrafish Pxr.

Interpreting the observed antagonism of KTC on PCN-induced R123 clearance is complicated by the known ability of KTC to inhibit P-gp and CYP3A activity in mammals (Takano et al, 1998; Zhang et al, 1998). Indeed, the inhibitory effects of KTC on

MDR/MXR activity have been used in the clinical setting to increase drug absorption of P-gp substrates such as cyclosporine A (Odocha et al, 1996). While KTC is known to bind with CYP3A and inhibit its catalytic activity, whether this interaction is competitive or non-competitive is not well understood (Greenblatt et al, 2011). The inhibitory effects of KTC on MDR/MXR have been observed in fish species, as reduced Cyp3a activity was demonstrated in trout and killifish treated to KTC (Hegelund et al, 2004). Similarly, KTC decreased Cyp3a and Cyp1a catalytic activity in juvenile rainbow trout, and increased the sensitivity of fish to exposure of 17 beta-estradiol (Hasselberg et al, 2008). Although the mechanism by which KTC inhibits P-gp is unclear, numerous reports have shown reduced clearance of P-gp substrates with co-administration of KTC (Yumoto et al, 1999; Wang et al, 2002; Fan and Rodriguez, 2008). One study reported the inhibitory effect of KTC *in vivo*, showing reduced R123 clearance from the liver of rats co-treated with KTC (Kageyama et al, 2005). Paradoxically, efflux of the radio-labeled P-gp substrates [^{3}H]vinblastine and [^{3}H]digoxin from MDCK-MDR1 cells (which express P-gp but no other ABC-transporter) was stimulated by KTC, but an inhibitory effect on P-gp-mediated transport was observed at higher concentrations of KTC (Taub et al, 2005). The above reported effects of KTC introduce confounding factors for interpreting the reduced hepatic R123 clearance in PCN + KTC-treated fish.

Similar to the R123 clearance assay, the mean AUC was estimated for each experimental group to represent the total hepatic exposure to R123 over the time course of the accumulation assay (0 - 3 h). The effect of the PCN treatment on P-gp functional activity in zebrafish resulted in a mean AUC significantly lower than both control and PCN + KTC-treated fish, with a 24% and 28% reduction in hepatic exposure to R123, respectively. Importantly, there was no significant difference in AUCs between control and PCN + KTC-treated fish, which reflects the potential of KTC to inhibit the effect of PCN on R123 kinetics in zebrafish. The observed response to PCN alone represents an increased barrier to R123 accumulation characteristic of the classic MDR/MXR mechanism, and adds supporting evidence that PCN can stimulate P-gp functional activity in zebrafish. Furthermore, the significantly lower AUC seen in PCN-treated fish suggests that the MDR/MXR response in zebrafish may be capable of altering P-gp substrate kinetics to physiologically relevant levels in fish. The physiological consequences of conferring protection against cytotoxic chemicals via increased MDR/MXR activity were not

specifically investigated in this study, but likely include the allocation of critical cellular resources in order to sustain the ATP-dependent functional activity of P-gp in the MDR/MXR response. Further work is required to investigate the physiological cost of sustaining MDR/MXR activity in fish.

As evidenced in the R123 clearance and uptake assays, a potential increase of P-gp activity following PCN treatment is consistent with an MDR/MXR mechanism in zebrafish that is regulated, at least in part, by the nuclear receptor, Pxr. PCN is an established PXR agonist in several species, including mice and rat, and has been shown to induce P-gp activity via the PXR pathway (Gu et al, 2013). The existence of a PXR-regulated MDR/MXR system in zebrafish has been indirectly supported by observations that PCN and the established mammalian PXR agonist clotrimazole can activate full-length zebrafish Pxr *in vitro* (Bainy et al, 2013). Furthermore, PCN was shown to induce zebrafish P-gp (*abcb5*) gene expression *in vivo* (Bresolin et al, 2005). This study provides further evidence that zebrafish P-gp functional activity may be regulated by a Pxr pathway through observations that KTC, a known PXR antagonist in mammals, can inhibit the stimulatory effects of PCN and the clearance of R123 *in vivo*.

While the response of altered R123 kinetics in zebrafish treated to PCN and PCN + KTC is consistent with a Pxr-regulated MDR/MXR mechanism in zebrafish, caution is warranted when drawing upon potential molecular mechanisms to interpret observations at higher levels of biological organization, such as whole tissues and organs. Although useful for describing P-gp activity in the liver, R123 assays fail to directly characterize the role of multiple layers of regulation at the subcellular level, including transcriptional, post-transcriptional, and post-translational mechanisms that could ultimately affect the functional activity of P-gp in response to drug treatment. Furthermore, it is possible that multiple pathways (in lieu of, or in addition to, Pxr) are involved with P-gp induction in zebrafish, as vertebrate nuclear receptor families have shown a considerable degree of overlap in ligand specificity and transcriptional activity (Pascussi et al, 2008). Despite these confounding variables, the investigation of specific transcriptional responses to PCN and KTC may help shed light into the molecular processes involved with the MDR/MXR response in zebrafish.

4.3. Effect of PCN and KTC on gene expression

The MDR/MXR mechanism in mammals is under the transcriptional regulation of the nuclear receptor, PXR. The PXR pathway responds to the intracellular accumulation of various cytotoxic ligands, including endogenous cellular waste products, and exogenous chemicals such as drugs and anthropogenic pollutants. Upon ligand–mediated activation of PXR, the MDR/MXR response is initiated by the transcription of PXR target genes, notably *ABCB1* (*MDR1*) and *CYP3A*, which code for P-gp and the phase I metabolizing enzyme, CYP3A (Masuyama et al, 2005). Although the precise mechanisms involved with regulating the MDR/MXR-response have yet to be characterized in fish species, emerging evidence suggests fish may possess a PXR pathway that is functionally homologous to the mammalian MDR/MXR mechanism (Bresolin et al, 2005; Wassmur et al, 2010). To help characterize the MDR/MXR mechanism in zebrafish, the expression of candidate MDR/MXR-associated genes (*abcb4*, *cyp3a65*, *cyp3c1*, and *nr1i2* (*pxr*)) was investigated in zebrafish liver following treatment to the PXR agonist PCN, and co-treatment with PCN and the PXR antagonist, KTC.

Zebrafish *abcb4* is a P-gp-like gene encoding a xenobiotic transporter involved with the MDR/MXR response in embryos (Fischer et al, 2013). Expression of this gene has not previously been verified in adult tissues, including the liver. Furthermore, hepatic *abcb4* gene expression has not been specifically investigated in terms of its transcriptional response to PXR modulators. In the current study, it was shown that *abcb4* mRNA levels are significantly modulated in adult zebrafish liver 48 h following treatment to PCN but not in zebrafish co-treated with PCN + KTC. The altered expression of hepatic *abcb4* mRNA following exposure to PCN is presented as a decrease in steady-state mRNA relative to control. Interestingly, similar gene expression patterns were observed with *abcb4* and *cyp3a65* mRNA levels in zebrafish liver. Because exposure to PXR agonists typically results in the induction of MDR/MXR-associated target genes in mammals, the decrease in *abcb4* and *cyp3a65* mRNA levels is a surprising response to PCN treatment in zebrafish. It is unclear why these genes were down-regulated following treatment to PCN in this study; however, the simultaneous modulation of *abcb4* and *cyp3a65* mRNA is consistent with a shared regulatory mechanism consistent with the PXR pathway in mammals.

Transcriptional responses commonly involve an initial gene induction followed by significant down-regulation to below basal levels (Wee et al, 2012; Lahav et al, 2004). It is worth noting that a PXR-mediated negative feedback loop has been identified which attenuates the expression of CYP3A in response to high levels of PCN *in vitro* (Bailey et al, 2011). Supporting the 'negative feedback' hypothesis, PCN has shown antagonistc effects on the activation of the glucocorticoid receptor (GR), which transcriptionally regulates PXR gene expression and indirectly influences the expression of PXR target genes such as CYP3A (Huss et al, 2000; Hosoe et al, 2005). It is conceivable that mechanisms have evolved to prevent hyper-stimulation of the Pxr pathway, which is implicated in bile salt and steroid homeostasis in addition to MDR/MXR (Jones et al, 2000; Ekins et al, 2008). Such negative transcriptional regulation of the Pxr pathway may result in below basal gene expression in fish exposed to Pxr agonists, which is consistent with the reduced *abcb4* and *cyp3a65* mRNA levels observed in fish treated with PCN (shown herein).

Similar to the unexpected decreases of *cyp3a65* mRNA levels observed in PCN-treated zebrafish in this study, decreased levels of *cyp3a* mRNA were observed in rainbow trout treated with the endogenous PXR agonist lithocholic acid (Wassmur et al, 2010). In one study, zebrafish embryos treated to 10 µM of the PXR agonist and the synthetic glucocorticoid, dexamethasone (DEX), showed induction of *cyp3a65* in the foregut while treatment with 100 µM DEX resulted in below-basal levels of *cyp3a65* mRNA in the same tissue (Tseng et al, 2005). Zebrafish exposed to crude microcystins (cyanobacterial toxins) which are substrates for P-gp (Contardo-Jara et al, 2008), showed below-basal *cyp3a65* and *nr1i2* (*pxr*) mRNA levels at low microcystin doses, while increased mRNA levels were reported at the highest microcystin exposure (Li et al, 2013). Similar discordant expression patterns were observed with P-gp mRNA levels in the gills and brain of one-sided livebearer (*Jenynsia multidentata*) treated to microcystins (Ame et al, 2009). While these studies did not directly investigate Pxr transcriptional activity, they demonstrate that the regulation of MDR/MXR-associated genes in fish species involve dynamic processes that result in fluctuations of steady state mRNA above or below basal levels. In order to better capture the transcriptional responses associated with the MDR/MXR mechanism, future experiments should include multiple time points and exposures.

Unlike *abcb4* and *cyp3a65* gene expression, *nr1i2* (*pxr*) and *cyp3c1* mRNA levels remained unchanged 48 h following treatment to PCN or PCN + KTC. This is in contrast to a previous study which used semi-quantitative PCR to show that *nr1i2* (*pxr*), *cyp3c1*, and *abcb5* mRNA was up-regulated in adult zebrafish liver 48 h following i.p. treatment with PCN (Bresolin et al, 2005). It is unclear why different transcriptional responses were observed for both *nr1i2* (*pxr*) and *cyp3c1* under similar conditions to this current study, although these contrasting observations may reflect the dynamic nature of PXR transcriptional activity. For example, Corley-Smith et al (2006) showed that zebrafish treated to the PXR agonist, dexamethasone (DEX), up-regulated *cyp3a65* but not *cyp3c1* mRNA *in vivo*. This pattern is consistent with the results presented herein, as *cyp3a65* mRNA levels were modulated during exposure to PCN, while *cyp3c1* mRNA levels remained at basal levels. Thus, while emerging evidence suggests the genes coding for *cyp3a65* and *cyp3c1* may be regulated by separate or overlapping pathways, further work is required to elucidate the precise mechanisms by which these genes are transcriptionally controlled.

Species differences in the modulation of PXR/Pxr are associated with variations in the ligand binding domain (LBD), which is known to bind numerous structurally unrelated ligands in mammals (Jones et al, 2000). PCN is a classic and potent activator of PXR in rodents, but its agonistic effect is relatively modest on human PXR (El-Sankary et al, 2001). Similarly, PCN and other mammalian PXR ligands are thought to induce fish Cyp3a, suggesting a possible role for Pxr in the regulation of the MDR/MXR response in fish species. For example, PCN has been shown to produce a 2-fold induction of *cyp3a27* in trout hepatocytes (Wassmur et al, 2010). Similar effects of PCN on Cyp3a induction have been observed in juvenile tilapia and rainbow trout *in vivo* (Celander et al, 1989; Pathiratne and George, 1996). Recently, PCN was shown to activate full-length zebrafish Pxr in COS-7 cells co-transfected with a Pxr-responsive reporter gene (Bainy et al, 2013). Thus, the modulating effects of PCN on zebrafish *cyp3a65* mRNA levels observed in this study are consistent with previous work that suggests Pxr could be a key regulator of *cyp3a* transcription in fish. In addition, the well-established co-regulation of *ABCB1* (*MDR1*) and *CYP3A* transcription by mammalian PXR is consistent with the PCN-mediated co-modulation of zebrafish P-gp (*abcb4*) and *cyp3a65* mRNA levels observed in this study, further supporting a role for Pxr in regulating the MDR/MXR response in fish.

Importantly, this is the first report of the modulation of zebrafish *abcb4* in response to a known PXR agonist.

Due to the clinical significance of PXR-mediated drug resistance in anti-cancer therapy, PXR has received much attention as a target for chemical inhibition. While the antagonistic effects of some azole antimycotics on the ligand-mediated activation of PXR are well known in mammals, these effects are less characterized in fish species (Eakins et al, 2007; Wang et al, 2007; Svecova et al, 2008). Ketoconazole (KTC), a potent inhibitor of CYP3A activity in various species, is also considered a prototypical PXR antagonist (Kageyama et al, 2005; Huang et al, 2007; Wang et al, 2007). In the presence of PXR agonists, KTC blocks the ligand-mediated activation of PXR and represses the transcription of MDR/MXR-associated genes such as *CYP3A* and *ABCB1* (*MDR1*) (Wang et al, 2007). The antagonistic interaction of KTC with PXR may explain, at least in part, the well-known inhibitory effects of KTC on P-gp-mediated transport activity (Fan and Rodrigues, 2008). The results reported in this current study show a similar antagonistic effect of KTC in zebrafish, as co-treatment of KTC and the PXR agonist, PCN, attenuates the PCN-mediated modulation of *cyp3a65* and *abcb4* mRNA levels in liver. This finding is consistent with a previous study by Corcoran et al (2012), who demonstrated KTC antagonizes the rifampicin-mediated induction of the *cyp3a* gene in carp. Thus, the effects of PCN and KTC in zebrafish provide further circumstantial evidence that Pxr plays a role in the regulation of MDR/MXR-associated genes in fish, as these established PXR modulators facilitate similar effects on the well-characterized mammalian PXR-pathway.

The complexity of the MDR/MXR mechanism is related to the variety of regulatory pathways and transcriptional responses involved with cellular defense mechanisms. This area of research is confounded by observations that a considerable amount of cross-talk may be involved with regulating multiple signalling pathways and down-stream target genes associated with cellular defense, which can result in conflicting reports in the literature (Pascussi et al, 2008). Unraveling the precise mechanisms of the MDR/MXR response can be challenging in fish species, as fish-specific data in the literature, as well as options for experimental methods (e.g., MDR/MXR-relevant transgenic fish lines and fish-specific antibodies) are currently limited for these organisms. Despite these challenges, characterizing the dynamic nature of the MDR/MXR mechanism in fish can be

aided by linking molecular processes with functional activity at higher levels of organization.

The work presented in this thesis contributes to the pursuit of uncovering the underlying mechanisms involved with the MDR/MXR response in the model teleost fish, zebrafish. The observations made here point to transcriptional and functional responses in zebrafish that share overlapping features with the well-characterized MDR/MXR mechanism in mammals; however, further investigations are required to corroborate these observations and to further describe the precise molecular and physiological responses involved with cellular defense mechanisms in fish. Such efforts will provide useful contributions to the existing 'toxicological toolbox' of zebrafish and will be directly applicable to areas of clinical pharmacology and environmental protection.

5. Conclusion and future directions

The results presented in this thesis demonstrate that the *in vivo* R123 assay can be a useful tool for investigating P-gp functional activity in zebrafish. Zebrafish treated with the PXR agonist (PCN) co-modulated P-gp (*abcb4*) and *cyp3a65* mRNA expression, and this co-modulation was associated with increased hepatic MDR/MXR functional activity *in vivo*. Consistent with a mammalian-like MDR/MXR mechanism regulated by PXR, zebrafish co-treated with PCN and the mammalian PXR antagonist, ketoconazole (KTC), attenuated the PCN-mediated modulation of hepatic *abcb4* and *cyp3a* mRNA levels, as well as attenuated the PCN-mediated modulation of MDR/MXR functional activity. These results suggest Abcb4 and Cyp3a65 may be involved with the MDR/MXR response in the adult zebrafish liver, and that Pxr may regulate this dynamic process. Finally, lack of Cyp3c1 mRNA modulation by PCN suggests Cyp3c1 and Cyp3a65 may be regulated by separate transcriptional pathways

Whether Pxr is directly involved with regulating P-gp (e.g., *abcb4* and *abcb5*) and *cyp3a65* transcriptional activity in zebrafish is still an open question, and the combined molecular and functional activity data presented in this thesis provide a basis on which to frame future investigations of the MDR/MXR mechanism in fish. In addition to continuing the use of P-gp functional activity assays (e.g., R123 influx /efflux), these investigations could simultaneously quantify Cyp3a metabolic activity via the benzyloxy-4-[trifluoromethyl]-coumarin-O-debenzyloxylase (BFCOD) assay (Miller et al, 2000). The BFCOD assay could help link PXR-mediated transcriptional responses to MDR/MXR functional activity, thus provide insight into the physiological significance of modulating the Pxr pathway in fish. In addition, further molecular techniques such as chromatin immunoprecipitation sequencing (ChIP-seq) could identify genome-wide protein-DNA interactions involved with the regulation of MDR/MXR-associated genes. Such target genes could include those under the transcriptional control of zebrafish Pxr, for example. Transcriptome-wide analyses (e.g., RNA-seq) to describe broad responses in gene expression to Pxr modulators would also help provide clues to the molecular

underpinnings of the MDR/MXR mechanism in zebrafish. The above approaches could be combined with RT-qPCR techniques to investigate with high sensitivity the induction of identified Pxr target genes during exposure to known PXR/Pxr modulators. If employed, these (or similar) approaches would significantly contribute to our understanding of PXR's role in regulating the MDR/MXR response in fish.

Because the protective role of the MDR/MXR response mechanism is vulnerable to impairment by xenobiotics, a deeper understanding of the MDR/MXR mechanism would also help describe the sensitivity of fish to specific exposures of aquatic contaminants. Chemicals known as 'chemosensitizers' inhibit the MDR/MXR mechanism (resulting in reduced P-gp activity) and can increase the bioaccumulation and toxic effects of other xenobiotics at environmental levels otherwise considered safe (Kurelec, 1997). Thus, the development of molecular biomarkers capable of accurately representing the degree of MDR/MXR activity in response to chemical exposures could help predict adverse effects in fish, as well as identify known (or previously unknown) environmental chemosensitizers relevant to ecotoxicology. Such capabilities would have important implications for regulatory guidelines designed to protect aquatic habitats from harmful levels of anthropogenic contamination.

References:

Ame, M. V., et al., 2009. Effects of microcystin-LR on the expression of P-glycoprotein in Jenynsia multidentata. Chemosphere. 74**,** 1179-1186.

Ando, H., et al., 2001. Effect of endotoxin on P-glycoprotein-mediated biliary and renal excretion of rhodamine-123 in rats. Antimicrobial Agents and Chemotherapy. 45**,** 3462-3467.

Bailey, I., et al., 2011. A PXR-mediated negative feedback loop attenuates the expression of CYP3A in response to the PXR agonist pregnenalone-16 alpha-carbonitrile. Plos One. 6.

Bain, L. J., LeBlanc, G. A., 1996. Interaction of structurally diverse pesticides with the human MDR1 gene product P-glycoprotein. Toxicology and Applied Pharmacology. 141**,** 288-298.

Bains, O. S., Kennedy, C. J., 2005. Alterations in respiration rate of isolated rainbow trout hepatocytes exposed to the P-glycoprotein substrate rhodamine 123. Toxicology. 214**,** 87-98.

Bard, S. M., 2000. Multixenobiotic resistance as a cellular defense mechanism in aquatic organisms. Aquatic Toxicology. 48**,** 357-389.

Bard, S. M., et al., 2002. Expression of P-glycoprotein in killifish (Fundulus heteroclitus) exposed to environmental xenobiotics. Aquatic Toxicology. 59**,** 237-251.

Blumberg, B., Evans R.M, 1998. Orphan nuclear receptors - new ligands and new possibilities. Genes & Development. 12, 3149-3155.

Boucher, B. A., et al., 2006. Pharmacokinetic changes in critical illness. Critical Care Clinics. 22**,** 255-+.

Box, G. E. P., Cox, D. R., 1964. An analysis of transformations. Journal of the Royal Statistical Society Series B-Statistical Methodology. 26**,** 211-252.

Bresolin, T., et al., 2005. Expression of PXR, CYP3A and MDR1 genes in liver of zebrafish. Comparative Biochemistry and Physiology C-Toxicology & Pharmacology. 140**,** 403-407.

Brodie, B. B., et al., 1958. Enzymatic metabolism of drugs and other foreign compounds. Annual Review of Biochemistry. 27**,** 427-454.

Bustin, S. A., et al., 2009. The MIQE guidelines: Minimum information for publication of

quantitative real-time PCR experiments. Clinical Chemistry. 55**,** 611-622.

Chan, K. M., et al., 1992. P-glycoprotein genes in the winter flounder, pleuronectes-americanus - isolation of 2 types of genomic clones carrying 3' terminal exons. Biochimica Et Biophysica Acta. 1171**,** 65-72.

Chang, C. T., et al., 2013. Regulation of zebrafish CYP3A65 transcription by AHR2. Toxicology and Applied Pharmacology. 270**,** 174-184.

Chang, G., 2003. Multidrug resistance ABC transporters. Febs Letters. 555**,** 102-105.

Chang, H., et al., 2009. Association of the ABCB1 gene polymorphisms 2677G > T/A and 3435C > T with clinical outcomes of paclitaxel monotherapy in metastatic breast cancer patients. Annals of Oncology. 20**,** 272-277.

Chaudhary, P. M., Roninson, I. B., 1991. Expression and activity of p-glycoprotein, a multidrug efflux pump, in human hematopoietic stem-cells. Cell. 66**,** 85-94.

Cheek, A. O., et al., 1998. Environmental signaling: A biological context for endocrine disruption. Environmental Health Perspectives. 106**,** 5-10.

Chin, J. E., et al., 1989. Structure and expression of the human MDR (P-glycoprotein) gene family. Molecular and Cellular Biology. 9**,** 3808-3820.

Cho, S., et al., 2011. Notch1 regulates the expression of the multidrug resistance gene ABCC1/MRP1 in cultured cancer cells. Proceedings of the National Academy of Sciences of the United States of America. 108**,** 20778-20783.

Choi, J. S., et al., 2011. Effects of quercetin on the bioavailability of doxorubicin in rats: Role of CYP3A4 and P-gp inhibition by quercetin. Archives of Pharmacal Research. 34**,** 607-613.

Cooper, P. S., et al., 1999. Altered expression of the xenobiotic transporter P-glycoprotein in liver and liver tumours of mummichog (Fundulus heteroclitus) from a creosote-contaminated environment. Biomarkers. 4**,** 48-58.

Corcoran, J., et al., 2012. Effects of pharmaceuticals on the expression of genes involved in detoxification in a carp primary hepatocyte model. Environmental Science & Technology. 46**,** 6306-6314.

Corley-Smith, G. E., et al., 2006. CYP3C1, the first member of a new cytochrome P450 subfamily found in zebrafish (Danio rerio). Biochemical and Biophysical Research Communications. 340**,** 1039-1046.

Dai, Y. J., et al., 2014. Zebrafish as a model system to study toxicology. Environmental Toxicology and Chemistry. 33**,** 11-17.

Damare, C. L., et al., 2009. Investigation of the multixenobiotic resistance mechanism in

the freshwater fishes western mosquitofish, *Gambusia affinis*, and bluegill sunfish, *Lepomis macrochirus*. Bulletin of Environmental Contamination and Toxicology. 83**,** 640-643.

Davey, M. W., et al., 1996. Comparison of drug accumulation in P-glycoprotein-expressing and MRP-expressing human leukaemia cells. Leukemia Research. 20, 657-664.

Dogan, A. L., et al., 2004. Evaluation and comparison of MRP1 activity with three fluorescent dyes and three modulators in leukemic cell lines. Leukemia Research. 28, 619-622.

Doyle, L. A., et al., 1998. A multidrug resistance transporter from human MCF-7 breast cancer cells. Proceedings of the National Academy of Sciences of the United States of America. 95**,** 15665-15670.

Ekins, S., et al., 2007. Human pregnane X receptor antagonists and agonists define molecular requirements for different binding sites. Molecular Pharmacology. 72**,** 592-603.

Ekins, S., et al., 2008. Evolution of pharmacologic specificity in the pregnane X receptor. Bmc Evolutionary Biology. 8.

El-Sankary, W., et al., 2001. Use of a reporter gene assay to predict and rank the potency and efficacy of CYP3A4 inducers. Drug Metabolism and Disposition. 29**,** 1499-1504.

Elferink, R., Paulusma, C. C., 2007. Function and pathophysiological importance of ABCB4 (MDR3 P-glycoprotein). Pflugers Archiv-European Journal of Physiology. 453**,** 601-610.

Enoch, H. G., Strittmatter, P., 1979. Cytochrome-b5 reduction by NADPH-cytochrome P450 reductase. Journal of Biological Chemistry. 254**,** 8976-8981.

Epel, D., et al., 2008. Efflux transporters: Newly appreciated roles in protection against pollutants. Environmental Science & Technology. 42, 3914-3920.

Fan, Y., Rodriguez-Proteau, R., 2008. Ketoconazole and the modulation of multidrug resistance-mediated transport in Caco-2 and MDCKII-MDR1 drug transport models. Xenobiotica. 38, 107-129.

Feller, N., et al., 1995. Functional detection of MDR1/P170 and MRP/P190-mediated multidrug-resistance in tumor-cells by flow-cytometry. British Journal of Cancer. 72, 543-549.

Fischer, S., et al., 2013. Abcb4 acts as multixenobiotic transporter and active barrier against chemical uptake in zebrafish (*Danio rerio*) embryos. Bmc Biology. 11.

Forman, B. M., et al., 1998. Androstane metabolites bind to and deactivate the nuclear receptor CAR-beta. Nature. 395**,** 612-615.

Forster, S., et al., 2012. Characterization of rhodamine-123 as a tracer dye for use in in vitro drug transport assays. Plos One. 7.

Frank, N. Y., Frank, M. H., 2009. *ABCB5* gene amplification in human leukemia cells. Leukemia Research. 33**,** 1303-1305.

Frank, N. Y., et al., 2005. ABCB5-mediated doxorubicin transport and chemoresistance in human malignant melanoma. Cancer Research. 65**,** 4320-4333.

Fromm, M. F., 2000. P-glycoprotein: a defense mechanism limiting oral bioavailability and CNS accumulation of drugs. International Journal of Clinical Pharmacology and Therapeutics. 38**,** 69-74.

Fuchs, I., et al., 2013. Effect of the CYP3A inhibitor ketoconazole on the PXR-mediated induction of CYP3A activity. European Journal of Clinical Pharmacology. 69**,** 507-513.

Galetin, A., Houston, J. B., 2006. Intestinal and hepatic metabolic activity of five cytochrome P450 enzymes: Impact on prediction of first-pass metabolism. Journal of Pharmacology and Experimental Therapeutics. 318**,** 1220-1229.

Geick, A., et al., 2001. Nuclear receptor response elements mediate induction of intestinal MDR1 by rifampin. Journal of Biological Chemistry. 276**,** 14581-14587.

Georgantzopoulou, A., et al., 2014. P-gp efflux pump inhibition potential of common environmental contaminants determined in vitro. Environmental Toxicology and Chemistry. 33, 804-813.

Goksoyr, A., 1995. Use of cytochrome-P450-1A (CYP1A) in fish as a biomarker of aquatic pollution. Toxicology in Transition. 80-95.

Gotoh, O., 2012. Evolution of Cytochrome P450 Genes from the Viewpoint of Genome Informatics. Biological & Pharmaceutical Bulletin. 35**,** 812-817.

Gottesman, M. M., Pastan, I., 1993. Biochemistry of multidrug-resistance mediated by the multidrug transporter. Annual Review of Biochemistry. 62**,** 385-427.

Gourley, M. E., Kennedy, C. J., 2009. Energy allocations to xenobiotic transport and biotransformation reactions in rainbow trout (*Oncorhynchus mykiss*) during energy intake restriction. Comparative Biochemistry and Physiology C-Toxicology & Pharmacology. 150**,** 270-278.

Gu, L., et al., 2013. Bioimaging real-time PXR-dependent *mdr1a* gene regulation in *mdr1a.fLUC* reporter mice. Journal of Pharmacology and Experimental Therapeutics. 345**,** 438-445.

Gu, X. S., et al., 2006. Role of NF-kappa B in regulation of PXR-mediated gene expression - A mechanism for the suppression of cytochrome P-450 3A4 by proinflammatory agents. Journal of Biological Chemistry. 281**,** 17882-17889.

Guengrich, F. P., 1999. Cytochrome P-450 3A4: Regulation and role in drug metabolism. Annual Review of Pharmacology and Toxicology. 39**,** 1-17.

Han, J. Y., et al., 2007. Associations of ABCB1, ABCC2, and ABCG2 polymorphisms with irinotecan-pharmacokinetics and clinical outcome in patients with advanced non-small cell lung cancer. Cancer. 110**,** 138-147.

Handschin, C., Meyer, U. A., 2003. Induction of drug metabolism: The role of nuclear receptors. Pharmacological Reviews. 55**,** 649-673.

Hasselberg, L., et al., 2008. Ketoconazole, an antifungal imidazole, increases the sensitivity of rainbow trout to 17 alpha-ethynylestradiol exposure. Aquatic Toxicology. 86**,** 256-264.

Higgins, C. F., 1992. ABC transporters - from microorganisms to man. Annual Review of Cell Biology. 8**,** 67-113.

Hirsch-Ernst, K.I., et al., 2001. Inhibitors of MDR1-dependent transport activity delay accumulation of the MDR1 substrate rhodamine 123 in primary rat hepatocyte cultures. Toxicology. 167, 47-57.

Hontoria, F., et al., 2013. Ketoconazole modulates the infectivity of *Ichthyophonus* sp (*Mesomycetozoa*) *in vivo* in experimentally injected European sea bass. Diseases of Aquatic Organisms. 105**,** 225-235.

Hosoe, T., et al., 2005. Divergent modes of induction of rat hepatic and pulmonary CYP3A1 by dexamethasone and pregnenolone 16 alpha-carbonitrile. Journal of Health Science. 51, 75-79.

Huang, H., et al., 2007. Inhibition of drug metabolism by blocking the activation of nuclear receptors by ketoconazole. Oncogene. 26**,** 258-268.

Huss, J. M., Kasper, C.B., 2000. Two-stage glucocorticoid induction of CYP3A23 through both the glucocorticoid and pregnane X receptors. Molecular Pharmacology. 58, 48-57.

Iyanagi, T., 2007. Molecular mechanism of phase I and phase II drug-metabolizing enzymes: Implications for detoxification. International Review of Cytology - a Survey of Cell Biology, Vol 260. 260**,** 35-112.

Jancova, P., et al., 2010. Phase II drug metabolizing enzymes. Biomedical Papers-Olomouc. 154**,** 103-116.

Janosek, J., et al., 2006. Environmental xenobiotics and nuclear receptors - Interactions, effects and in vitro assessment. Toxicology in Vitro. 20, 18-37.

Jin, S., et al., 2013. P-glycoprotein and multidrug resistance-associated protein 2 are oppositely altered in brain of rats with thioacetamide-induced acute liver failure. Liver International. 33**,** 274-282.

Johnatty, S. E., et al., 2008. ABCB1 (MDR 1) polymorphisms and progression-free survival among women with ovarian cancer following paclitaxel/carboplatin chemotherapy. Clinical Cancer Research. 14**,** 5594-5601.

Johnson, D. R., et al., 2006. Regulation and binding of pregnane X receptor by nuclear receptor corepressor silencing mediator of retinoid and thyroid hormone receptors (SMRT). Molecular Pharmacology. 69**,** 99-108.

Johnson, L. V., et al., 1980. Localization of mitochondria in living cells with rhodamine-123. Proceedings of the National Academy of Sciences of the United States of America-Biological Sciences. 77**,** 990-994.

Jones, S. A., et al., 2000. The pregnane x receptor: A promiscuous xenobiotic receptor that has diverged during evolution. Molecular Endocrinology. 14**,** 27-39.

Joshi, T., Xu, D., 2007. Quantitative assessment of relationship between sequence similarity and function similarity. Bmc Genomics. 8.

Kageyama, M., et al., 2006. Relationship between excretion clearance of rhodamine 123 and P-glycoprotein (Pgp) expression induced by representative Pgp inducers. Biological & Pharmaceutical Bulletin. 29**,** 779-784.

Kageyama, M., et al., 2005. In vivo effects of cyclosporin A and ketoconazole on the pharmacokinetics of representative substrates for P-glycoprotein and cytochrome P450 (CYP) 3A in rats. Biological & Pharmaceutical Bulletin. 28**,** 316-322.

Karuppasamy, R., et al., 2010. Karyotype of a bagrid catfish, *Mystus vittatus*, from the freshwater system of Chidambaram, Tamil Nadu, India. Scienceasia. 36**,** 157-160.

Kawanobe, T., et al., 2012. Expression of human ABCB5 confers resistance to taxanes and anthracyclines. Biochemical and Biophysical Research Communications. 418**,** 736-741.

Kennedy, S. W., Jones, S. P., 1994. Simultaneous measurement of cytochrome p4501a catalytic activity and total protein-concentration with a fluorescence plate reader. Analytical Biochemistry. 222**,** 217-223.

Keppler, C., Ringwood, A. H., 2001. Expression of P-glycoprotein in the gills of oysters, *Crassostrea virginica*: seasonal and pollutant related effects. Aquatic Toxicology. 54**,** 195-204.

Kliewer, S. A., et al., 2002. The nuclear pregnane X receptor: A key regulator of xenobiotic metabolism. Endocrine Reviews. 23**,** 687-702.

Kliewer, S. A., et al., 1998. An orphan nuclear receptor activated by pregnanes defines a novel steroid signaling pathway. Cell. 92**,** 73-82.

Kohler, A., et al., 1998. Detection of P-glycoprotein mediated MDR/MXR in *Carcinus maenas* hepatopancreas by immuno-gold-silver labeling. Marine Environmental Research. 46**,** 411-414.

Kroetz, D. L., et al., 2003. Sequence diversity and haplotype structure in the human *ABCB1* (*MDR1*, multidrug resistance transporter) gene. Pharmacogenetics. 13**,** 481-494.

Kurata, Y., et al., 2002. Role of human *MDR1* gene polymorphism in bioavailability and interaction of digoxin, a substrate of P-glycoprotein. Clinical Pharmacology & Therapeutics. 72**,** 209-219.

Kurelec, B., et al., 1996. Expression of multixenobiotic resistance mechanism in a marine mussel *Mytilus galloprovincialis* as a biomarker of exposure to polluted environments. Comparative Biochemistry and Physiology C-Pharmacology Toxicology & Endocrinology. 113**,** 283-289.

Kurelec, B., et al., 1992. Expression of P-glycoprotein gene in marine sponges - identification and characterization of the 125 kDa drug-binding glycoprotein. Carcinogenesis. 13**,** 69-76.

Kurelec, B., Pivcevic, B., 1991. Evidence for a multixenobiotic resistance mechanism in the mussel, *Mytilus galloprovincialis*. Aquatic Toxicology. 19**,** 291-302.

Lahav, G., et al., 2004. Dynamics of the p53-Mdm2 feedback loop in individual cells. Nature Genetics. 36**,** 147-150.

Lampidis, T. J., et al., 1984. Effects of the mitochondrial probe rhodamine-123 and related analogs on the function and viability of pulsating myocardial-cells in culture. Agents and Actions. 14**,** 751-757.

LeCluyse, E. L., 2001. Pregnane X receptor: molecular basis for species differences in CYP3A induction by xenobiotics. Chemico-Biological Interactions. 134**,** 283-289.

Lee, G., Piquette-Miller, M., 2001. Influence of IL-6 on MDR and MRP-mediated multidrug resistance in human hepatoma cells. Canadian Journal of Physiology and Pharmacology. 79**,** 876-884.

Lee, J. S., et al., 1994. Rhodamine efflux patterns predict p-glycoprotein substrates in the national-cancer-institute drug screen. Molecular Pharmacology. 46**,** 627-638.

Lee, S. D., et al., 2013. Evaluation of the contribution of the ATP binding cassette transporter, p-glycoprotein, to in vivo cholesterol homeostasis. Molecular Pharmaceutics. 10**,** 3203-3212

Leslie, E. M., et al., 2005. Multidrug resistance proteins: role of P-glycoprotein, MRP1, MRP2, and BCRP (ABCG2) in tissue defense. Toxicology and Applied Pharmacology. 204**,** 216-237.

Li, H., et al., 2013. Novel yeast-based strategy unveils antagonistic binding regions on the nuclear xenobiotic receptor PXR. Journal of Biological Chemistry. 19, 13655 – 13668.

Li, X. Y., et al., 2013. Transcription alterations of microRNAs, cytochrome P4501A1 and

3A65, and AhR and PXR in the liver of zebrafish exposed to crude microcystins. Toxicon. 73**,** 17-22.

Liu, H. Y., et al., 2006. Impaired function and expression of P-glycoprotein in blood-brain barrier of streptozotocin-induced diabetic rats. Brain Research. 1123**,** 245-252.

Long, Y., et al.,. 2011. Molecular characterization and functions of zebrafish ABCC2 in cellular efflux of heavy metals. Comparative Biochemistry and Physiology C-Toxicology & Pharmacology. 153, 381-391.

Loo, T. W., Clarke, D. M., 1998. Nonylphenol ethoxylates, but not nonylphenol, are substrates of the human multidrug resistance P-glycoprotein. Biochemical and Biophysical Research Communications. 247**,** 478-480.

Ludden, T. M., 1991. Nonlinear pharmacokinetics - clinical implications. Clinical Pharmacokinetics. 20**,** 429-446.

Maglich, J. M., et al., 2002. Nuclear pregnane X receptor and constitutive androstane receptor regulate overlapping but distinct sets of genes involved in xenobiotic detoxification. Molecular Pharmacology. 62, 638-646.

Martin, P., et al., 2008. Comparison of the induction profile for drug disposition proteins by typical nuclear receptor activators in human hepatic and intestinal cells. British Journal of Pharmacology. 153**,** 805-819.

Martin, P., et al., 2010. Effect of prototypical inducers on ligand activated nuclear receptor regulated drug disposition genes in rodent hepatic and intestinal cells. Acta Pharmacologica Sinica. 31**,** 51-65.

Masuyama, H., et al., 2005. The pregnane X receptor regulates gene expression in a ligand- and promoter-selective fashion. Molecular Endocrinology. 19**,** 1170-1180.

Meunier, B., et al., 2004. Mechanism of oxidation reactions catalyzed by cytochrome P450 enzymes. Chemical Reviews. 104**,** 3947-3980.

Miller, V. P., et al., 2000. Fluorometric high-throughput screening for inhibitors of cytochrome P450. Annals of the New York Academy of Sciences. 919**,** 26-32.

Muller, W. E. G., et al., 1996. The multixenobiotic resistance mechanism in the marine sponge *Suberites domuncula*: Its potential applicability for the evaluation of environmental pollution by toxic compounds. Marine Biology. 125**,** 165-170.

Nebert, D. W., et al., 1989. Evolution of the cytochrome-P450 genes. Xenobiotica. 19**,** 1149-1160.

Nelson, D. R., et al., 2013. The cytochrome P450 genesis locus: the origin and evolution of animal cytochrome P450s. Philosophical Transactions of the Royal Society B-Biological Sciences. 368.

Ourlin, J. C., et al., 2003. The small heterodimer partner interacts with the pregnane X

receptor and represses its transcriptional activity. Molecular Endocrinology. 17**,** 1693-1703.

Parks, D.J., et al., 1999. Bile acids: Natural ligands for an orphan nuclear receptor. Science. 284, 1365-1368.

Pathiratne, A., George, S., 1996. Comparison of xenobiotic metabolizing enzymes of Tilapia with those of other fish species and interspecies relationships between gene families. Marine Environmental Research. 42**,** 293-296.

Pelkonen, O., et al., 1998. Inhibition and induction of human cytochrome P450 (CYP) enzymes. Xenobiotica. 28**,** 1203-1253.

Pelkonen, O., Turpeinen, M., 2007. In vitro-in vivo extrapolation of hepatic clearance: Biological tools, scaling factors, model assumptions and correct concentrations. Xenobiotica. 37, 1066-1089.

Pondugula, S. R., et al., 2009. Phosphorylation and protein-protein interactions in PXR-mediated CYP3A repression. Expert Opinion on Drug Metabolism & Toxicology. 5**,** 861-873.

Reschly, E. J., et al., 2007. Functional evolution of the vitamin D and pregnane X receptors. Bmc Evolutionary Biology. 7.

Reschly, E. J., Krasowski, M. D., 2006. Evolution and function of the NR1I nuclear hormone receptor subfamily (VDR, PXR, and CAR) with respect to metabolism of xenobiotics and endogenous compounds. Current Drug Metabolism. 7**,** 349-365.

Richards, D. J., Shieh, W. K., 1986. Biological fate of organic priority pollutants in the aquatic environment. Water Research. 20**,** 1077-1090.

Ritter, L., et al., 2002. Sources, pathways, and relative risks of contaminants in surface water and groundwater: A perspective prepared for the Walkerton inquiry. Journal of Toxicology and Environmental Health-Part a-Current Issues. 65**,** 1-142.

Rumpold, H., et al., 2005. RNAi-mediated knockdown of P-glycoprotein using a transposon-based vector system durably restores imatinib sensitivity in imatinib-resistant CML cell lines. Experimental Hematology. 33**,** 767-775.

Sarkadi, B., et al., 2006. Human multidrug resistance ABCB and ABCG transporters: Participation in a chemoimmunity defense system. Physiological Reviews. 86**,** 1179-1236.

Schuetz, E. G., et al., 1996. Modulators and substrates of P-glycoprotein and cytochrome P4503A coordinately up-regulate these proteins in human colon carcinoma cells. Molecular Pharmacology. 49**,** 311-318.

Seelig, A., 1998. A general pattern for substrate recognition by P-glycoprotein. European Journal of Biochemistry. 251**,** 252-261.

Shuilleabhain, S. N., et al., 2005. Identification of a multixenobiotic resistance mechanism in primary cultured epidermal cells from *Oncorhynchus mykiss* and the effects of environmental complex mixtures on its activity. Aquatic Toxicology. 73**,** 115-127.

Sladek, F. M., 2011. What are nuclear receptor ligands? Molecular and Cellular Endocrinology. 334**,** 3-13.

Smital, T., et al., 2003. Inducibility of the P-glycoprotein transport activity in the marine mussel *Mytilus galloprovincialis* and the freshwater mussel *Dreissena polymorpha*. Aquatic Toxicology. 65**,** 443-465.

Snyder, M. J., Glendinning, J. I., 1996. Causal connection between detoxification enzyme activity and consumption of a toxic plant compound. Journal of Comparative Physiology a-Sensory Neural and Behavioral Physiology. 179**,** 255-261.

Sturm, A., Cravedi, JP., et al., 2001. Prochloraz and nonylphenol diethoxylate inhibit an MDR1-like activity in vitro, but do not alter hepatic levels of P-glycoprotein in trout exposed in vivo. Aquatic Toxicology. 53**,** 215-228.

Sturm, A., Zeimann, C., et al., 2001. Expression and finctional activity of P-glycoprotein in cultured hepatocytes from *Oncorhynchus mykiss*. American Journal of physiology - Regulatory integrative and comparative physiology. 281, R1119-R1126.

Svecova, L., et al., 2008. Azole antimycotics differentially affect rifampicin-induced pregnane x receptor-mediated CYP3A4 gene expression. Drug Metabolism and Disposition. 36**,** 339-348.

Takano, M., et al., 1998. Interaction with P-glycoprotein and transport of erythromycin, midazolam and ketoconazole in Caco-2 cells. European Journal of Pharmacology. 358, 289-294.

Taub, M. E., et al., 2005. Functional assessment of multiple P-glycoprotein (P-gp) probe substrates: Influence of cell line and modulator concentration on P-GP activity. Drug Metabolism and Disposition. 33, 1679-1687.

Thiebaut, F., et al., 1987. Cellular-localization of the multidrug-resistance gene-product p-glycoprotein in normal human-tissues. Proceedings of the National Academy of Sciences of the United States of America. 84**,** 7735-7738.

Tran, C. D. H., et al., 2002. Investigation of the coordinated functional activities of cytochrome P450 3A4 and P-glycoprotein in limiting the absorption of xenobiotics in Caco-2 cells. Journal of Pharmaceutical Sciences. 91**,** 117-128.

Tseng, H. P., et al., 2005. Constitutive and xenobiotics-induced expression of a novel *CYP3A* gene from zebrafish larva. Toxicology and Applied Pharmacology. 205**,** 247-258.

Turner, P. V., et al., 2011. Administration of Substances to Laboratory Animals: Routes of Administration and Factors to Consider. Journal of the American Association for Laboratory Animal Science. 50**,** 600-613.

Twentyman, P. R., et al., 1994. A comparison of rhodamine-123 accumulation and efflux in cells with p-glycoprotein-mediated and mrp-associated multidrug-resistance phenotypes. European Journal of Cancer. 30A, 1360-1369.

Ueda, K., et al., 1986. The *MDR1* gene, responsible for multidrug-resistance, codes for P-glycoprotein. Biochemical and Biophysical Research Communications. 141**,** 956-962.

vanHelvoort, A., et al., 1996. MDR1 P-glycoprotein is a lipid translocase of broad specificity, while MDR3 P-glycoprotein specifically translocates phosphatidylcholine. Cell. 87**,** 507-517.

Vilella, A. J., et al., 2009. EnsemblCompara GeneTrees: Complete, duplication-aware phylogenetic trees in vertebrates. Genome Research. 19**,** 327-335.

Wacher, V. J., et al., 1995. Overlapping substrate specificities and tissue distribution of cytochrome-P450 3a and P-glycoprotein - implications for drug-delivery and activity in cancer-chemotherapy. Molecular Carcinogenesis. 13**,** 129-134.

Wagner, M., et al., 2005. CAR and PXR agonists stimulate hepatic bile acid and bilirubin detoxification and elimination pathways in mice. Hepatology. 42**,** 420-430.

Wang, Y. J., et al., 2002. Ketoconazole potentiates the antitumor effects of nocodazole: In vivo therapy for human tumor xenografts in nude mice. Molecular Carcinogenesis. 34, 199-210.

Wang, H. W., et al., 2007. Activated pregnenolone X-receptor is a target for ketoconazole and its analogs. Clinical Cancer Research. 13**,** 2488-2495.

Wang, R. X., et al., 2009. Compensatory Role of P-glycoproteins in knockout mice lacking the bile salt export pump. Hepatology. 50**,** 948-956.

Wang, W., et al., 2008. Construction and characterization of a fully active PXR/SRC-1 tethered protein with increased stability. Protein Engineering Design & Selection. 21**,** 425-433.

Ward, K. W., et al., 2004. Development of an in vivo preclinical screen model to estimate absorption and first-pass hepatic extraction of xenobiotics. II. Use of ketoconazole to identify P-glycoprotein/CYP3A-limited bioavailability in the monkey. Drug Metabolism and Disposition. 32**,** 172-177.

Wassmur, B., et al., 2010. Interactions of pharmaceuticals and other xenobiotics on hepatic pregnane X receptor and cytochrome P450 3A signaling pathway in rainbow trout (*Oncorhynchus mykiss*). Aquatic Toxicology. 100**,** 91-100.

Watkins, R. E., et al., 2003. Coactivator binding promotes the specific interaction between ligand and the pregnane X receptor. Journal of Molecular Biology. 331**,** 815-828.

Waxman, D. J., Holloway, M. G., 2009. Sex differences in the expression of hepatic drug metabolizing enzymes. Molecular Pharmacology. 76**,** 215-228.

Wee, K. B., et al., 2012. Transcription factor oscillations induce differential gene expressions. Biophysical Journal. 102**,** 2413-2423.

Yang, H., Wang, H. B., 2014. Signaling control of the constitutive androstane receptor (CAR). Protein & Cell. 5**,** 113-123.

Yumoto, R., et al.,. 1999. Transport of rhodamine 123, a P-glycoprotein substrate, across rat intestine and Caco-2 cell monolayers in the presence of cytochrome P-450 3A-related compounds. Journal of Pharmacology and Experimental Therapeutics. 289, 149-155.

Yumoto, R., et al., 2001. Pharmacokinetic interaction of cytochrome P450 3A-related compounds with rhodamine 123, a P-glycoprotein substrate, in rats pretreated with dexamethasone. Drug Metabolism and Disposition. 29, 145-151.

Yeh, G. C., et al., 1992. A new functional-role for P-glycoprotein - efflux pump for benzo(a)pyrene in human breast-cancer MCF-7 cells. Cancer Research. 52**,** 6692-6695.

Zhang, Y. C., et al., 1998. Effects of ketoconazole on the intestinal metabolism, transport and oral bioavailability of K02, a novel vinylsulfone peptidomimetic cysteine protease inhibitor and a P450 3A, P-glycoprotein dual substrate, in male Sprague-Dawley rats. Journal of Pharmacology and Experimental Therapeutics. 287, 246-252.

Appendices

Appendix A.

Figure A.1: Rhodamine 123 standard curve

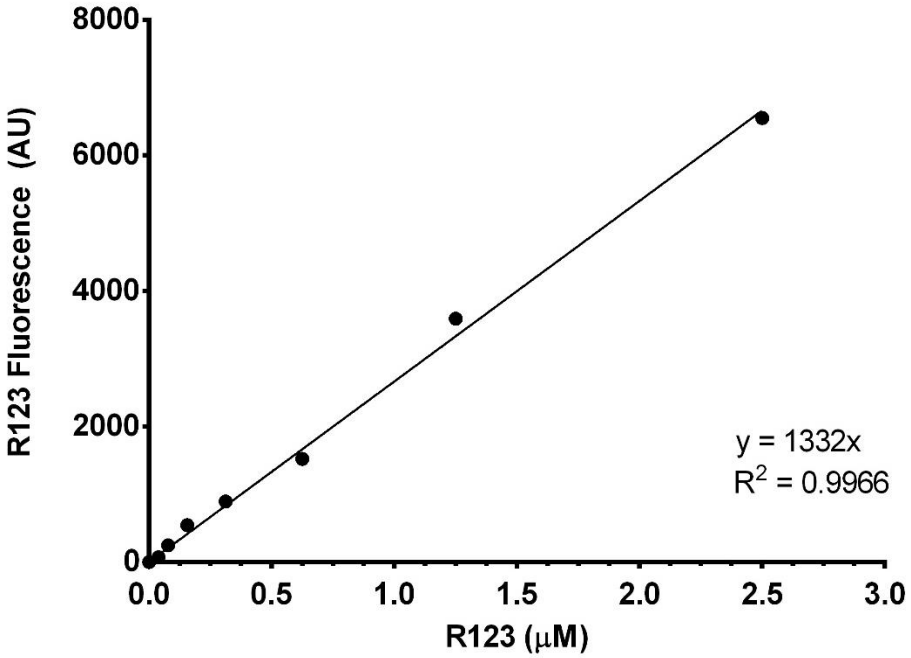

Raw R123 fluorescence (arbitrary units) *v.* μM R123 in homogenization buffer (HBSS + 0.05% Triton X-100).

Figure A.2: Bovine serum albumin (BSA) standard curve

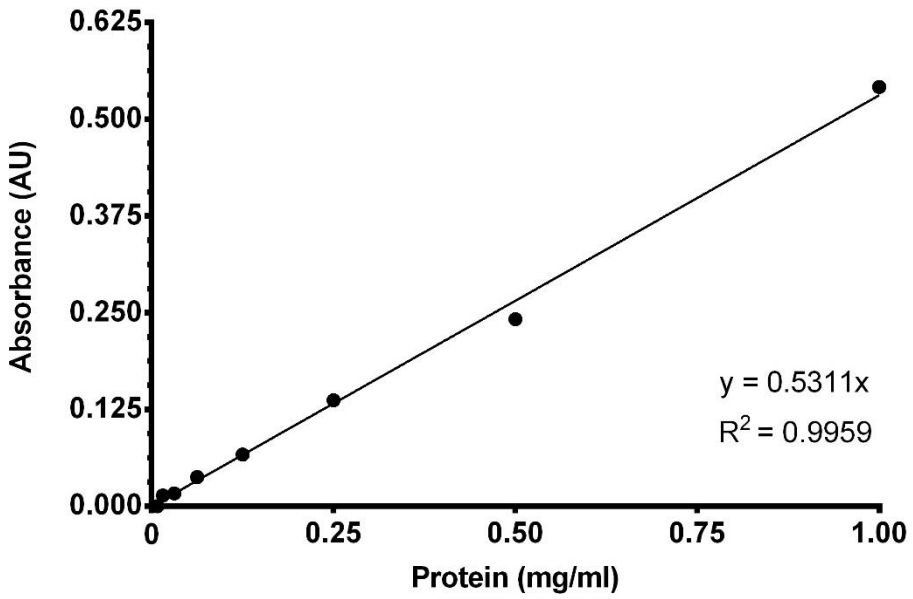

Sample absorbance (arbitrary units) at 595 nm vs. bovine serum albumin (BSA) concentration (mg/ml) in homogenization buffer (HBSS + 0.05% Triton X-100). Protein content was determined by the Bradford assay.

Appendix B.

Box-Cox transformation

If data were suspected of violating the statistical model (ANOVA) assumptions, a Box-Cox transformation of the original data (anchored at 1) was attempted in JMP software to improve the fit of the data. Briefly, the Box-Cox transformations are a suite of power transformations based on the following formula (Box and Cox, 1964):

$$Y_\lambda = \begin{cases} \dfrac{y^\lambda - 1}{\lambda y^{\lambda-1}} & if\ \lambda \neq 0 \\ \dot{y}\ln(y) & if\ \lambda = 0 \end{cases}$$

Where $\dot{y}$ is the geometric mean.

JMP software's factor profiling function for Box-Cox transformations returns an optimal value for λ, which ranges from -2 to 2 in increments of 0.2. More information pertaining to the Box-Cox method in JMP software can be found online at *www.jmp.com*. Where applicable, the statistical diagnostics of residuals from the original and transformed data are presented along with the associated λ value in appendices B - I.

Appendix C.

Diagnostics report and summary statistics of R123 concentration assay

Statistical diagnostics of the residuals (error terms) revealed the data failed to show significant departure from equal variance (Figure 1), independence of errors (Figure 2), and normality (Figure 3). Thus, the assumptions of the analysis of variance (ANOVA) were fulfilled and a one-way ANOVA with Tukey's HSD multiple comparison test was used to analyze significant differences of mean hepatic R123 uptake in fish.

Figure C.1: Assessment of homoscedasticity

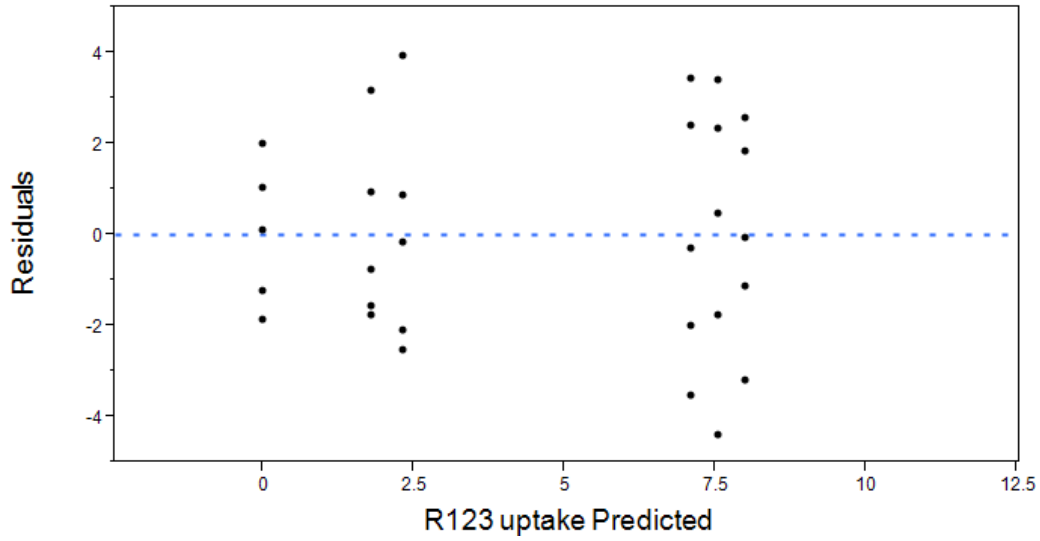

Plot of the residuals *vs.* the predicted response. No extreme differences in the variance of error terms (residuals) across the fitted response values are apparent. The Brown-Forsythe test failed to reject the null hypothesis of equal sample variation across experimental groups, F (5, 24) = 1.2297, p = 0.3260.

Figure C.2: Assessment of independent errors

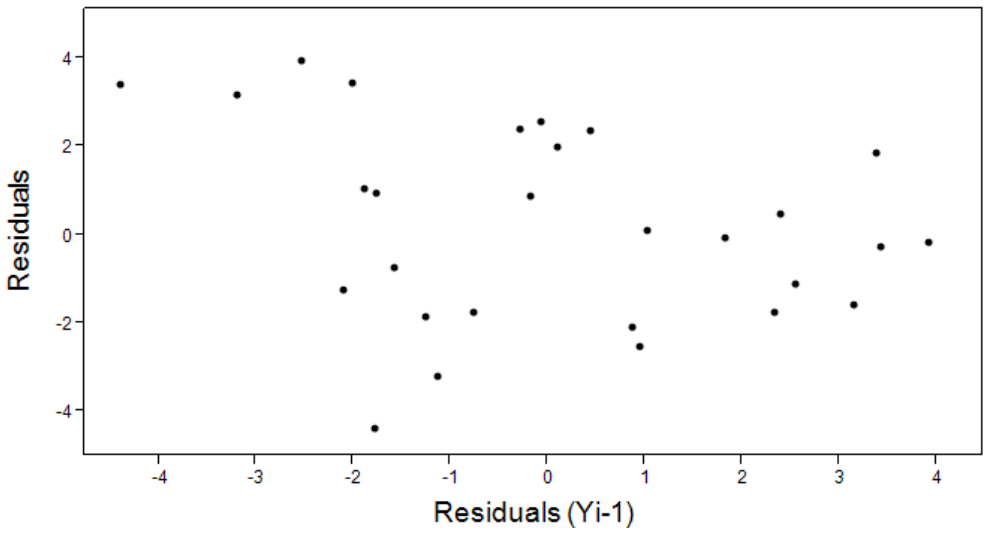

Residual lag plot of residuals vs. residual (Y_{i-1}) to check the assumption of independent errors. The residual values show random scattering with no clear pattern, suggesting the errors are independent.

Figure C.3: Assessment of normal distribution

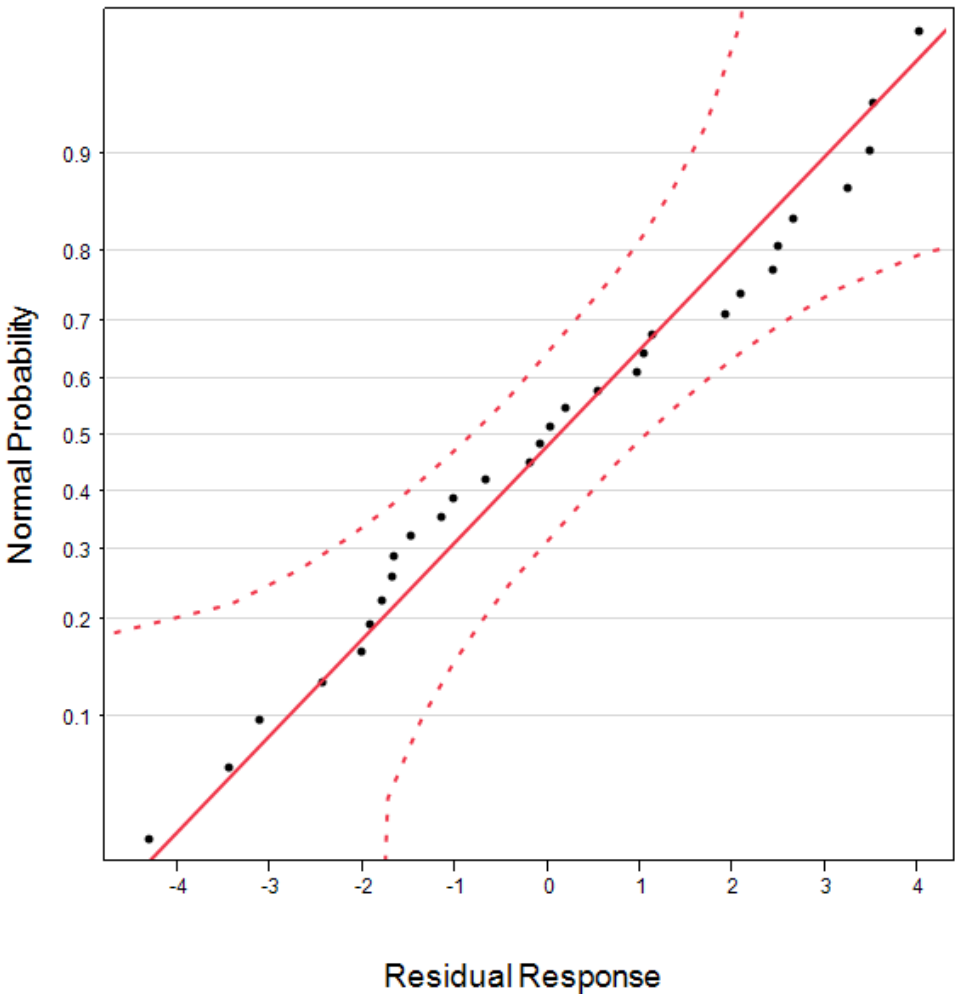

A normal probability plot showing normal probability vs. residual response. The solid diagonal line represents an ideal Gaussian distribution. The residuals appear to be approximately normally distributed, showing a quantile plot that is roughly linear and falling well within the Lilliefors confidence intervals (curved dashed lines). Parameter estimates N (μ, σ) show the distribution of the residuals is centered around 0 (mean distribution, $\mu \approx 0$) with standard deviation (σ) ≈ 2.3. The Shapiro-Wilk goodness-of-fit test failed to reject the null hypothesis (Ho) that the residuals are from a normal distribution ($W = 0.9578$, $p = 0.2724$).

Analysis of variance (ANOVA) and multiple-comparison report for R123 concentration assay

Table C.1: ANOVA report

Source	DF	Sum of Squares	Mean Square	F Ratio	Prob > F
Factor	5	29.5901	5.9180	9.7561	<.0001
Error	24	14.5583	0.6066		
Total	29	44.1483			

Summary statistics of one-way ANOVA for R123 concentration assay. Factor = R123 concentration (μM).

Table C.2: Multiple comparisons of means report

Comparison (μM R123)	Mean Dif	SE	DF	p-value
0 vs. 1.25	-2.335	1.576	24	0.6786
0 vs. 2.5	-1.796	1.576	24	0.8599
0 vs. 5	-8.003	1.576	24	0.0004
0 vs. 10	-7.56	1.576	24	0.0009
0 vs. 20	-7.094	1.576	24	0.0018
1.25 vs. 2.5	0.539	1.576	24	0.9993
1.25 vs. 5	-5.667	1.576	24	0.0162
1.25 vs. 10	-5.225	1.576	24	0.0306
1.25 vs. 20	-4.759	1.576	24	0.0585
2.5 vs. 5	-6.206	1.576	24	0.0072
2.5 vs. 10	-5.764	1.576	24	0.014
2.5 vs. 20	-5.298	1.576	24	0.0276
5 vs. 10	0.4421	1.576	24	0.9997
5 vs. 20	0.9087	1.576	24	0.9917
10 vs. 20	0.4666	1.576	24	0.9997

Summary of Tukey's HSD post-hoc test for the R123 concentration assay. Mean R123 uptake is compared to the 0 μM R123 control group. Mean Dif = difference in means; SE Diff. = standard error of the difference of means; p-values less than the significance level of $\alpha = 0.05$ are bolded.

Appendix D.

Diagnostics report and summary statistics of R123 exposure duration assay

Figure D.1: Assessment of homoscedasticity

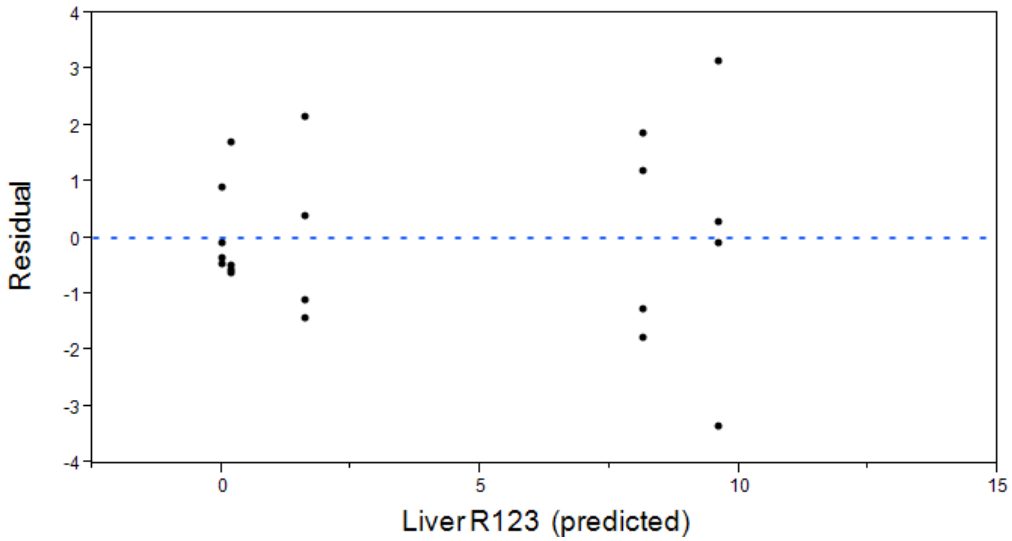

A plot of the error terms (residuals) *vs.* the predicted response (R123 uptake). Visual inspection of the residuals (above) reveals a pattern of increasing residual variance as the fitted (predicted) response increases, indicating the ANOVA assumption of homoscedasticity may be violated.

Figure D.2: Assessment of independent errors

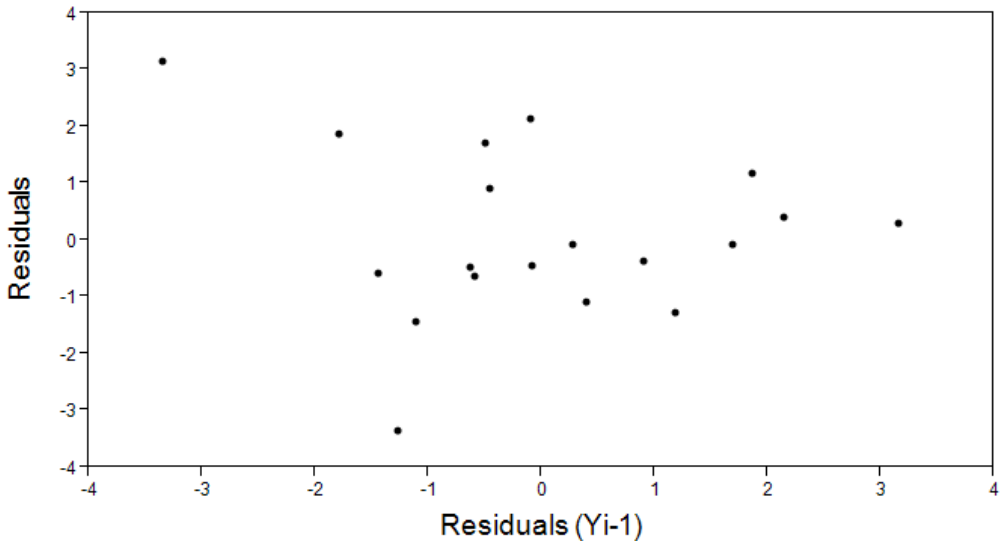

A residual lag plot of residuals vs. residual (Y_{i-1}),) to visually check the assumption of independent errors. The residual values show random scattering with no clear pattern, suggesting the errors are independent.

Figure D.3: Assessment of normal distribution

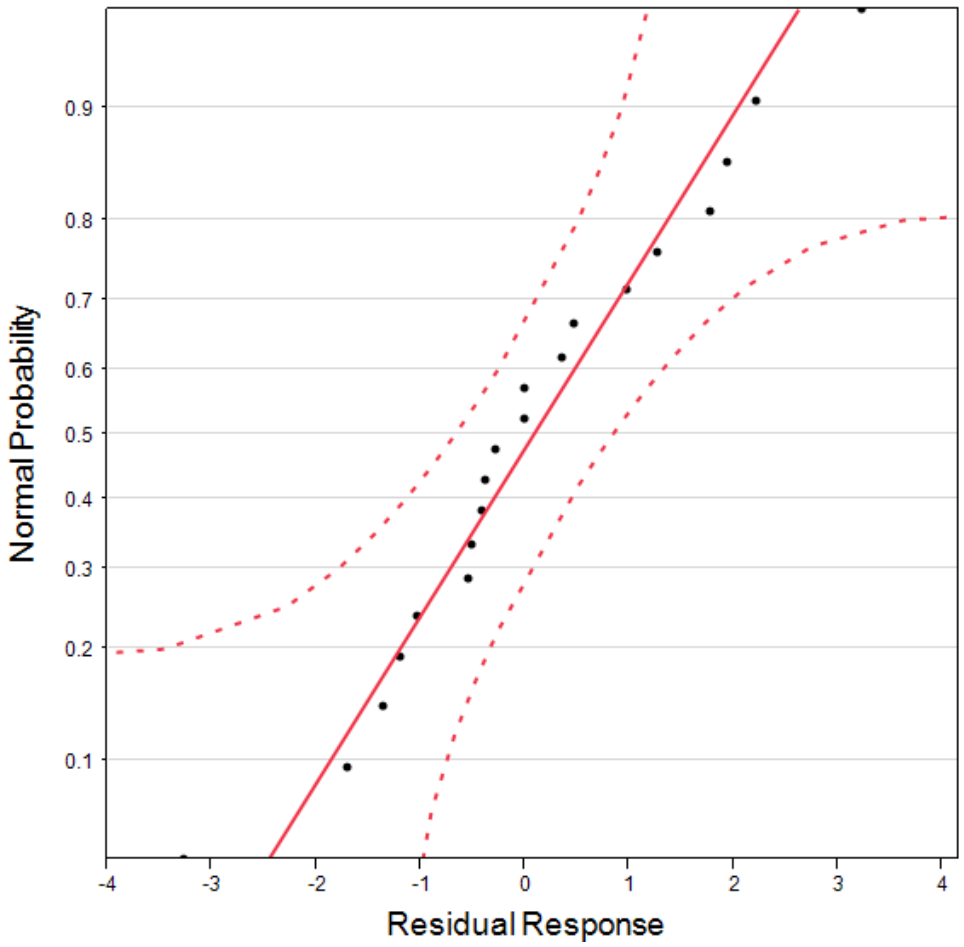

A normal probability plot showing normal probability *vs.* residual response. The solid diagonal line represents an ideal Gaussian distribution. The residuals appear to be approximately normally distributed, showing a probability plot that is roughly linear and falling within the Lilliefors confidence intervals (curved dashed lines). Parameter estimates N (μ, σ) show the distribution of the residuals is centered around 0 (mean distribution, $\mu \approx 0$) with standard deviation (σ) ≈ 1.5. The Shapiro-Wilk goodness-of-fit test failed to reject the null hypothesis that the residuals are from a normal distribution ($W = 0.9811$, $p = 0.9479$).

Diagnostics report of R123 exposure duration assay following a Box-Cox transformation

Diagnostics of the residuals from the R123 exposure duration assay revealed potential violations of the critical ANOVA assumptions of homoscedasticity and independence of errors, thus a Box-Cox transformation (λ = 0.4) was applied to the original data to improve the fit of the statistical model. The transformation moderately reduced the linearity of the normal probability plot (Figure 6); however, the Shapiro-Wilk test failed to detect a significant departure from normality. Importantly, the transformation greatly improved homoscedasticity of the residuals and independence of errors, thus the transformation resulted in an improved overall fit for the ANOVA (Figures 4 – 6). For ease of interpretation, all transformed data were back-transformed to construct the graph of the results (see Figure 2, Results section).

Figure D.4: Assessment of homoscedasticity following Box-Cox transformation

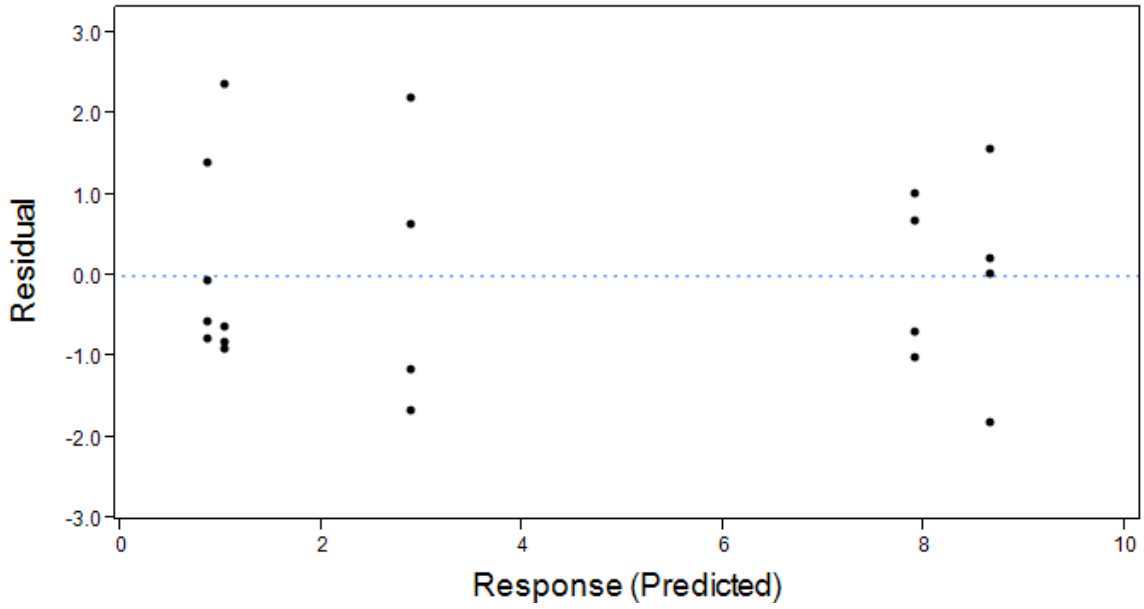

Plot of the error terms (residuals) *vs.* the predicted response (R123 uptake) following a Box-Cox transformation (λ = 0.4). Relative to the original data, the transformed data generates a higher degree of homoscedasticity (equal variance). The Brown-Forsythe test failed to reject the null hypothesis of equal sample variance across experimental groups, F (4, 15) = 0.3706, p = 0.8259.

Figure D.5: Assessment of independent errors following square root transformation

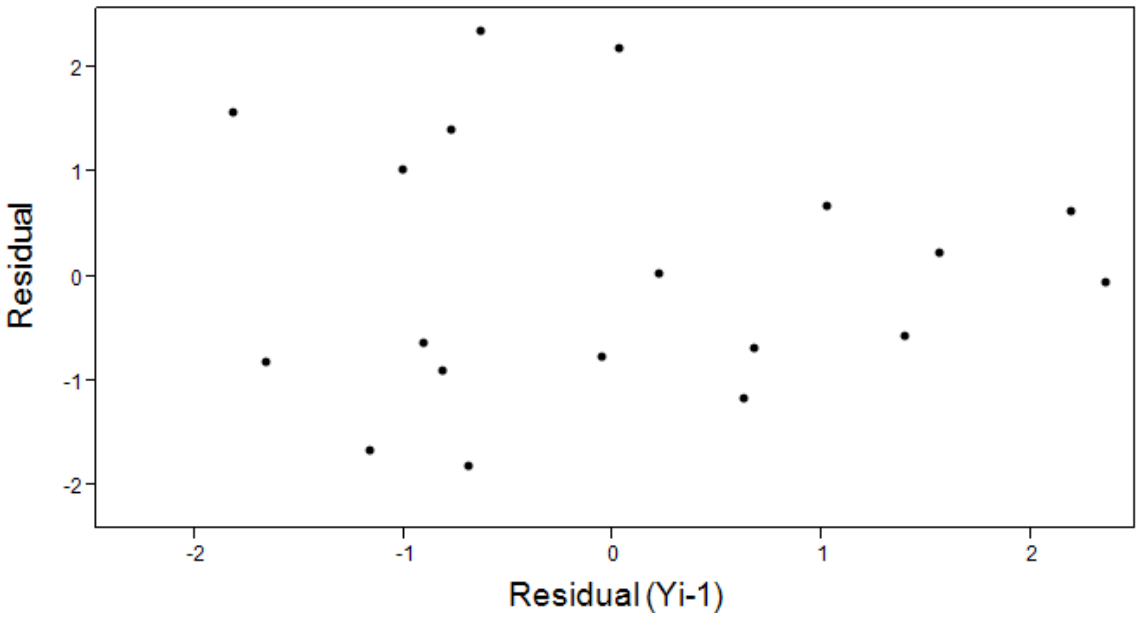

A residual lag plot of residuals vs. residual (Y_{i-1}) following a Box-Cox transformation ($\lambda = 0.4$), to visually check the assumption of independent errors. The residual values show random scattering with no clear pattern, suggesting the errors are independent.

Figure D.6: Assessment of normal distribution following Box-Cox transformation

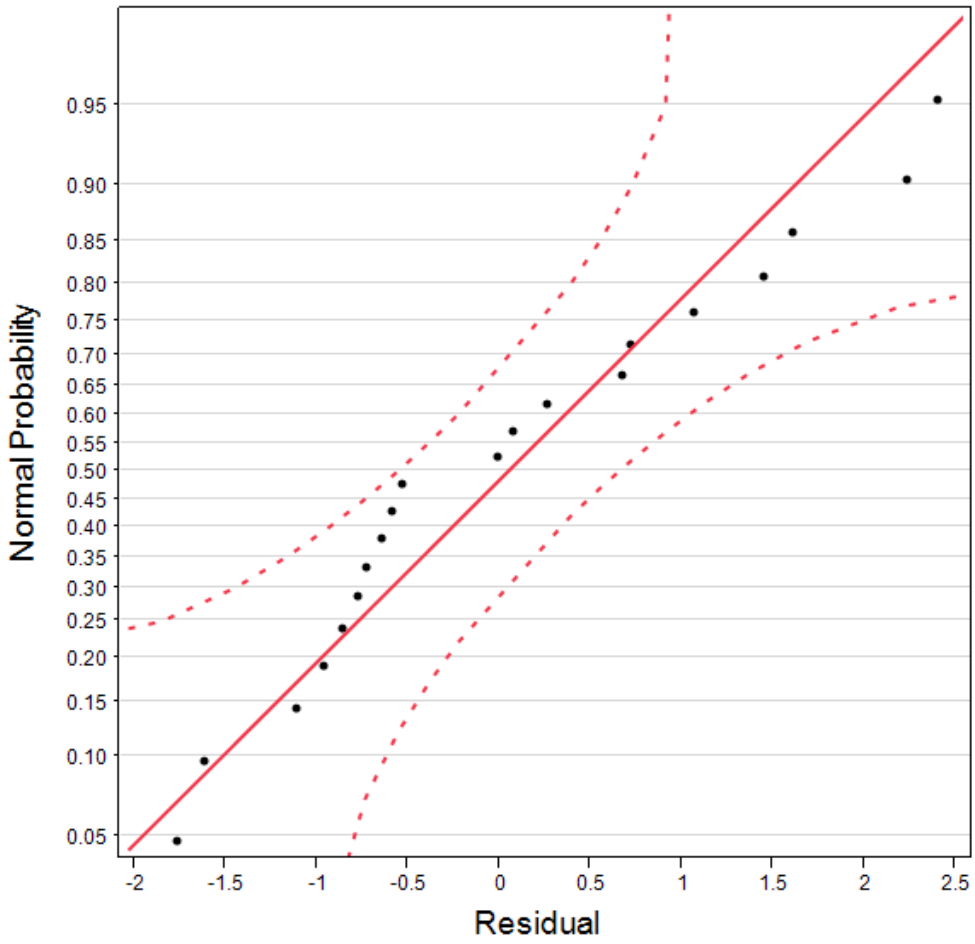

A normal probability plot showing normal probability *vs.* residual response following a Box-Cox transformation ($\lambda = 0.4$) of the data. The solid diagonal line represents an ideal Gaussian distribution. Parameter estimates $N(\mu, \sigma)$ show the distribution of the residuals is centered around 0 (mean distribution, $\mu \approx 0$) with standard deviation (σ) ≈ 1.22. Relative to original data, the transformed plot has reduced linearity. The Shapiro-Wilk goodness-of-fit test again failed to reject the null hypothesis that the residuals are from a normal distribution ($W = 0.9439$, $p = 0.2841$).

Analysis of variance (ANOVA) and multiple-comparison report for R123 exposure duration assay following Box-Cox transformation

Table D.1: ANOVA report

Source	DF	Sum of Squares	Mean Square	F Ratio	Prob > F
Factor	4	225.78	56.44	29.81	<.0001
Error	15	28.41	1.89		
Total	19	254.19			

Summary statistics of one-way ANOVA on Box-Cox transformed data (λ = 0.4) from R123 concentration assay. Factor = R123 exposure duration (hours).

Table D.2: Multiple comparisons of means report

Comparison (hours)	Mean Dif	SE	DF	p-value
0 vs. 0.5	-0.1892	1.212	15	0.9998
0 vs. 1	-1.613	1.212	15	0.6771
0 vs. 2	-9.6	1.212	15	< **0.0001**
0 vs. 4	-8.133	1.212	15	< **0.0001**
0.5 vs. 1	-1.424	1.212	15	0.7648
0.5 vs. 2	-9.411	1.212	15	< **0.0001**
0.5 vs. 4	-7.944	1.212	15	< **0.0001**
1 vs. 2	-7.987	1.212	15	< **0.0001**
1 vs. 4	-6.52	1.212	15	**0.0006**
2 vs. 4	1.467	1.212	15	0.7456

Summary of Tukey's HSD post-hoc test for the R123 exposure duration assay. Mean R123 uptake is compared across every time point (0.5, 1, 2, 4 h). Mean Diff. = difference in means; SE = standard error of the difference of means; p-values less than the significance level of α = 0.001 are bolded.

Appendix E.

Diagnostics report and summary statistics of R123 efflux assay

Diagnostics of the residuals (error terms) revealed an outlier in the R123 efflux data. After visual inspection of the residual vs. predicted response plot as well as Cook's distance plot, the outlier was considered a highly influential observation to the statistical model (Figures 1 and 2). On this basis, the data point was removed from the analysis. Further diagnostics indicated the assumptions of homoscedasticity, independence of errors, and normality were upheld (Figures 3, 4, and 5).

Figure E.1: Assessment of homoscedasticity

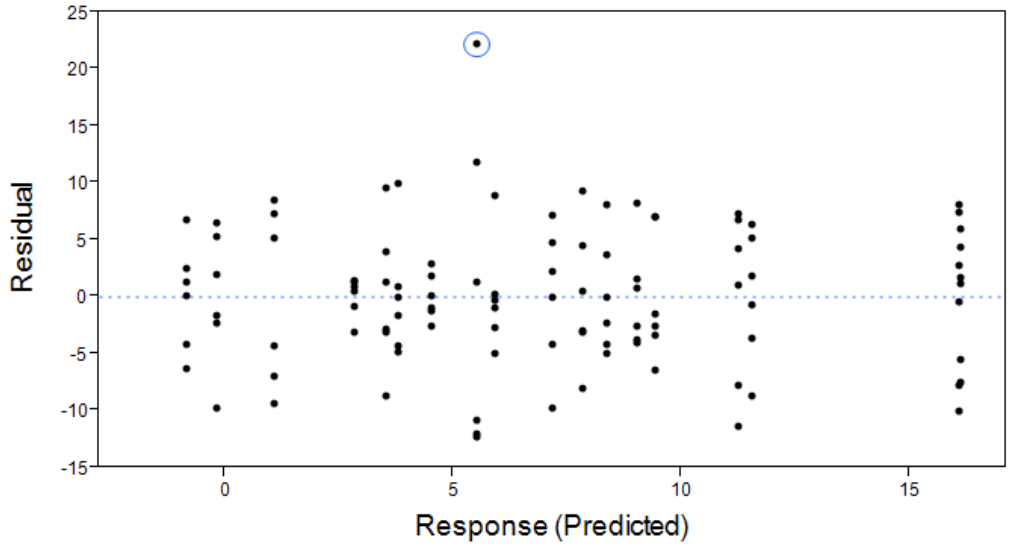

A plot of the error terms (residuals) *vs.* the predicted response (liver R123). The residuals appear roughly homoscedastic; however, a possible influential error term is seen (circled).

Figure E.2: Influence of residual outliers on model estimates

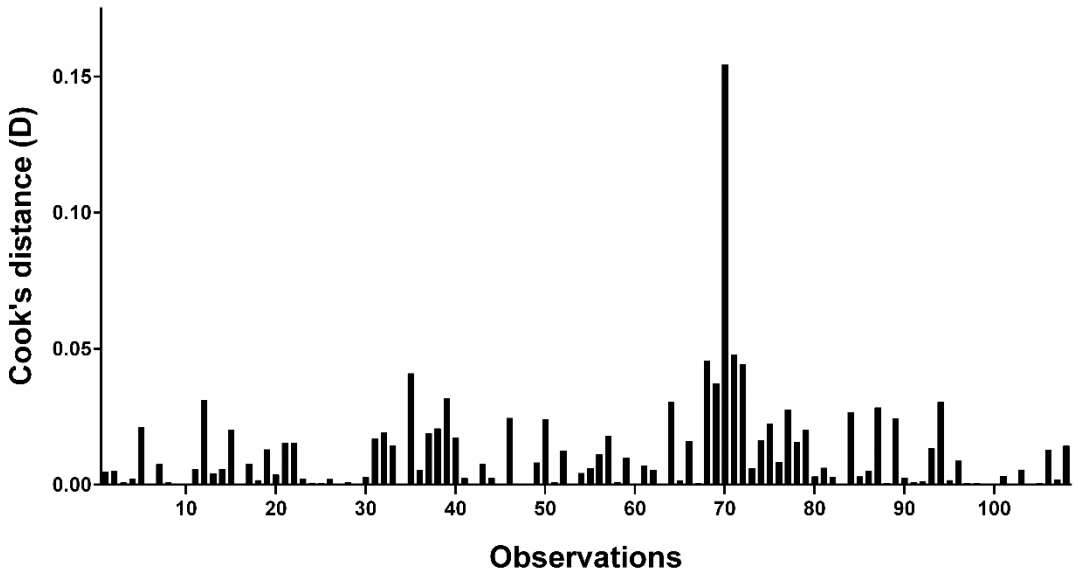

A plot of Cook's distance for each observation. Observations with relatively high Cook's distances are considered influential to the model estimates. The observation with the largest Cook's distance (observation # 70, D = 0.154) belongs to the outlier in question (Figure 11).

Figure E.3: Assessment of homoscedasticity following outlier removal

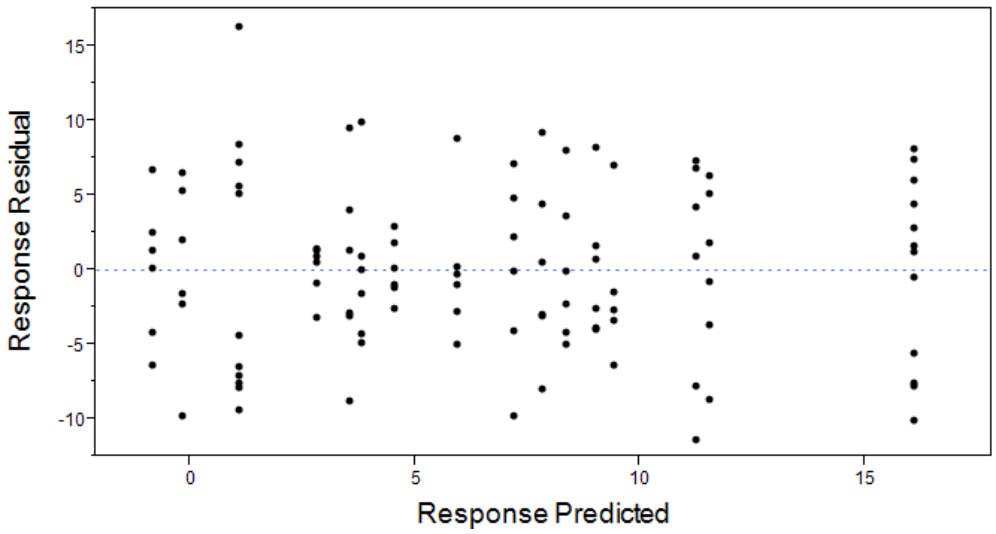

A plot of the error terms (residuals) vs. the predicted response (liver R123) following removal of the outlier (data point #70 from Cook's distance plot, figure 12). Removal of the outlier resulted in improved homoscedasticity to meet the model assumption of equal variance of errors. No extreme differences in the variance of error terms (residuals) across the fitted response values (predicted R123 uptake) are apparent. In addition, the Brown-Forsythe test failed to reject the null hypothesis of equal sample variation across experimental groups, F (17, 89) = 0.8737, p = 0.6056.

Figure E.4: Independence of errors following outlier removal

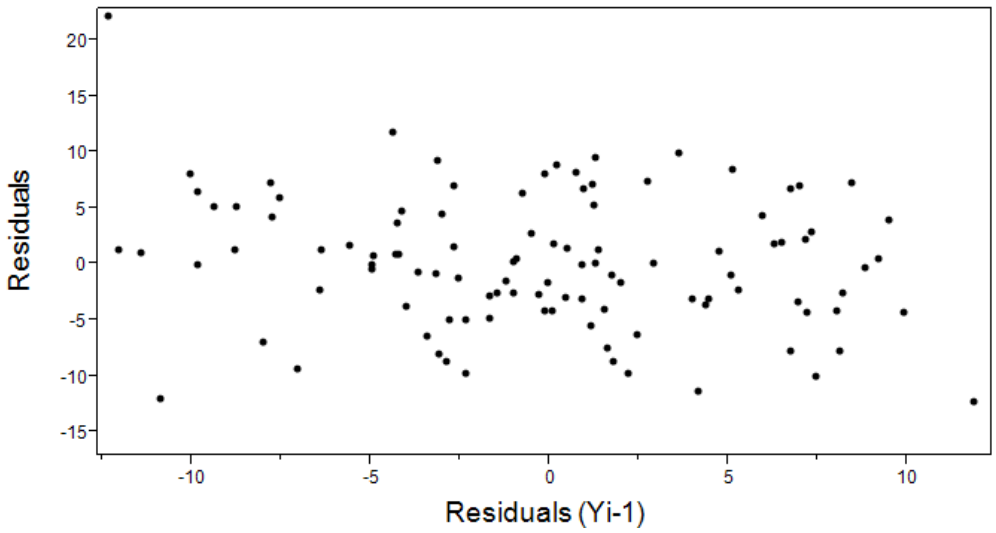

A residual lag plot of residuals vs. residuals (Y_{i-1}),) to visually check the assumption of independent errors. The residual values show random scattering with no clear pattern, suggesting the errors are independent.

Figure E.5: Assessment of normal distribution

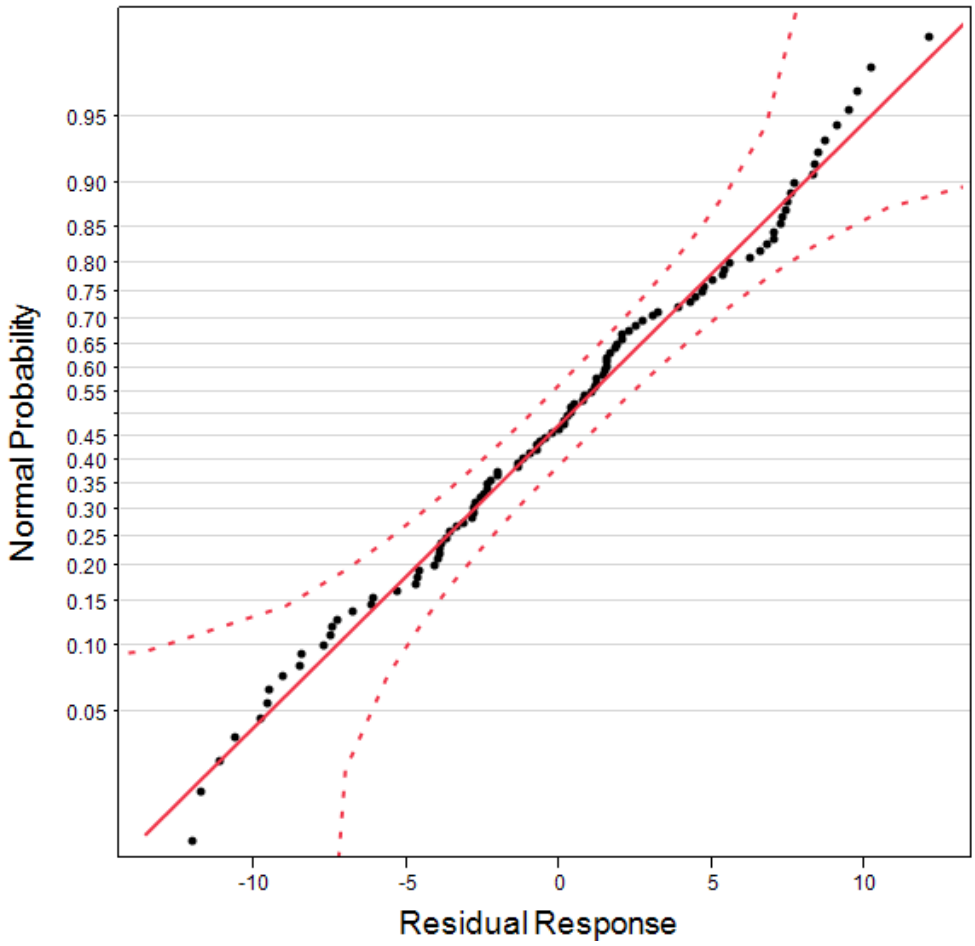

A normal probability plot showing normal probability *vs.* residual response. The solid diagonal line represents an ideal Gaussian distribution. Parameter estimates N (μ, σ) show the distribution of the residuals is centered on 0 (mean distribution, $\mu \approx 0$) with standard deviation (σ) ≈ 5.97. The Shapiro-Wilk goodness-of-fit test failed to reject the null hypothesis that the residuals are from a normal distribution ($W = 0.9799$, $p = 0.1025$).

Analysis of variance (ANOVA) and multiple-comparison report for R123 efflux assay

Table E.1: ANOVA report

Source	DF	Sum of Squares	Mean Square	F Ratio	Prob > F
Model	17.0	2629.79	154.69	4.2617	<.0001
Error	89.0	3230.58	36.30		
Total	106.0	5860.37			

Summary statistics of two-way ANOVA on data from R123 efflux assay.

Table E.2: Parameter effects

Source	DF	Sum of Squares	F Ratio	Prob > F
Drug	2.00	219.69	3.0261	0.0535
Time (h)	5.00	1235.37	6.8067	<.0001
Drug*Time (h)	10.00	1159.37	3.194	0.0015

Parameter effects of two-way ANOVA. A significant interaction exists between factors.

Figure E.6: Assessment of interaction between factors (drug vs time)

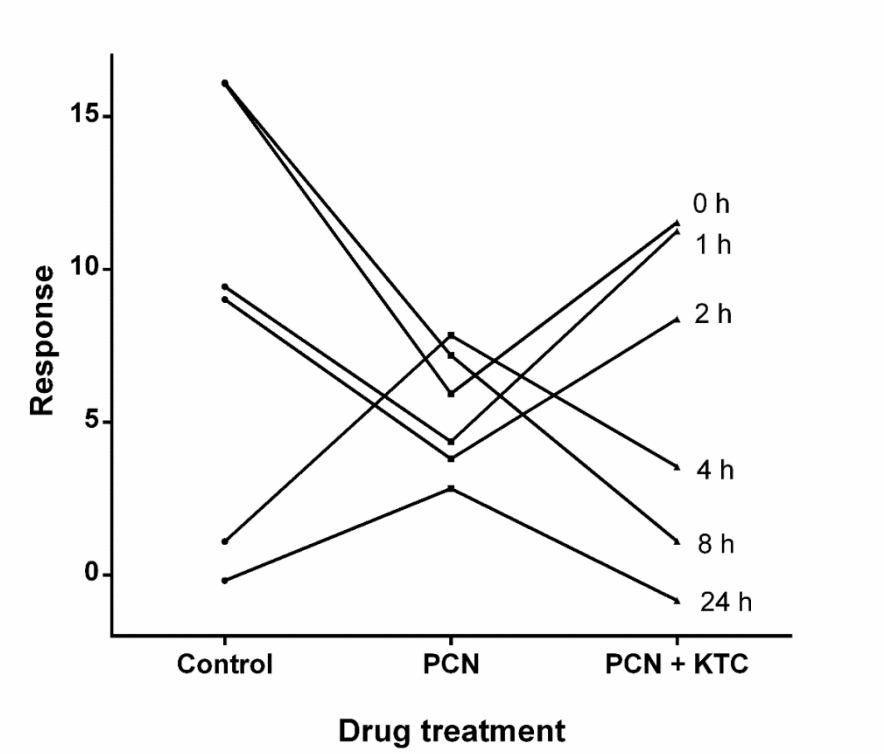

Interaction plot between factor levels (drug treatments and time points). Non-parallelism of the lines indicates an interaction between factors (drug treatment and time). The effect of drug treatment (control, PCN, or PCN + KTC) on the measured response (liver R123 quantity) depends on the time point of the assay (0 – 24 h).

Table E.3: Summary of multiple comparisons test

Test details	Mean Diff.	SE of diff.	N1	N2	q	DF	***p*-value**
0 h							
Control vs. PCN	5.224	3.506	6	6	2.107	89	0.3006
Control vs. PCN + KTC	0.6502	3.506	6	6	0.262	89	0.9812
PCN vs. PCN + KTC	-4.574	3.506	6	6	1.845	89	0.3964
1 h							
Control vs. PCN	5.068	3.506	6	6	2.044	89	0.3223
Control vs. PCN + KTC	-1.817	3.506	6	6	0.733	89	0.8627
PCN vs. PCN + KTC	-6.885	3.506	6	6	2.777	89	0.1273
2 h							
Control vs. PCN	10.15	3.506	6	6	4.094	89	0.0131
Control vs. PCN + KTC	4.544	3.506	6	6	1.833	89	0.4011
PCN vs. PCN + KTC	-5.606	3.506	6	6	2.261	89	0.2514
4 h							
Control vs. PCN	8.925	3.506	6	6	3.600	89	0.0335
Control vs. PCN + KTC	15.01	3.677	6	5	5.773	89	0.0003
PCN vs. PCN + KTC	6.084	3.677	6	5	2.340	89	0.2285
8 h							
Control vs. PCN	-6.748	3.506	6	6	2.722	89	0.1377
Control vs. PCN + KTC	-2.452	3.506	6	6	0.989	89	0.7644
PCN vs. PCN + KTC	4.295	3.506	6	6	1.733	89	0.4416
24 h							
Control vs. PCN	-3.014	3.506	6	6	1.216	89	0.6670
Control vs. PCN + KTC	0.6531	3.506	6	6	0.263	89	0.9811
PCN vs. PCN + KTC	3.667	3.506	6	6	1.479	89	0.5500

Summary of Tukey's HSD post-hoc test for the R123 efflux assay. Comparison of means between drug treatments (Control, PCN, or PCN +KTC) is organized by each time point (0 – 24 h). Mean Diff. = difference in means; SE Diff. = standard error of the difference of means; N1 and N2 are the sample sizes of compared means; q = Tukey's critical q value; p-values less than the significance level of $\alpha = 0.05$ are bolded.

Appendix F.

Diagnostics report and summary statistics of R123 uptake assay

Diagnostics of the residuals from this assay revealed potential violations of the critical ANOVA assumptions of homoscedasticity (Figure 1) and normal distribution (Figure 3), thus a Box-Cox transformation (λ = 0.4) was applied to the original data to improve the fit of the statistical model. The transformation greatly improved homoscedasticity of the residuals (Figure 4), while no significant departure from normality was observed (Figure 6). Thus, the transformation resulted in an improved overall fit for the ANOVA. While the statistics were performed on the transformed data, all data were back-transformed to the original data to present the results (see Figure 4, Results section).

Figure F.1: Assessment of homoscedasticity

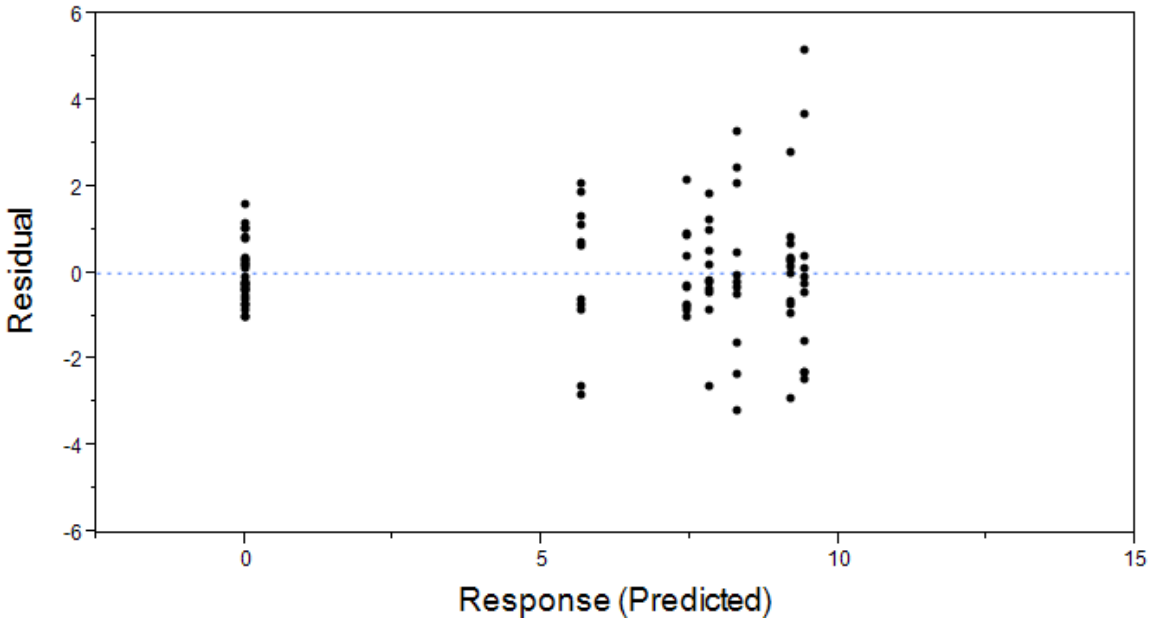

A plot of the error terms (residuals) *vs.* the predicted response (liver R123). Note: Prior to the diagnostic analysis of residuals, one outlier was identified by the Grubbs test (α = 0.05), and removed from the analysis. The residuals show moderate heteroscadisticity with relatively uneven distributions about the y = 0 regression line. However, the Brown-Forsythe test failed to reject the null-hypothesis of equal sample variance, F (8, 86) = 1.7678, p = 0.0946.

Figure F.2: Independence of errors

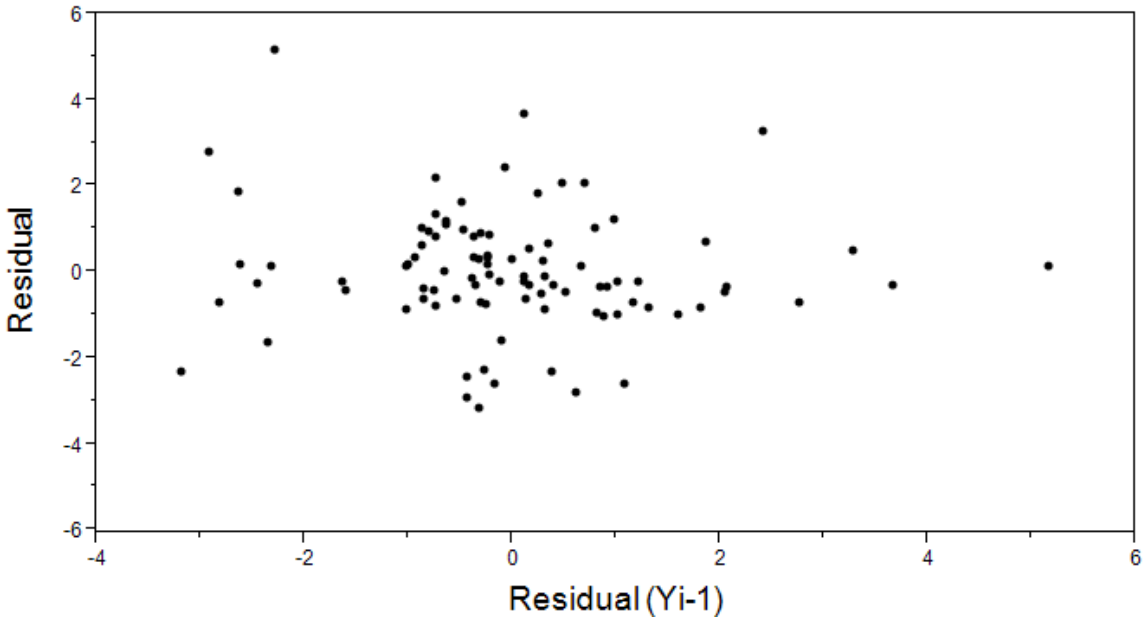

A lag plot of residuals vs. residual (Y_{i-1}) to visually check the assumption of independent errors. The residual values show random scattering with no clear pattern, suggesting the errors are independent.

Figure F.3: Assessment of normal distribution

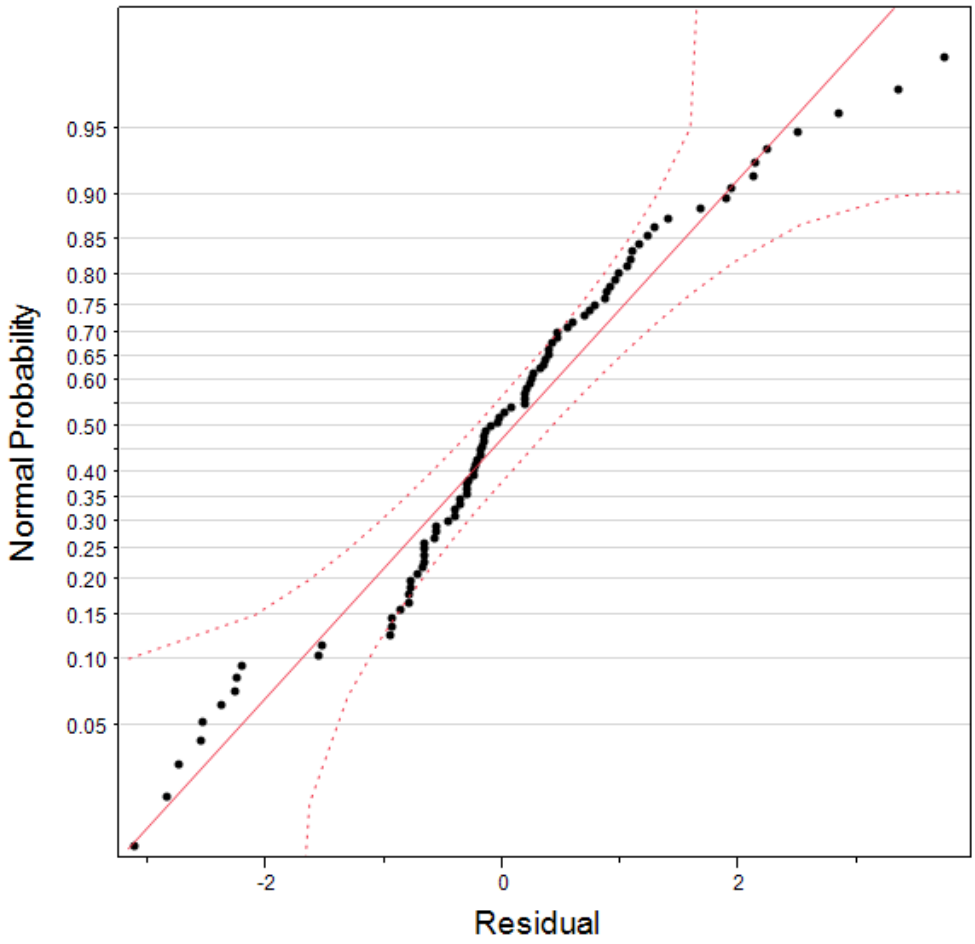

A normal probability plot showing normal probability vs. residual response. The solid diagonal line represents an ideal Gaussian distribution. Parameter estimates *N* (μ, σ) show the distribution of the residuals is approximately centered around 0 (mean distribution, μ ≈ 0) with standard deviation (σ) ≈ 1.47. The Shapiro-Wilk goodness-of-fit test rejected the null hypothesis that the residuals are from a normal distribution (W = 0.9679, p = 0.0197). Therefore, normality of the residuals (error terms) cannot be assumed in this model.

Figure F.4: Assessment of homoscedasticity following Box-Cox transformation

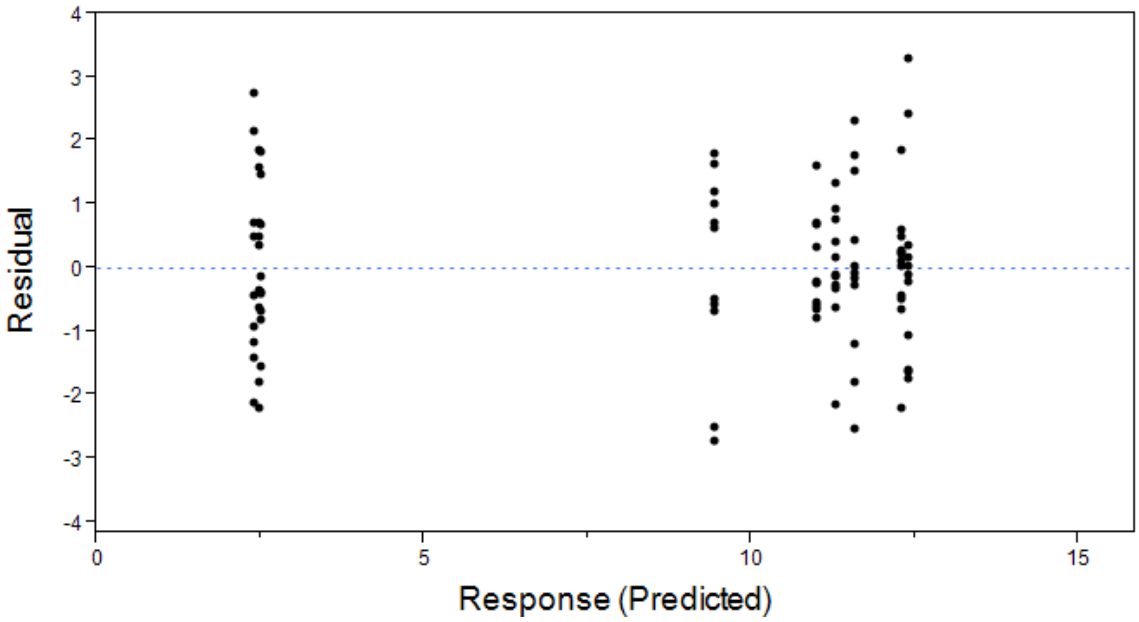

A plot of the error terms (residuals) *vs.* the predicted response (liver R123). After converting the original data using a Box-Cox transformation (λ = 0.4), the residuals show an improved degree of homoscedasticity (by visual inspection). The Brown-Forsythe test failed to reject the null-hypothesis of equal sample variance, F (8, 86) = 1.1774, p = 0.3221.

Figure F.5: Independence of errors following Box-Cox transformation

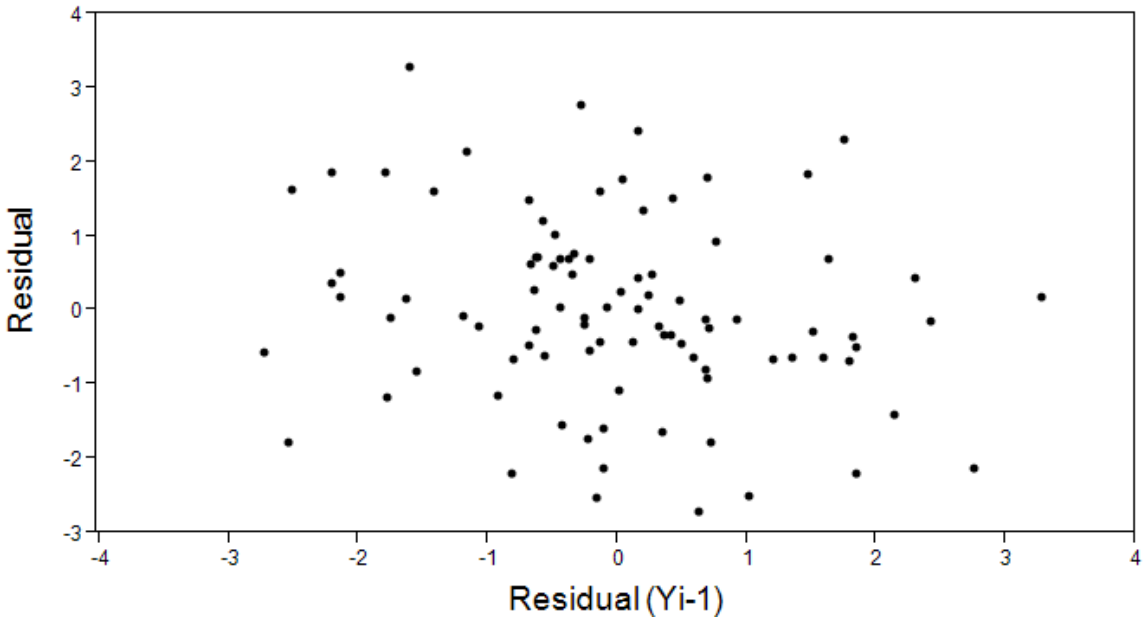

A lag plot of residuals vs. residual (Y_{i-1}) to visually check the assumption of independent errors following Box-Cox transformation ($\lambda = 0.4$) of data. The residual values show random scattering with no clear pattern, suggesting the errors are independent.

Figure F.6: Assessment of normal distribution following Box-Cox transformation

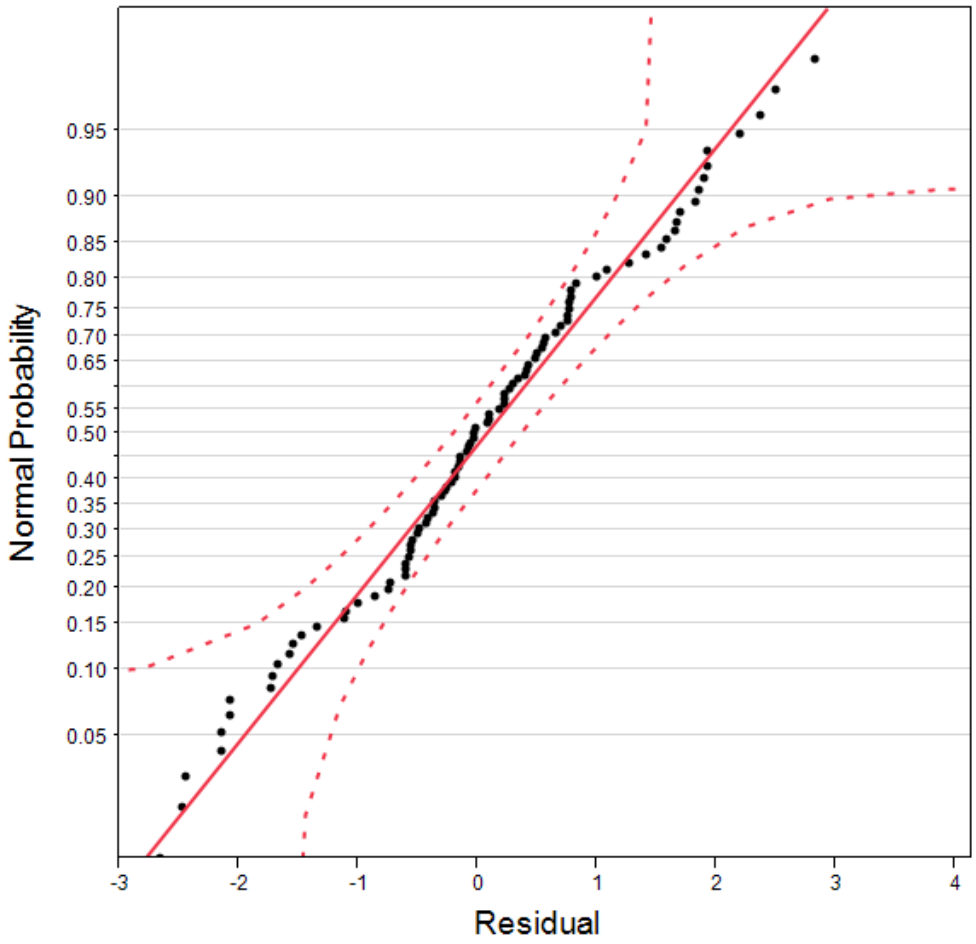

A normal probability plot showing normal probability vs. residual response following a Box-Cox transformation ($\lambda = 0.4$) of the original data. Parameter estimates *N* (μ, σ) show the distribution of the residuals is approximately centered around 0 (mean distribution, $\mu \approx 0$) with standard deviation (σ) $\approx$ 1.24. The Shapiro-Wilk goodness-of-fit test failed to reject the null hypothesis that the residuals are from a normal distribution ($W = 0.9863$, $p = 0.4307$). Thus, a square root transformation of the original data successfully improved the assumption of normality.

Analysis of variance (ANOVA) and multiple-comparison report for R123 uptake assay

Table F.1: ANOVA report

Source	DF	Sum of Squares	Mean Square	F Ratio	Prob > F
Model	8	1595.29	199.41	119.36	<.0001
Error	86	143.68	1.67		
Total	94	1738.97			

Summary statistics of two-way ANOVA on Box-Cox transformed data (λ = 0.4) from the R123 uptake assay.

Table F.2: Parameter effects

Source	DF	Sum of Squares	F Ratio	Prob > F
Drug	2	24.49	7.33	0.0012
Time	2	1546.18	462.74	<.0001
Drug*Time	4	14.69	2.20	0.0759

Summary statistics of two-way ANOVA on data from R123 uptake assay.

Figure F.7: Assessment of interaction between factors (drug and time)

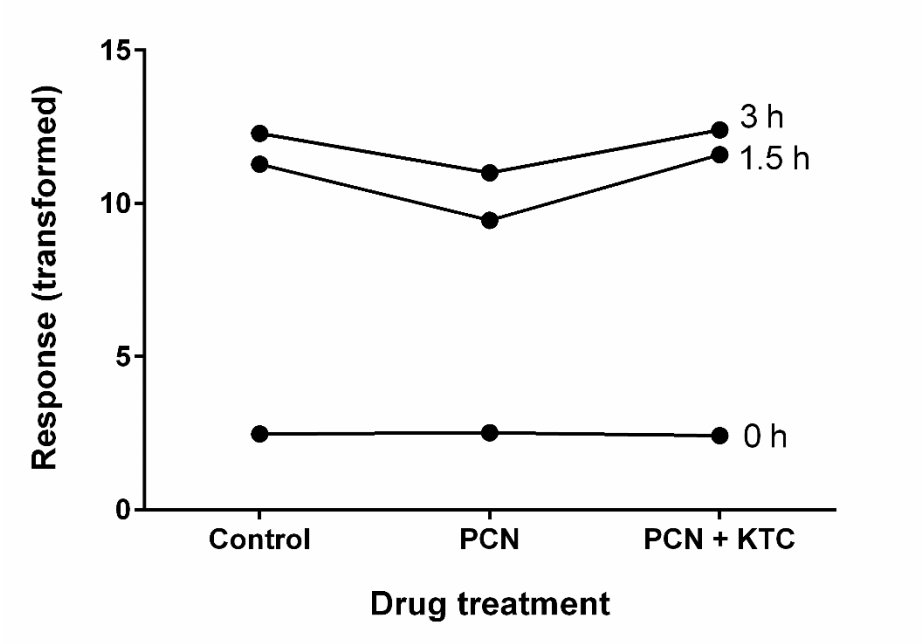

An interaction plot between factor levels (drug treatments and time points). The zero-hour (no R123) time point shows a moderate degree of anti-parallelism with the 1.5 and 3 h time points. However, the overall effect of drug treatment (control, PCN, or PCN + KTC) on the measured response (liver R123 quantity) does not significantly depend on the time point of the assay (see table X above).

Table F.3: Summary of multiple comparisons test

Test details	Mean Dif	SE	N1	N2	q	DF	p-value
0 h							
Control vs. PCN	-0.04524	0.6093	9	9	0.105	86	0.997
Control vs. PCN + KTC	0.05608	0.6093	9	9	0.1302	86	0.9953
PCN vs. PCN + KTC	0.1013	0.6093	9	9	0.2352	86	0.9849
1.5 h							
Control vs. PCN	1.827	0.5511	11	11	4.687	86	**0.0038**
Control vs. PCN + KTC	-0.3136	0.5511	11	11	0.8047	86	0.8369
PCN vs. PCN + KTC	-2.14	0.5511	11	11	5.492	86	**0.0006**
3 h							
Control vs. PCN	1.285	0.5395	12	11	3.368	86	0.0504
Control vs. PCN + KTC	-0.1103	0.5277	12	12	0.2957	86	0.9762
PCN vs. PCN + KTC	-1.395	0.5395	11	12	3.657	86	**0.0303**

Summary of Tukey's HSD post-hoc test for the R123 uptake assay. Comparison of means between drug treatments (Control, PCN, or PCN +KTC) is organized by each time point (0 – 3 h). Mean Diff. = difference in means; SE Diff. = standard error of the difference of means; N1 and N2 are the sample sizes of compared means; q = Tukey's critical q value; p-values less than the significance level of $\alpha = 0.05$ are bolded. One outlier from the PCN, 3h group was identified by Grubbs outlier test and removed from the analysis.

Appendix G.

Diagnostics and summary statistics of gene expression data

Residual analysis of *abcb4* expression data support the assumptions of homoscedasticity (equal variance) and independence of errors; however, the assumption of normal distribution could not be upheld (Figure 3). Because a Box-Cox transformation did not improve departure from normality, the statistical analysis was performed using the non-parametric Wilcoxon Rank Sums and Steel-Dwass multiple-comparison tests on the untransformed data (α = 0.05) (Table 1

Figure G.1: Assessment of homoscedasticity

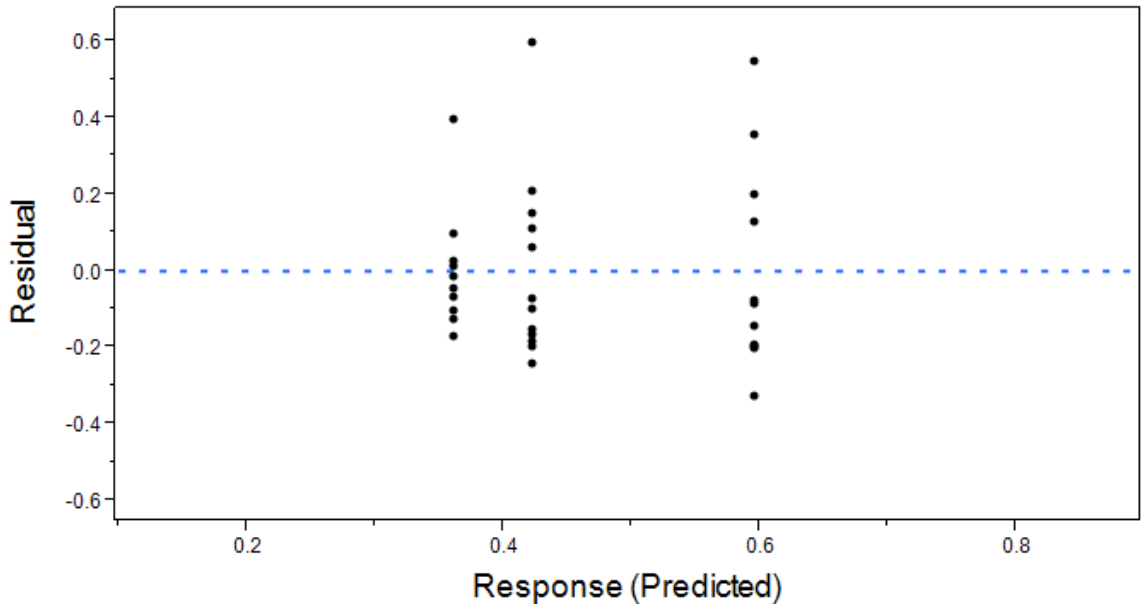

A plot of the error terms (residuals) *vs.* the predicted response (liver R123)., and removed from the analysis. The residuals show homoscedasticity with relatively even distributions about the y = 0 regression line. Furthermore, the Brown-Forsythe test failed to reject the null-hypothesis of equal sample variance, F (2, 30) = 0.9522, p = 0.3973. The assumption of equal variance is upheld.

.

Figure G.2: Assessment of independent errors

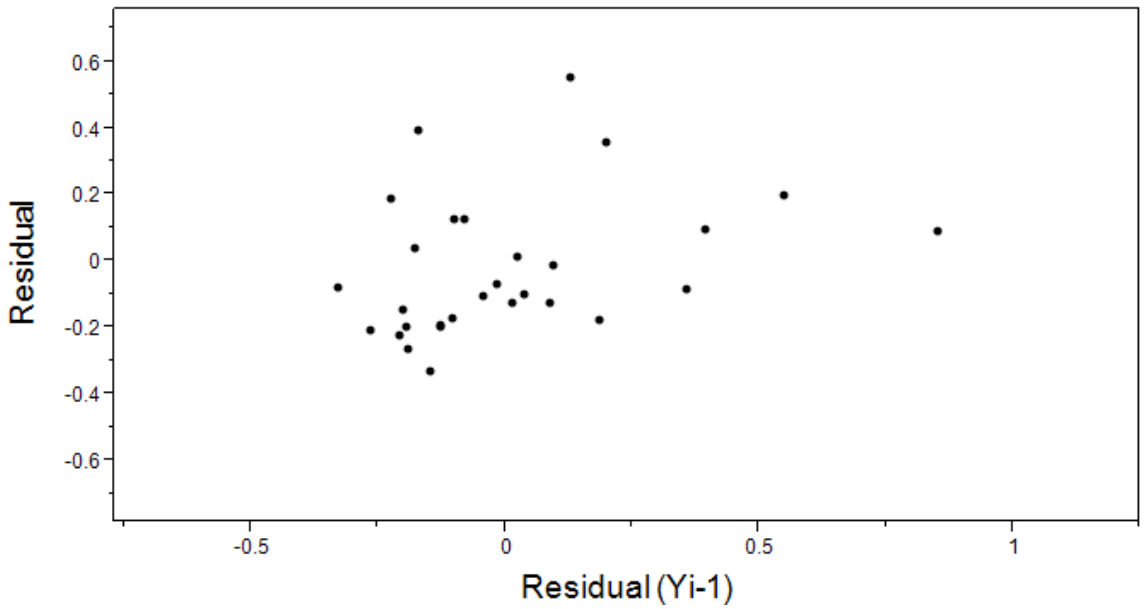

A lag plot of residuals vs. residual (Y_{i-1}) to visually check the assumption of independent errors. The residual values show random scattering with no clear pattern, suggesting the errors are independent.

Figure G.3: Assessment of normal distribution

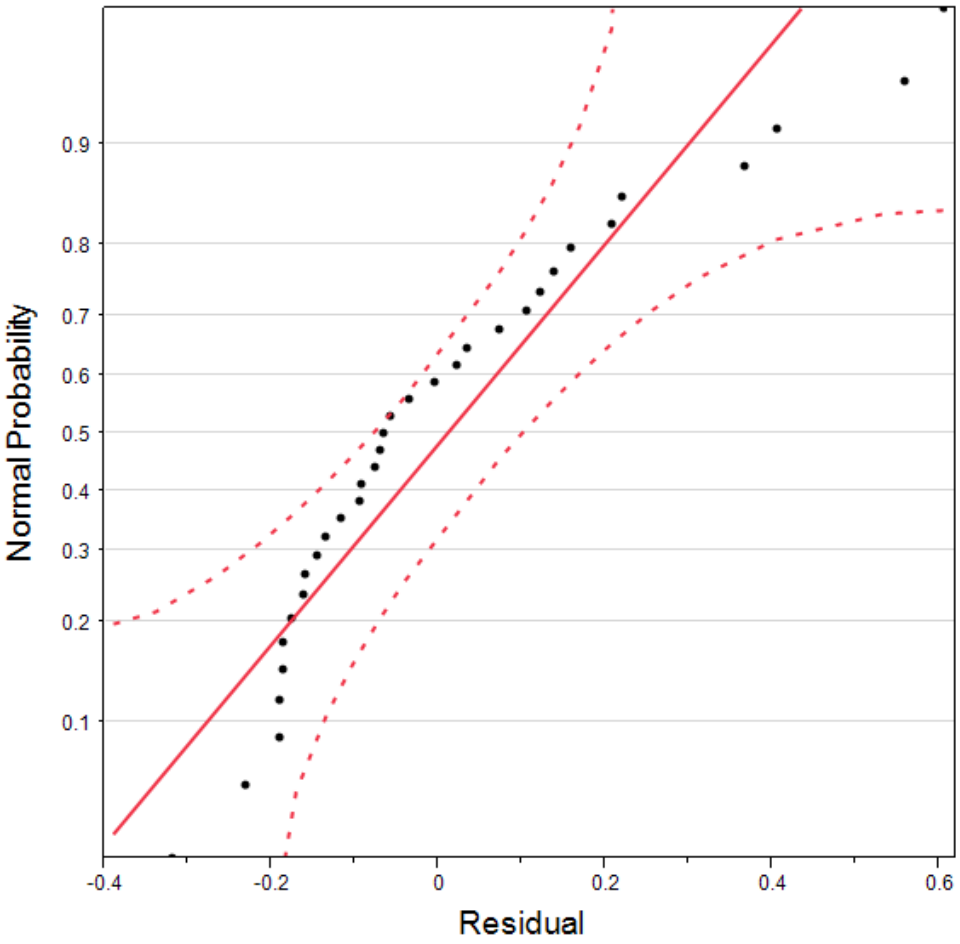

A normal probability plot showing normal probability vs. residual. Parameter estimates *N* (μ, σ) show the distribution of the residuals is approximately centered around 0 (mean distribution, μ ≈ 0) with standard deviation (σ) ≈ 0.22. Curvature of the normal probability vs. residual line indicates some departure from normality. The Shapiro-Wilk goodness-of-fit test rejected the null hypothesis that the residuals are from a normal distribution (W = 0.8937, p = 0.0037). Thus, the assumption of normality cannot be met.

Kruskal-Wallis Rank Sums and multiple comparisons summary statistics

Table G.1: Kruskal-Wallis Rank Sums report

Level	N	Score Sum	Expected Score	Score Mean
Control	11	251	187	22.8182
PCN + KTC	12	182	204	15.1667
PCN	10	128	170	12.8

Chi-Square	DF	Prob > Chi-Sq.
6.3005	2	0.0428

Summary statistics of the non-parametric Kruskall-Wallis Rank Sums test. N = sample number in each level; DF = Degrees of freedom; Prob. > Chi-Square = p-value of test.

Table G.2: Steel-Dwass multiple-comparisons report

Comparison	Mean Dif	SE Dif	Z	p-Value	95% C.I.
PCN vs. PCN + KTC	-0.825	2.780	-0.297	0.9526	[-0.28, 0.14]
Control vs. PCN + KTC	-4.617	2.831	-1.631	0.2326	[-0.47, 0.09]
Control vs. PCN	-6.968	2.711	-2.570	**0.0274**	[-0.53, -0.01]

Summary statistics of the non-parametric Steel-Dwass multiple comparisons test. Mean Dif = mean difference between compared levels; SE Dif = Standard error of the difference in means; Z = standardized test statistic; 95% C.I. = 95% confidence interval of the mean difference.

Appendix H.

Diagnostics and summary statistics of *cyp3a65* gene expression

Residual analysis of the *cyp3a65* expression data revealed the assumptions of homoscedasticity and normality could not be supported (Figure 1). Thus, a Box-Cox transformation (λ = - 2) was performed on the original data (anchored at 1) in order to improve the fit of the data to the statistical model. The transformation increased homoscedasticity (Figure 4), and improved the departure from normality to satisfy the model assumptions (Figure 6), thus the statistical analysis was performed on the transformed data by one-way ANOVA and Tukey's Honest Significant Differences (HSD) multiple-comparisons tests (α = 0.05) (Table 1).

Figure H.1: Assessment of homoscedasticity

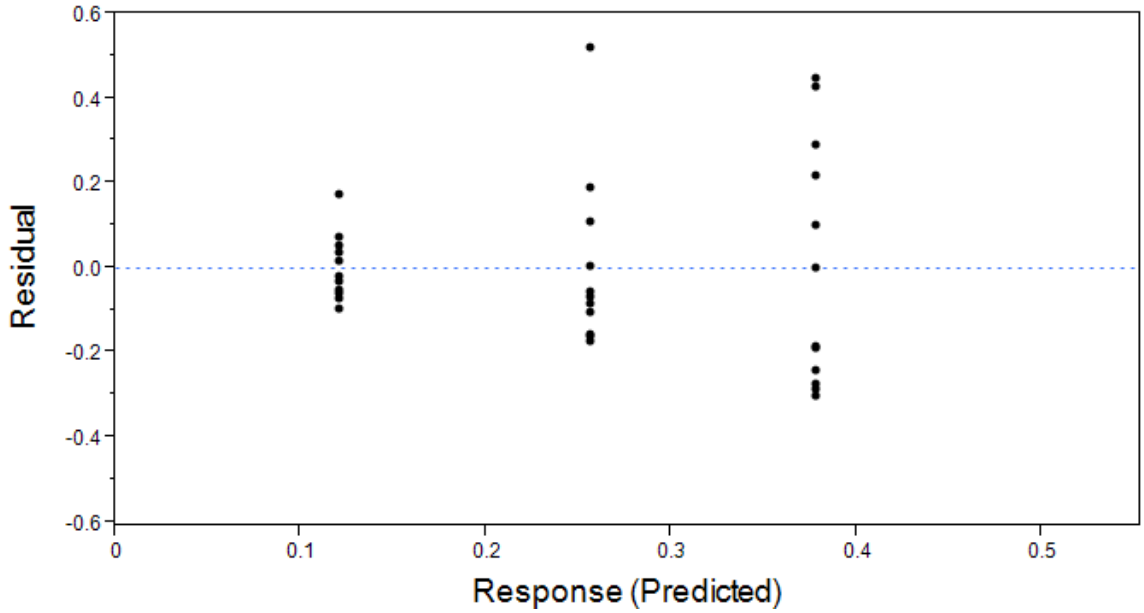

A plot of the error terms (residuals) *vs.* the predicted response (liver R123), The residuals show considerable heteroscedasticity (unequal variance), as variance increases with the predicted response. Furthermore, the Brown-Forsythe test rejected the null-hypothesis of equal variance, $F(2, 31) = 5.3595$, $p = 0.0100$.

.

Figure H.2: Assessment of independent errors

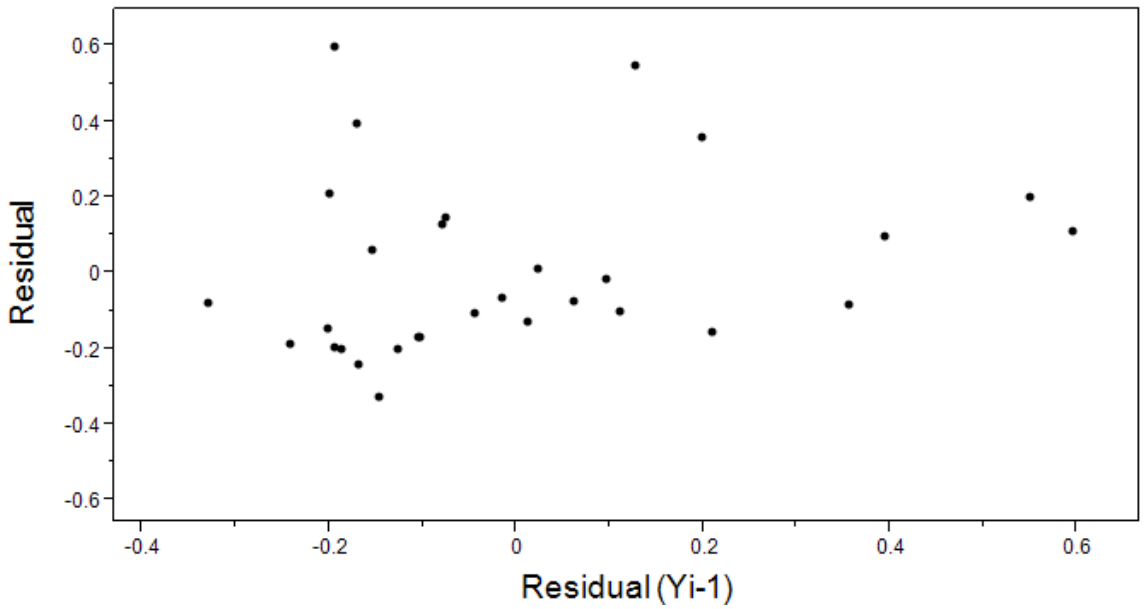

A lag plot of residuals vs. residual (Y_{i-1}) to visually check the assumption of independent errors. The residual values show random scattering with no clear pattern, suggesting the errors are independent.

Figure 3: Assessment of normal distribution

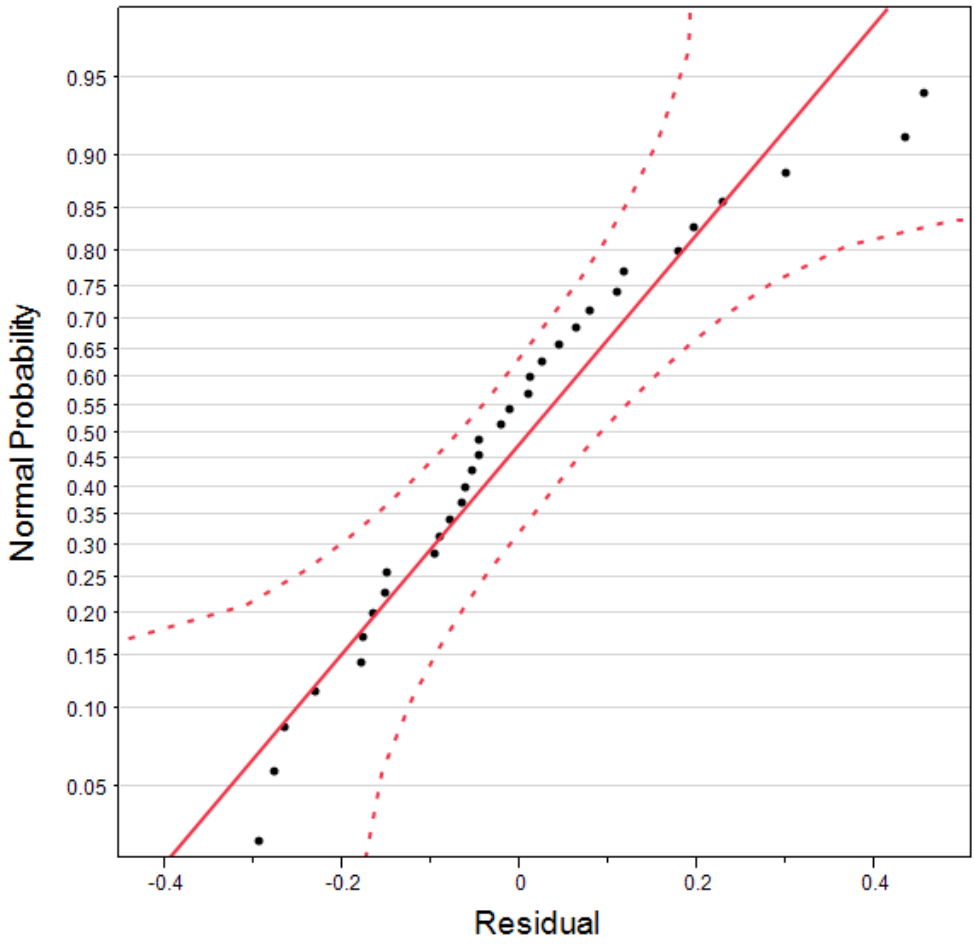

A normal probability plot showing normal probability vs. residual. Parameter estimates *N* (μ, σ) show the distribution of the residuals is approximately centered around 0 (mean distribution, μ ≈ 0) with standard deviation (σ) ≈ 0.21. Moderate curvature of the normal probability vs. residual line indicates departure from normality. The Shapiro-Wilk goodness-of-fit test rejected the null hypothesis that the residuals are from a normal distribution (W = 0.9352, p = 0.0447). Thus, the assumption of normal distribution cannot be met.

Diagnostics and summary statistics of *cyp3a65* gene expression following Box-Cox transformation

Figure H.4: Assessment of homoscedasticity following Box-Cox transformation

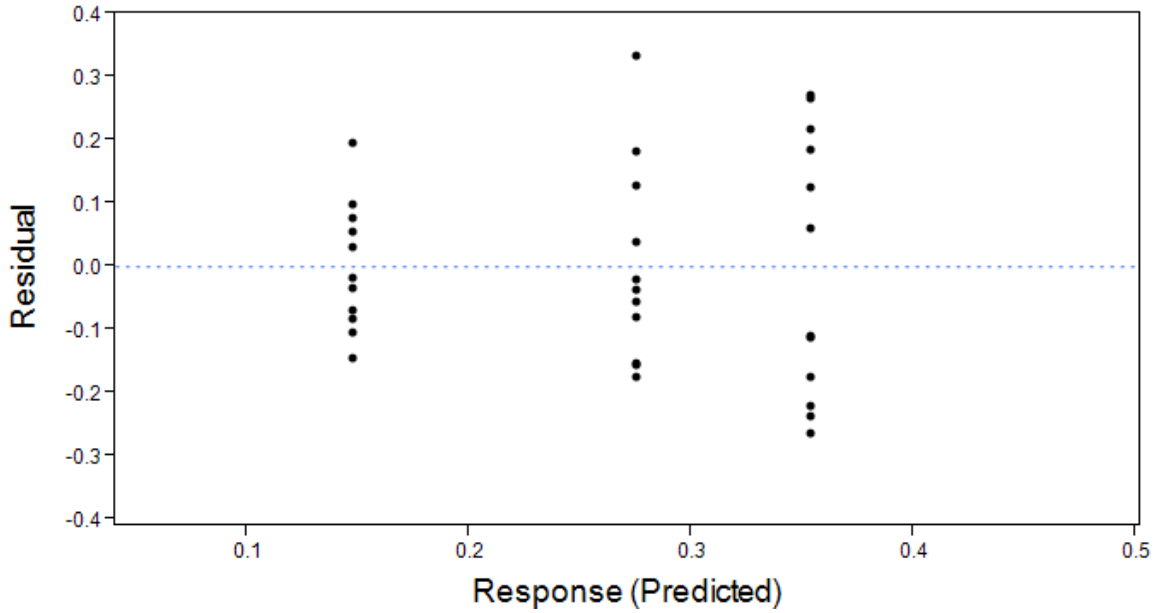

A plot of the error terms (residuals) *vs.* the predicted response (liver R123)., Following a Box-Cox transformation (λ = -2), the residuals show a marked improvement in homoscedasticity. The Brown-Forsythe test failed to reject the null-hypothesis of equal sample variance, F (2, 30) = 0.9522, p = 0.3973.

.

Figure H.5: Assessment of independent errors following Box-Cox transformation

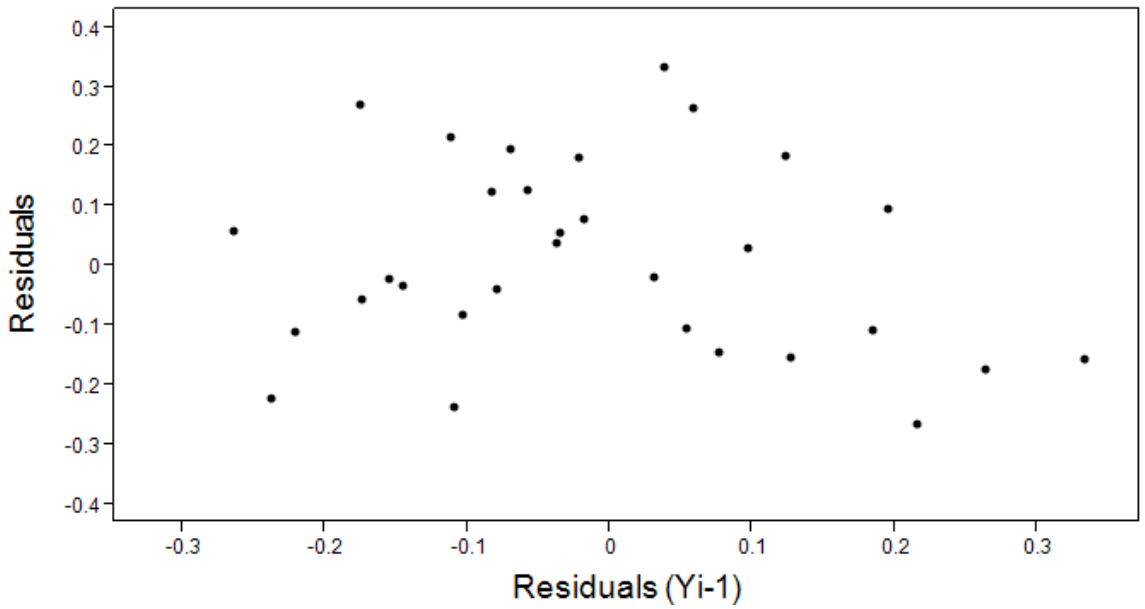

A lag plot of residuals vs. residual (Y_{i-1}) to visually check the assumption of independent errors. Following the Box-Cox transformation ($\lambda = -2$), the residuals appear randomly distributed about the plot. The assumption of independent errors is therefore upheld.

Figure H.6: Assessment of normal distribution following Box-Cox transformation

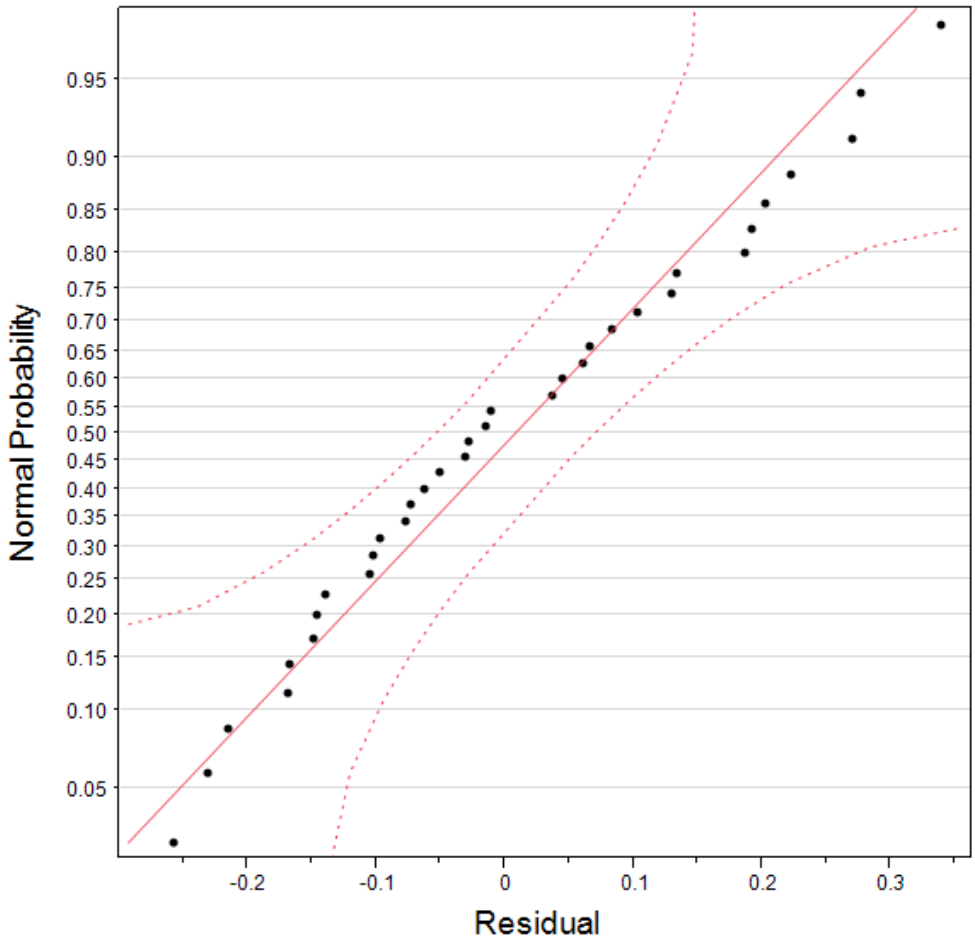

A normal probability plot showing normal probability vs. residual following a Box-Cox transformation (λ = -2). Parameter estimates *N* (μ, σ) show the distribution of the residuals is approximately centered on 0 (mean distribution, μ ≈ 0) with standard deviation (σ) ≈ 0.16. Relative to the original data, the transformed residuals show increased linearity in the plot, indicating a closer fit to normality. In addition, the Shapiro-Wilk goodness-of-fit test failed to reject the null hypothesis that the residuals are from a normal distribution (W = 0.9540, p = 0.1621). Thus, normality can be assumed and the log transformed data show an improved fit for the statistical model.

Analysis of variance (ANOVA) and multiple comparisons summary statistics

Table H.1: ANOVA report

Source	DF	Sum of Squares	Mean Square	F Ratio	*p*-value
Factor	2	0.247	0.124	4.641	**0.0173**
Error	31	0.826	0.027		
C. Total	33	1.074			

Summary statistics of one-way ANOVA. DF = degrees of freedom. Factor = drug treatment.

Table H.2: Tukey's HSD multiple-comparisons report

Comparison	Mean Dif	SE	p-Value	95% C.I.
Control vs. PCN	0.206	0.068	0.0133	[0.04, 0.37]
PCN vs. PCN + KTC	0.128	0.070	0.1745	[-0.04, 0.30]
Control vs. PCN + KTC	0.078	0.068	0.4903	[-0.09, 0.25]

Summary statistics of Tukey's honest significant differences (HSD) multiple comparisons test. Mean Dif = mean difference between compared levels; SE = Standard error of the difference in means; 95% C.I. = 95% confidence interval.

Appendix I.

Diagnostics and summary statistics of *nr1i2 (pxr)* gene expression

. Residual analysis of the *nr1i2* expression data revealed sufficient homoscedasticity and independence of errors; however, the residuals showed a moderate departure from normality with curvature in the normality plot. A Box-Cox transformation did not improve the assumption of normality, therefore the statistical analysis for differences in means was performed using the non-parametric Wilcoxon Rank Sums test (α = 0.05) on the original data (Appendix H).

Figure I.1: Assessment of homoscedasticity

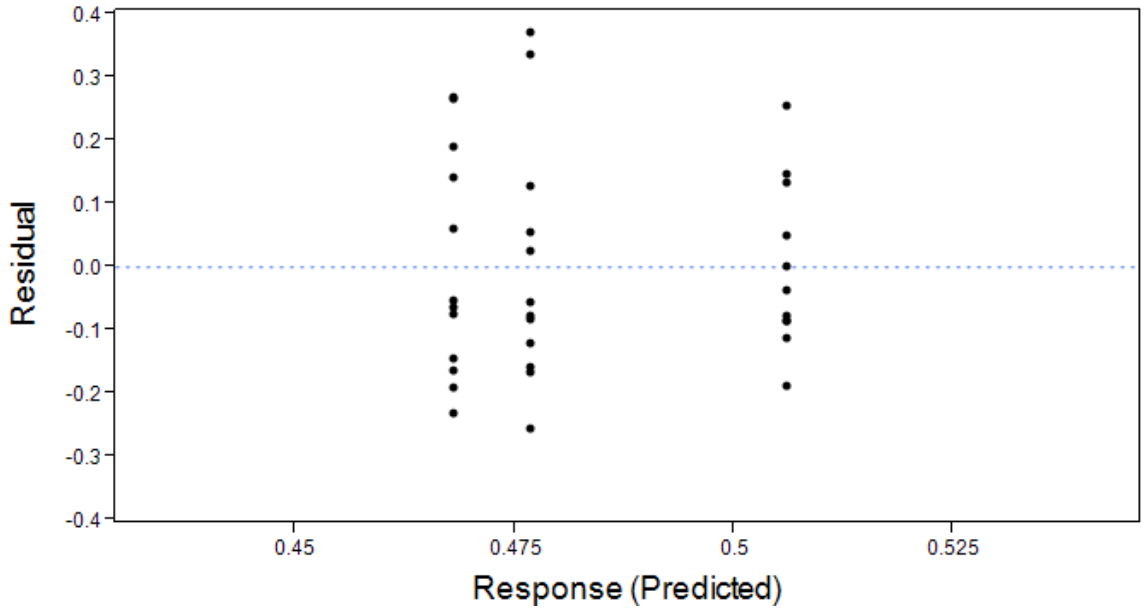

A plot of the error terms (residuals) *vs.* the predicted response from the regression, and removed from the analysis. The residuals show homoscedasticity with relatively even distributions about the y = 0 regression line. Furthermore, the Brown-Forsythe test failed to reject the null-hypothesis of equal sample variance, F (2, 30) = 0.9522, p = 0.3973. The assumption of equal variance is upheld.

Figure I.2: Assessment of independent errors

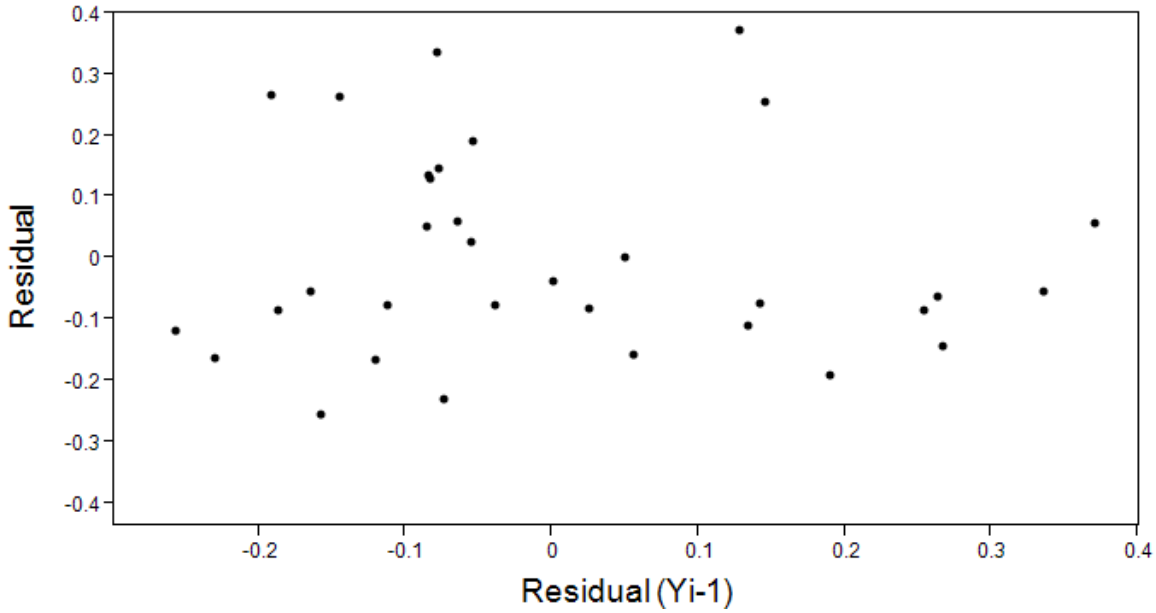

A lag plot of residuals vs. residual (Y_{i-1}) to visually check the assumption of independent errors. The residual values show random scattering with no clear pattern, suggesting the errors are independent.

Figure I.3: Assessment of normal distribution

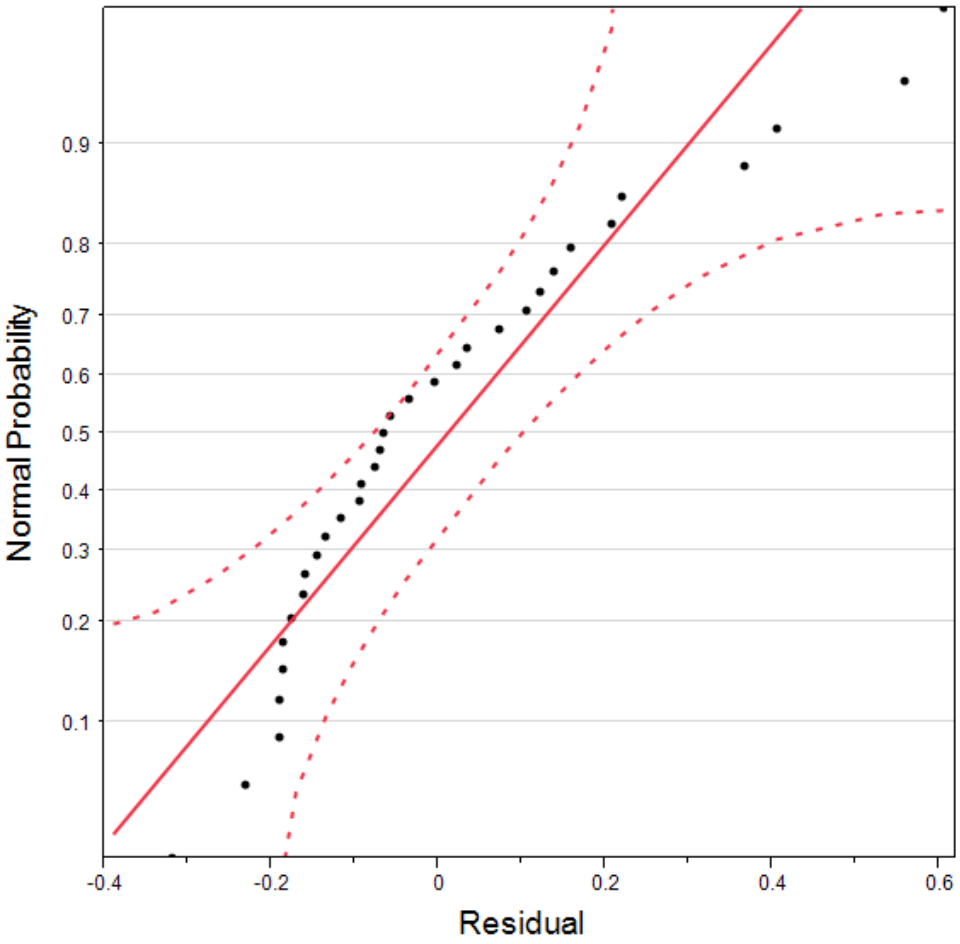

A normal probability plot showing normal probability vs. residual. Parameter estimates $N(\mu, \sigma)$ show the distribution of the residuals is approximately centered around 0 (mean distribution, $\mu \approx 0$) with standard deviation (σ) ≈ 0.17. Curvature of the normal probability vs. residual line indicates some departure from normality. The Shapiro-Wilk goodness-of-fit test barely failed to reject the null hypothesis that the residuals are from a normal distribution ($W = 0.9386$, $p = 0.0509$). Thus, the assumption of normality is not confidently met with this data.

Wilcoxon Rank Sums and multiple comparisons summary statistics

Table I.1: Wilcoxon Rank Sums report

Level	N	Score Sum	Expected Score	Score Mean
Control	12	204	216	17
PCN + KTC	12	201	216	16.75
PCN	11	225	198	20.45

Chi-Square	DF	Prob > Chi-Sq.
0.924	2	0.6300

Summary statistics of the non-parametric Wilcoxon Rank Sums test. N = sample number in each level; DF = Degrees of freedom; Prob. > Chi-Square = p-value of test.

Appendix J.

Diagnostics and summary statistics of *cyp3c1* gene expression

Residual analysis of the *cyp3c1* expression data revealed sufficient homoscedasticity and independence of errors, but normality could not be assumed (Figure 3). A Box-Cox transformation (λ = -0.2) improved all underlying assumptions of the model, including normality (Figures 4 - 6). Thus, the statistical analysis for differences in means was performed by one-way ANOVA (α = 0.05).

Figure J.1: Assessment of homoscedasticity

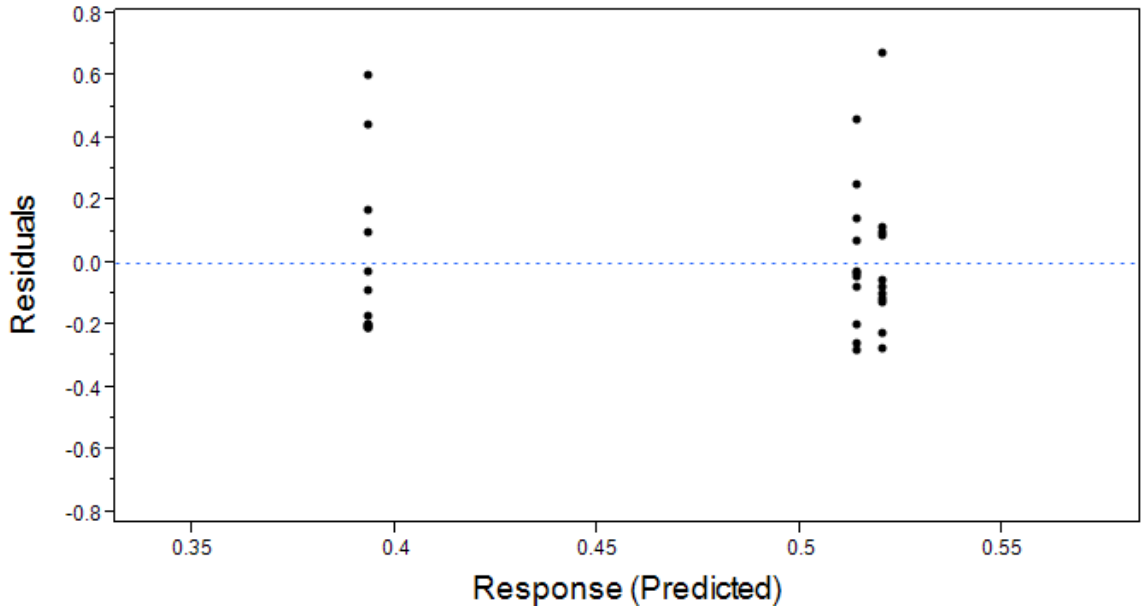

A plot of the error terms (residuals) *vs.* the predicted response (nr1i2 gene expression) from the regression, and removed from the analysis. The residuals show homoscedasticity. Furthermore, the Brown-Forsythe test failed to reject the null-hypothesis of equal sample variance, F (2, 31) = 0.1370, p = 0.8725. The assumption of equal variance is upheld.

Figure J.2: Assessment of independent errors

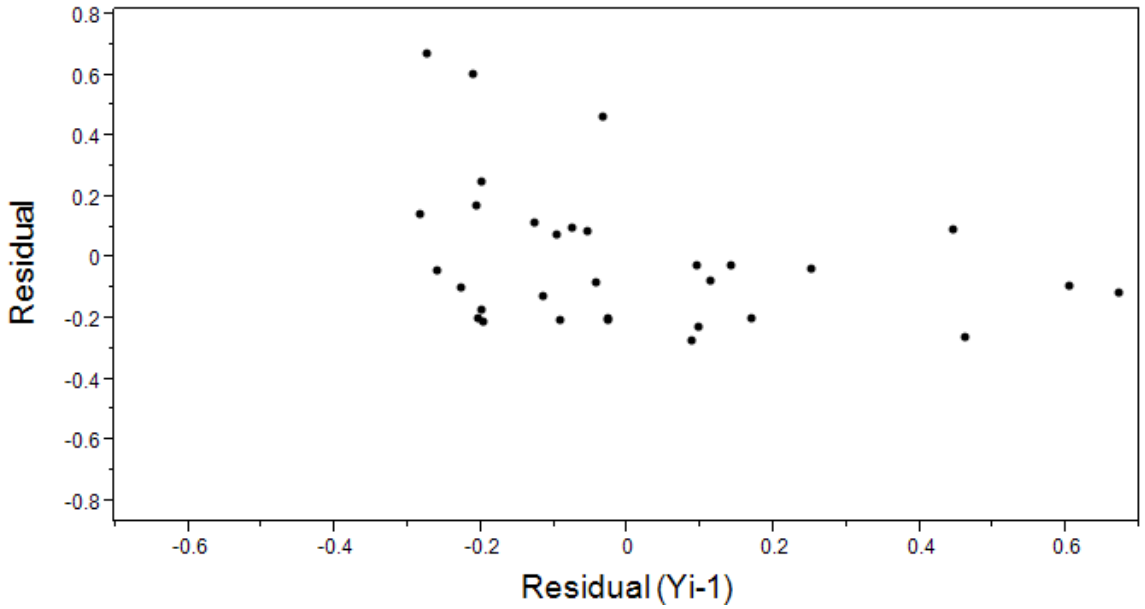

A lag plot of residuals vs. residual (Y_{i-1}) to visually check the assumption of independent errors. The residuals show some random scattering in the plot, suggesting the assumption of independent errors is upheld.

Figure J.3: Assessment of normal distribution

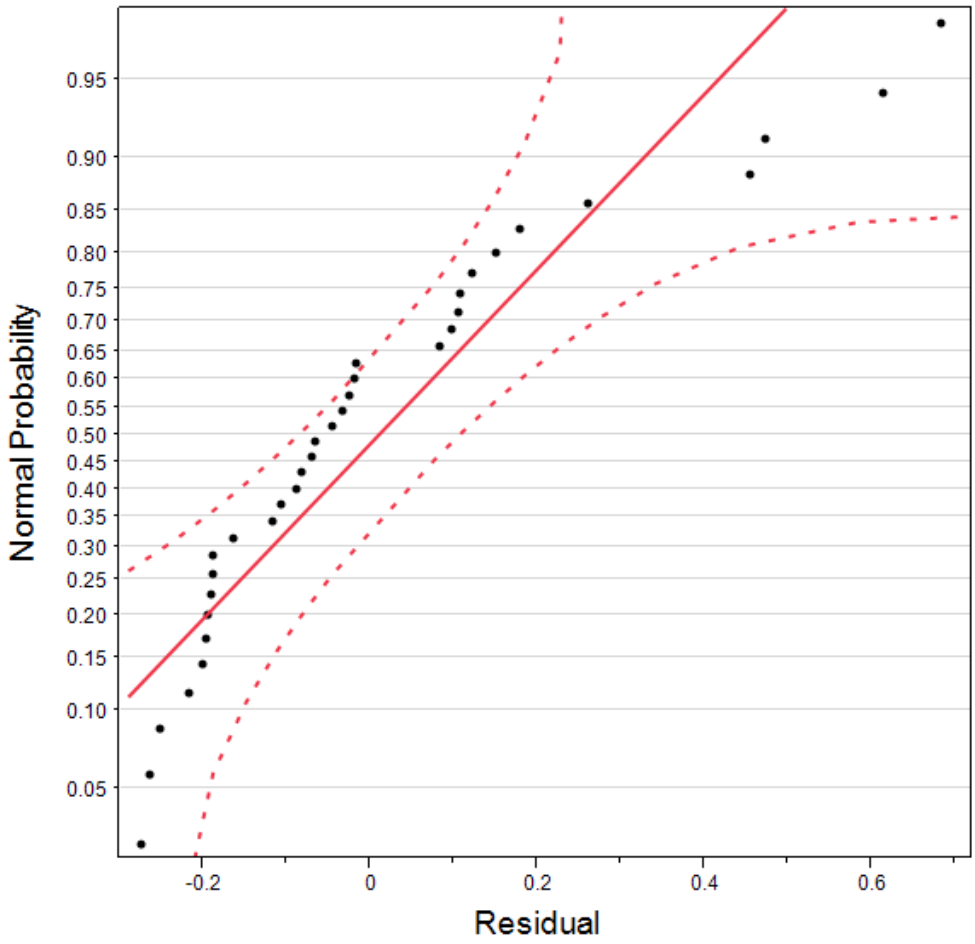

A normal probability plot showing normal probability vs. residual. Parameter estimates N (μ, σ) show the distribution of the residuals is approximately centered around 0 (mean distribution, $\mu \approx 0$) with standard deviation (σ) ≈ 0.25. Curvature of the normal probability vs. residual line indicates some departure from normality. Furthermore, the Shapiro-Wilk goodness-of-fit test rejected the null hypothesis that the residuals are from a normal distribution (W = 0.8665, p = 0.0007). Thus, the assumption of normality is not upheld.

Diagnostics and summary statistics of *cyp3c1* gene expression following Box-Cox transformation

Figure J.4: Assessment of homoscedasticity

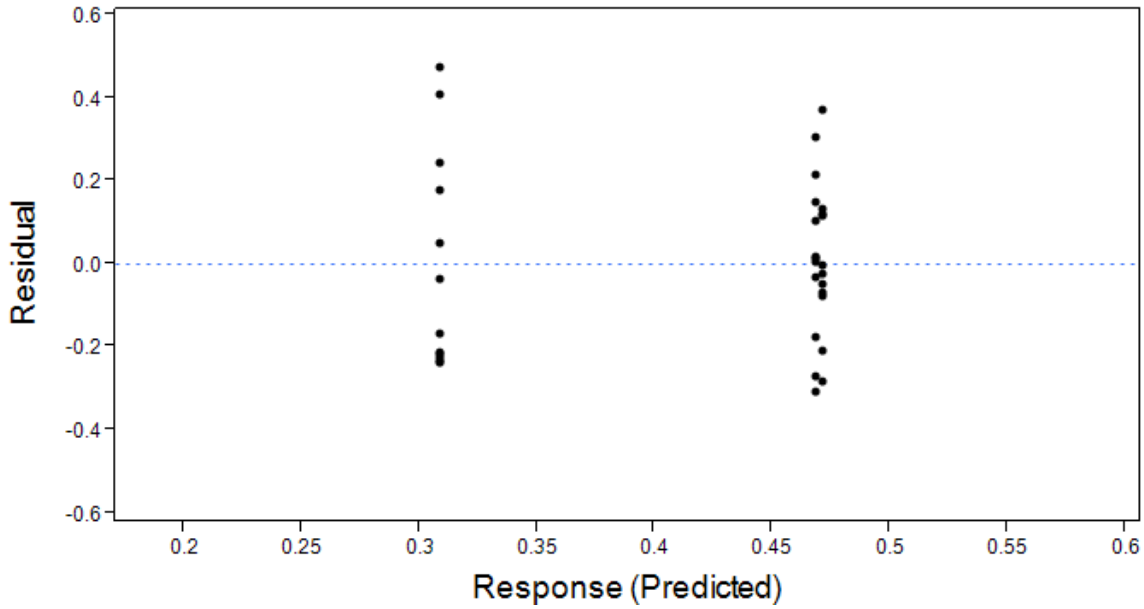

A plot of the error terms (residuals) *vs.* the predicted response from the regression. Following the Box-Cox transformation (λ = -0.2), the residuals show increased homoscedasticity with relatively even distributions about the y = 0 regression line. Furthermore, the Brown-Forsythe test failed to reject the null-hypothesis of equal sample variance, F (2, 31) = 1.2947, p = 0.2884. The assumption of equal variance is upheld.

Figure J.5: Assessment of independent errors following Box-Cox transformation

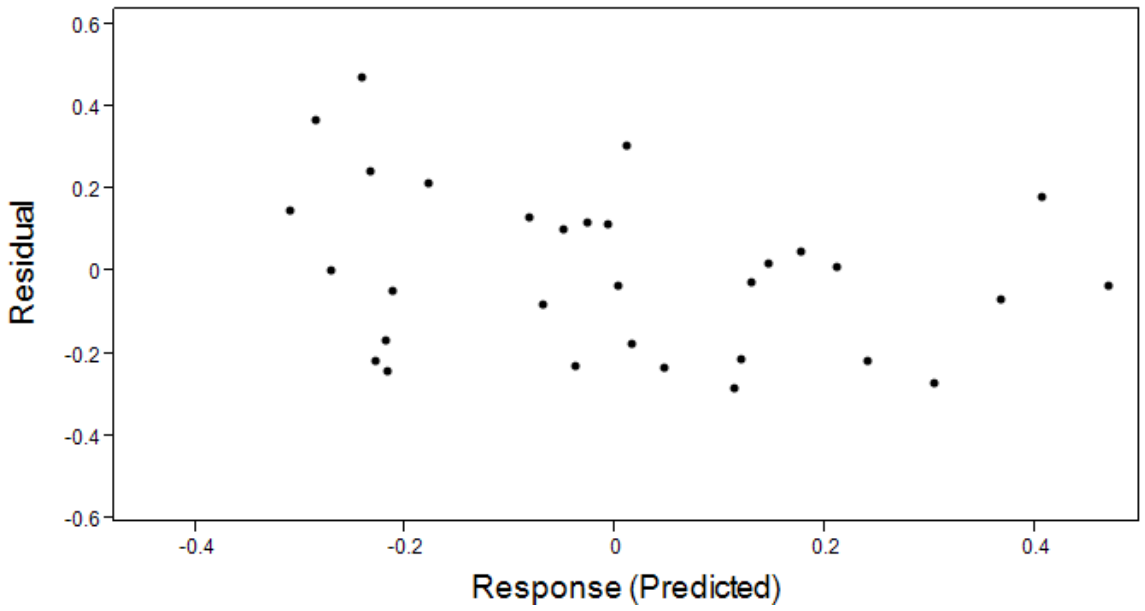

A lag plot of residuals vs. residual (Y_{i-1}) to visually check the assumption of independent errors following a Box-Cox transformation ($\lambda = -0.2$). The residuals show random scattering in the plot, suggesting the assumption of independent errors is upheld.

Figure J.6: Assessment of normal distribution following Box-Cox transformation

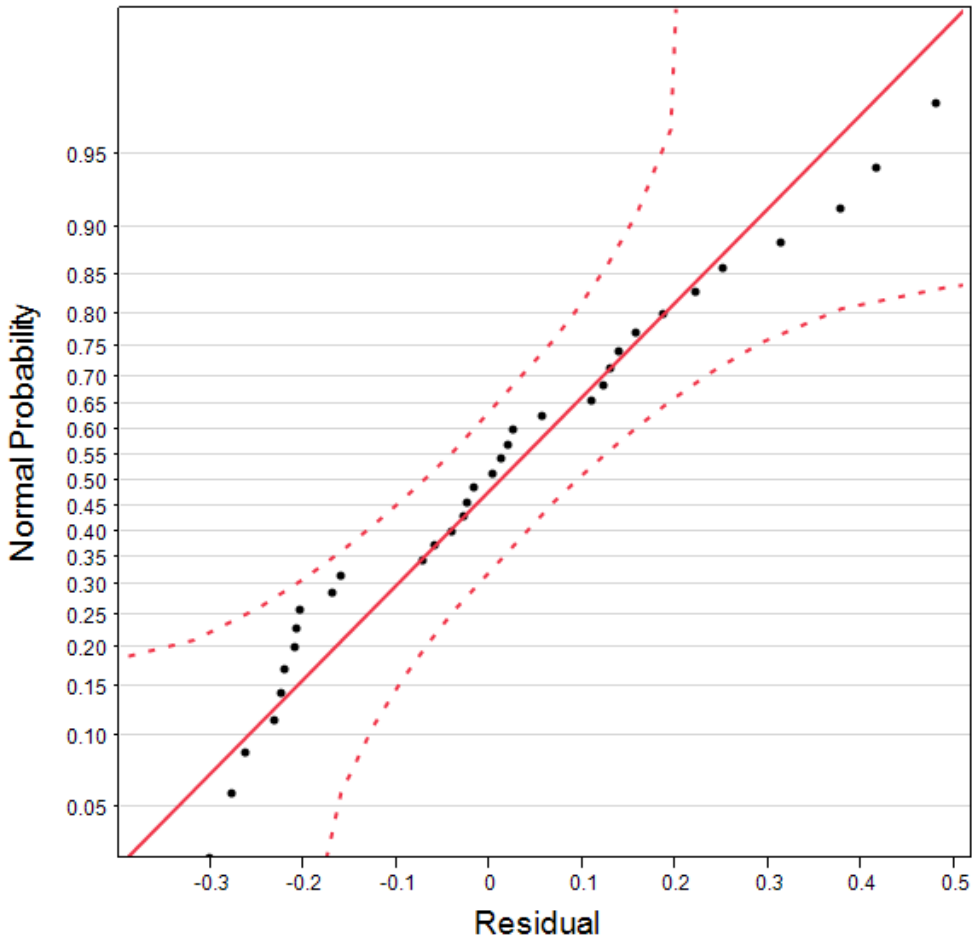

A normal probability plot showing normal probability vs. residual following a Box-Cox transformation ($\lambda = -0.2$). Parameter estimates $N(\mu, \sigma)$ show the distribution of the residuals is approximately centered around 0 (mean distribution, $\mu \approx 0$) with standard deviation (σ) ≈ 0.21. The residuals show improved linearity. The Shapiro-Wilk goodness-of-fit test failed to reject the null hypothesis that the residuals are from a normal distribution ($W = 0.9540$, $p = 0.1615$). Thus, the assumption of normality is upheld following the transformation.

Analysis of variance (ANOVA) report following Box-Cox transformation

Table J.1: ANOVA report

Source	DF	Sum of Squares	Mean Square	F Ratio	Prob > F
Factor	2	0.201	0.101	2.1341	0.1354
Error	31	1.461	0.047		
C. Total	33	1.663			

Summary statistics of the ANOVA. DF = Degrees of freedom.

Appendix K.

Area under curve (AUC) analysis of R123 kinetics

To assess the effect of chemical treatment on overall R123 kinetics, the area under the curve (AUC) method was performed on the R123 concentration vs. time curves for the R123 efflux and accumulation assays. The AUC analysis for serial sacrifice designs is described in detail by Bailer (1987). First, for each experimental group *g* at time *t* (note *t* = 1, 2, and 3 correspond to time points p_1 = 0 h, p_2 = 1.5 h, and p_3 = 3 h, respectively), the mean liver R123 concentration $\bar{y}_{g,t}$ and associated variance $s_{g,t}^2$ were calculated. Next, the linear trapezoid method was used to estimate the area under the curve AUC_g as follows:

$$AUC_g = \sum_{t=1}^{3} c_t \, \bar{y}_{g,t}$$

Where:

$$C_t = \begin{cases} \frac{1}{2}(p_2 - p_1) & \text{for } t = 1 \\ \frac{1}{2}[(p_2 - p_1) + (p_3 - p_2)] & \text{for } t = 2 \\ \frac{1}{2}(p_3 - p_2) & \text{for } t = 3 \end{cases}$$

According to Bailer, variance can be directly estimated for AUC_g because the area under the R123 concentration-time curve is determined by a "linear combination of independent variables" $\bar{y}_{g,t}$ with variance $s^2_{g,t}$ and sample size $n_{g,t}$ (for experimental group *g* at time *t*). Thus, the estimate of variance for each AUC_g was calculated as follows:

$$s^2(AUC_g) = \sum_{t=1}^{3} {c_t}^2 \left(\frac{{s_{g,t}}^2}{n_{g,t}} \right)$$

The two-tailed hypothesis test for significant differences of AUC_g is based around Z_{crit}, which is the critical Z value of a standard normal distribution with an upper tail probability of α/2 (α = significance level). Thus, Z_{crit} = 1.96 when α = 0.05 and Z_{crit} = 2.33 when α = 0.01. A contrast between two AUC_g produces Z_{obs} (the observed Z value), which is compared against Z_{crit} to determine significance. The Z_{obs} value for a contrast between experimental groups *g*= *i* and *j* is calculated using independent variances for each AUC_g as follows:

$$Z_{obs} = \frac{AUC_i - AUC_j}{\sqrt{s^2(AUC_i) + s^2(AUC_j)}}$$

Bonferroni's adjustment to account for the family-wise error rate was incorporated into the hypothesis test, whereby contrasts were considered statistically significant when $|Z_{obs}|$ was greater than the Bonferroni-adjusted Z_{crit} value of 2.394 ($\alpha = 0.05$) or 2.93 ($\alpha = 0.01$). The adjusted Z_{crit} for significance level $\alpha = 0.05$ was used to construct 95% confidence intervals for $AUC_j - AUC_j$ as follows:

$$(AUC_i - AUC_j) \pm Z_{crit} \sqrt{s^2(AUC_i) + s^2(AUC_j)}$$

Appendix L.

Figure L.1: RNA quality of control group

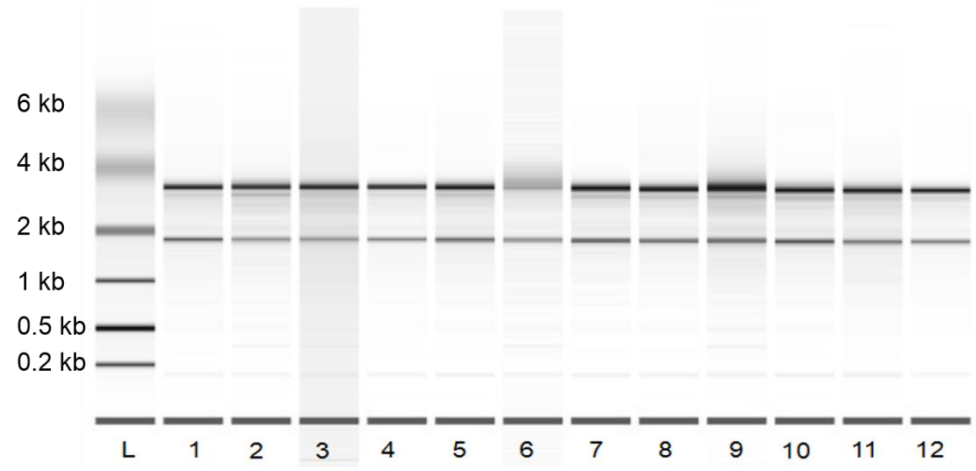

A simulated denaturing gel of total RNA from the control group, as generated by Agilent 2100 Expert software. The "L" lane is the RNA ladder (0.2 – 6.0 kb) used to verify the size of RNA fragments in each sample (lanes 1 – 12). The 28s and 18s ribosomal subunits are approximately 3.8 and 1.9 kb, respectively.

Table L.1: RNA quality of control group

Sample	1	2	3	4	5	6	7	8	9	10	11	12
RIN	8.4	8.2	n/a	8.8	8.4	n/a	8.7	8.8	8.1	8.5	8.2	8.9
28s : 18s	1.4	1.6	2.3	1.9	1.5	1.7	1.5	1.6	1.6	1.4	1.8	1.7

Sample RNA integrity numbers (RINs) and ratio of 28s to 18s ribosomal subunits generated by the Agilent Bioanalyzer 2100. The algorithm that calculates the RIN incorporates the curve of the electrophoretic trace (not shown) to provide a score ranging from 1 (severe degradation) to 10 (high quality, intact RNA). In cases where a RIN was not computable (samples 3 and 6), the ratio of 28s to 18s ribosomal RNA was used as an indicator of RNA quality. In general, RINs greater than 6 and rRNA ratios greater than 1 are adequate for downstream applications such as qPCR (Mueller et al, 2004).

Figure L.2: RNA quality of PCN-treated group

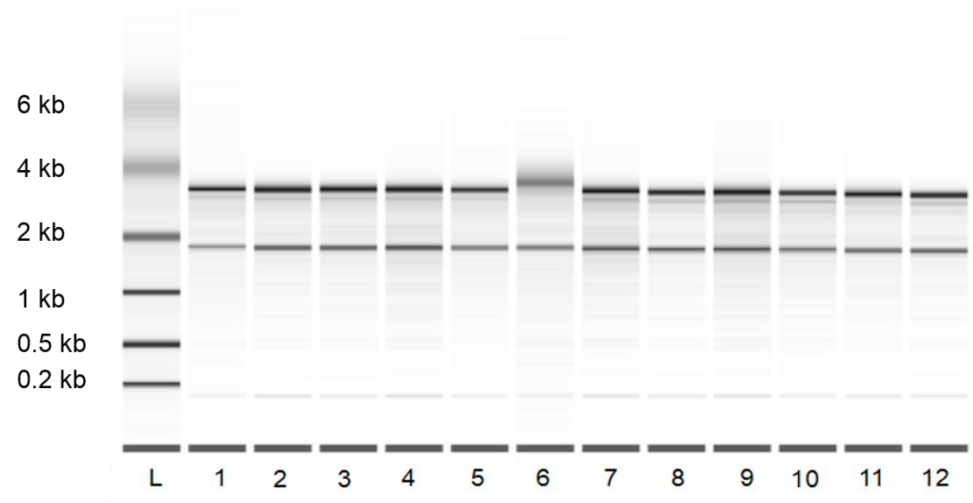

A simulated denaturing gel of total RNA from the PCN-treated group, as generated by Agilent 2100 Expert software. The "L" lane is the RNA ladder (0.2 – 6.0 kb) used to verify the size of RNA fragments in each sample (lanes 1 – 12). The 28s and 18s ribosomal subunits are approximately 3.8 and 1.9 kb, respectively.

Table L.2: RNA quality of PCN-treated group

Sample	**1**	**2**	**3**	**4**	**5**	**6**	**7**	**8**	**9**	**10**	**11**	**12**
RIN	8.4	8.4	8.2	7.7	8.3	8.7	7.7	8.5	7.7	8.1	8.5	8.6
28s : 18s	1.8	1.4	1.4	1.3	1.4	2.2	1.2	1.2	1.3	1.3	1.4	1.7

Sample RNA integrity numbers (RINs) and ratio of 28s to 18s ribosomal subunits produced by the Agilent Bioanalyzer 2100.

Figure L.3: RNA quality of PCN + KTC-treated group

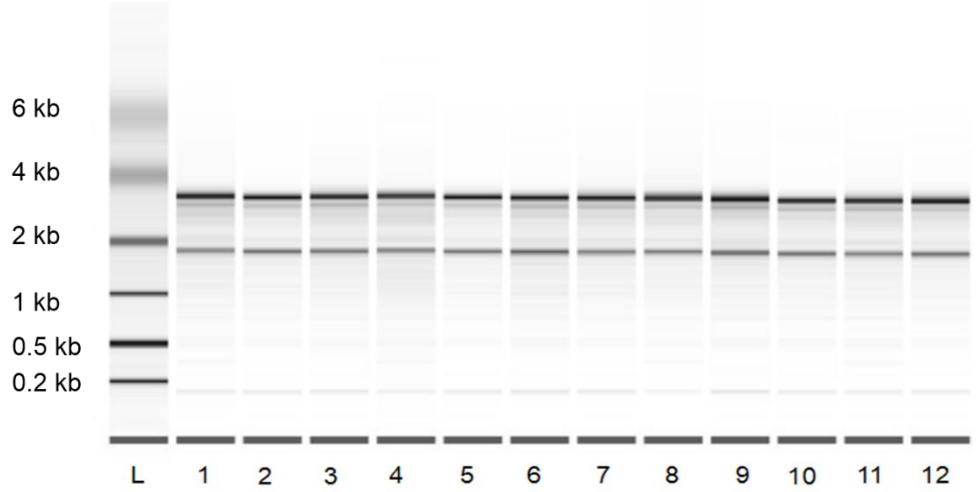

A simulated denaturing gel of total RNA from the PCN+KTC-treated group, as generated by Agilent 2100 Expert software. The "L" lane is the RNA ladder (0.2 – 6.0 kb) used to verify the size of RNA fragments in each sample (lanes 1 – 12). The 28s and 18s ribosomal subunits are approximately 3.8 kb and 1.9 kb, respectively.

Table L.3: RNA quality for PCN + KTC-treated group

Sample	1	2	3	4	5	6	7	8	9	10	11	12
RIN	7.8	8.3	8	7.8	8.6	7.9	8.1	8.4	8.1	8.3	8.1	8.5
28s : 18s	1.6	1.4	1.4	1.5	1.5	1.2	1.6	1.7	1.4	1.3	1.5	1.6

Sample RNA integrity numbers (RINs) and ratio of 28s to 18s ribosomal subunits produced by the Agilent Bioanalyzer 2100.

Appendix M.

Table M.1: Target genes and primer pair sequences

Gene name	Primer sequence (5´- 3´)	Amplicon length	RefSeq (ncbi) accession no.
abcb4	F: TACTGATGATGCTTGGCTTAATC R: TCTCTGGAAAGGTGAAGTTAGG	159	NM_001114583.1
*abcb5**	F: CCATCGGAGAGCTGAACATTAG R: CGTCAACTTCCAGCCAAAGA	146	XM_005157969.1
nr1i2	F: AGTTCCGGCCTTTAGATCG R: GTCTGTGATCGATCCAGCT	81	NM_001098617.1
cyp3a65	F: CTTCGGCACCATGCTGAGAT R: AGATACCCCAGATCCGTCCATA	86	NM_001037438.1
cyp3c1	F: CACTAACAGACGGAATATGAATCC R: CTCCACCTCTCATCTTTAACCA	81	NM_212673.1
bactin2	F: GCAGAAGGAGATCACATCCCTGGC R: CATTGCCGTCACCTTCACCGTTC	322	NM_181601.4
ef1a	F: CTGTACCTGTGGGTCGTGTGGAGACTG R: CAGCCTTCTGTGCAGACTTTGTGACC	594	NM_131263.1

Primer pairs (F: forward, R: reverse) used for quantitative real time PCR of zebrafish target genes. * The primer pair shown for abcb5 was one of 5 primer pairs attempted for this target gene. All abcb5 primer pairs produced consistent qPCR standard curves indicating low transcript abundance at the limit of detection. Consequently, abcb5 expression analyses were not performed in this study. See a “typical” abcb5 qPCR standard curve and its associated melting curve in appendix figures 4 and 5, respectively.

Appendix N.

Figure N.1: -RT control

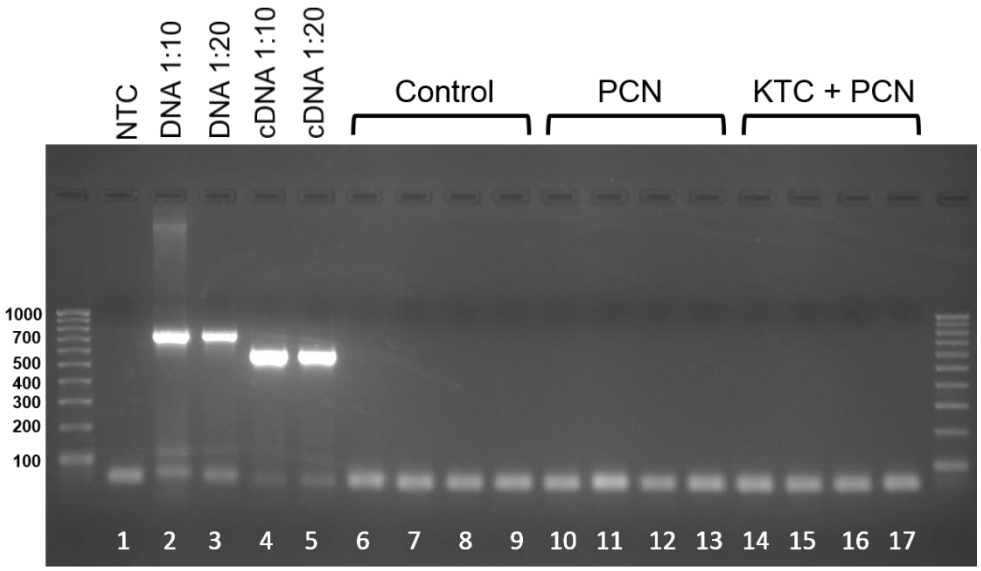

To ensure the reverse transcription from mRNA to cDNA was carried out without genomic DNA contamination, each liver mRNA sample (n = 36) was treated to reverse transcription conditions without reverse transcriptase (-RT). The resulting samples and controls underwent PCR targeting ef1α followed by gel electrophoresis (2% agarose stained with ethidium bromide). Expected amplicons are 751 bp (DNA) and 575 bp (cDNA). Lane 1: no template control (NTC); lanes 2 and 3: pooled zebrafish DNA diluted 1:10 and 1:20; lanes 4 and 5: pooled zebrafish liver cDNA diluted 1:10 and 1:20; lanes 6 – 9: four pooled -RT samples per treatment (n = 3 samples per pool).

Appendix O.

Figure O.1: Temperature gradients of target genes

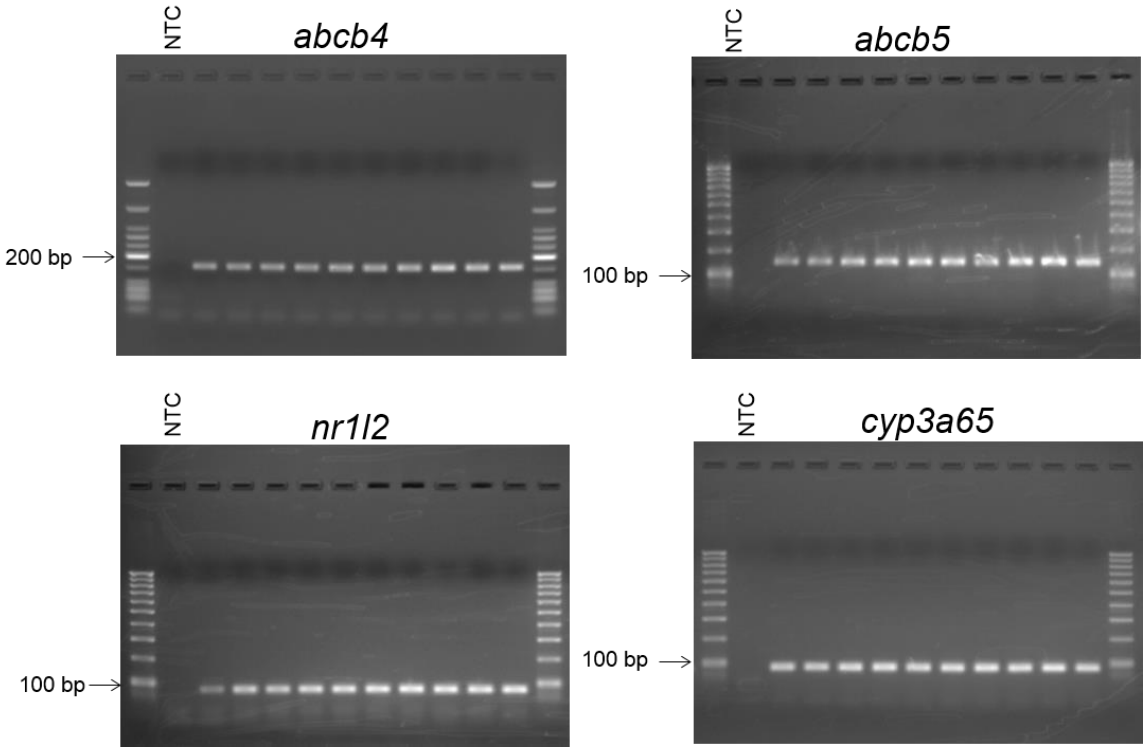

To determine the optimal annealing temperature (Ta) for each primer pair, end-point PCR was carried out using a Ta gradient. For all primer pairs, the PCR conditions included a 5 min denaturing period at 95°C, followed by 35 cycles of 95°C (30 sec denaturing step), 42 – 62°C (30 sec annealing step), and 72°C (30 sec elongation step). The final phase of PCR was 72°C for 5 minutes. PCR products were loaded into a 2% agarose gel stained with ethidium bromide and photographed under UV light following electrophoresis. Results indicate that each primer pair produces specific bands of the expected size (bp) across a range of annealing temperatures. Based on these data, all subsequent qPCR reactions were carried out with an annealing temperature of 55°C unless specific attempts to optimize reaction conditions were carried out (i.e., for abcb5).

Figure O.1 (continued): Temperature gradients of cyp3c1 and endogenous reference genes

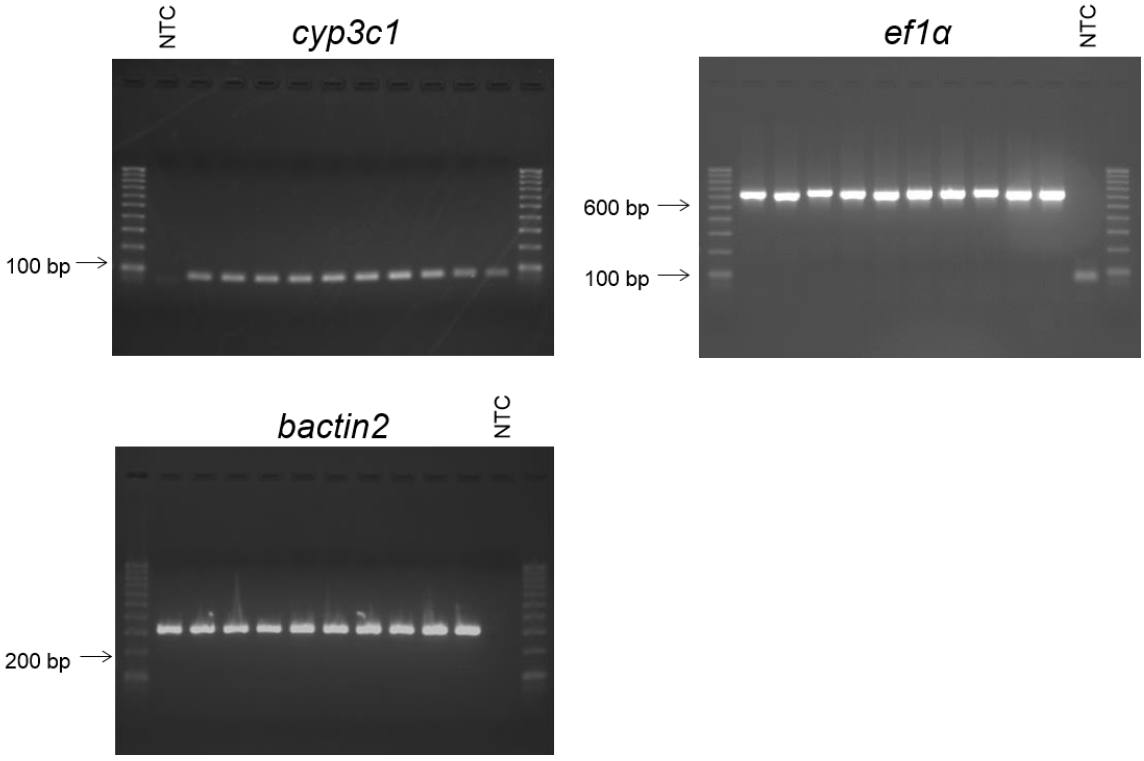

To determine the optimal annealing temperature (Ta) for cyp3c1 and the endogenous reference genes, ef1a and cyp3c1, end-point PCR was carried out using Ta gradient PCR as described (on previous page).

Appendix P.

Figure P.1: qPCR standard curves

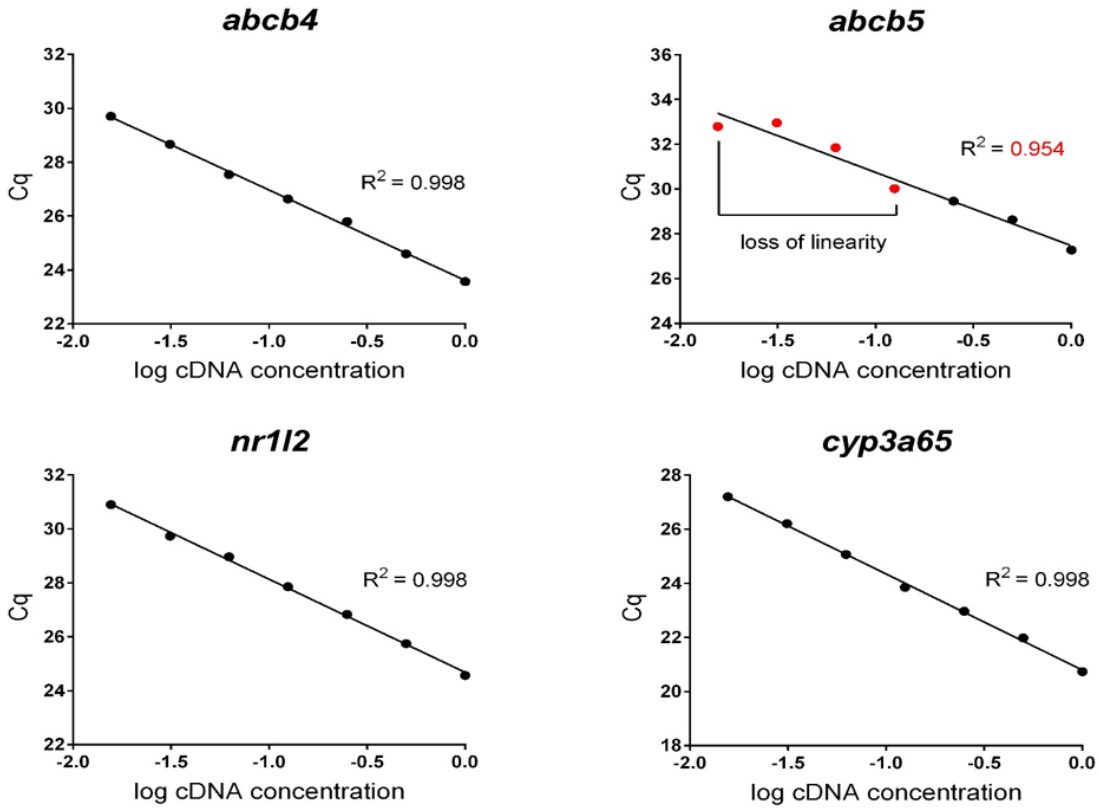

To check the qPCR amplification efficiency of each primer pair, cDNA was diluted 2-fold (1:5 – 1:320) to build 7-point standard curves. The qPCR conditions included a 5 min denaturing period at 95°C, followed by 40 cycles of 95°C (30 sec denaturing step), 55°C (30 sec annealing step), and 72°C (30 sec elongation step). The final phase of qPCR was 72°C for 5 minutes, followed by melting curve analysis (Figure 5). The R^2 value shows how well the standard curve data fit the linear regression. After numerous attempts, *abcb5* consistently showed loss of linearity (red data points) at lower cDNA concentrations, resulting in poor R^2 values. All other target genes show sufficient optimization for qPCR (table 1). Figure 1 continues on following page.

Figure P.1 (continued): qPCR standard curves

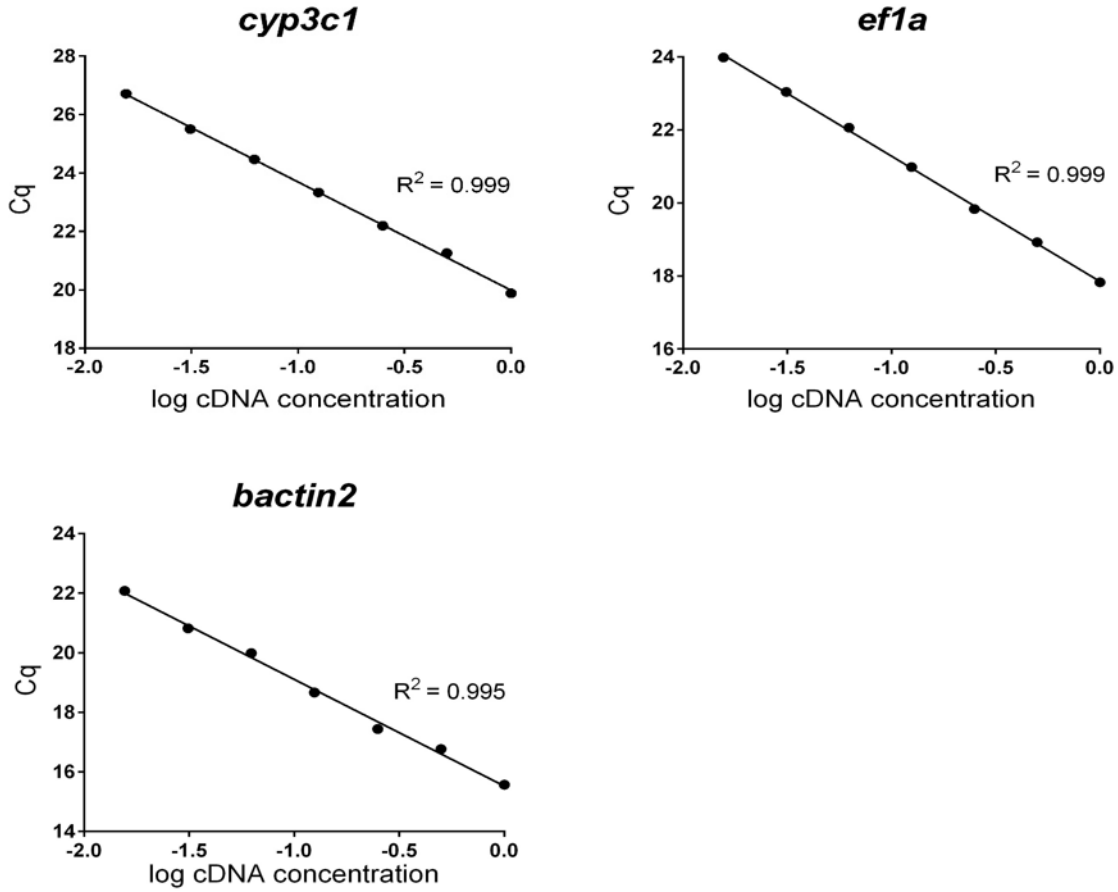

Seven-point standard curves (as described on previous page) for *cyp3c1* and the endogenous reference genes, *efla* and *bactin2*.

Table P.1: qPCR standard curves

Gene	Efficiency	Efficiency %	Slope (m)	SE (E)	R^2	NTC > 5 Cq from unknown?
abcb4	1.96	95.60	-3.4332	0.0587	0.998	YES
*abcb5**	2.02	102.04	-3.2739	0.4660	0.962	NO
nr1i2	1.95	94.75	-3.4537	0.1097	0.998	YES
cyp3a65	1.91	91.18	-3.553	0.0960	0.998	YES
cyp3c1	1.86	86.03	-3.7093	0.0907	0.999	YES
ef1a	1.95	94.64	-3.4573	0.0588	0.999	YES
bactin2	1.90	90.20	-3.5814	0.1633	0.995	YES

A summary of the optimization parameters for each amplicon. The criteria for performing qPCR gene expression analyses were as follows: (1) reaction efficiency between 85% - 115% (1.85 < E < 2.15), (2) a linear standard curve with R2 > 0.99, (3) any NTC signals should appear at least 5 Cqs higher than the most dilute sample, and (4) a single peak in the melting curve (figure 5). All target genes passed these criteria except abcb5, which was left out of the gene expression analysis. *The summary presented for abcb5 is representative of numerous primer pairs and reaction conditions attempted.

Appendix Q.

Figure Q.1: qPCR melting curves

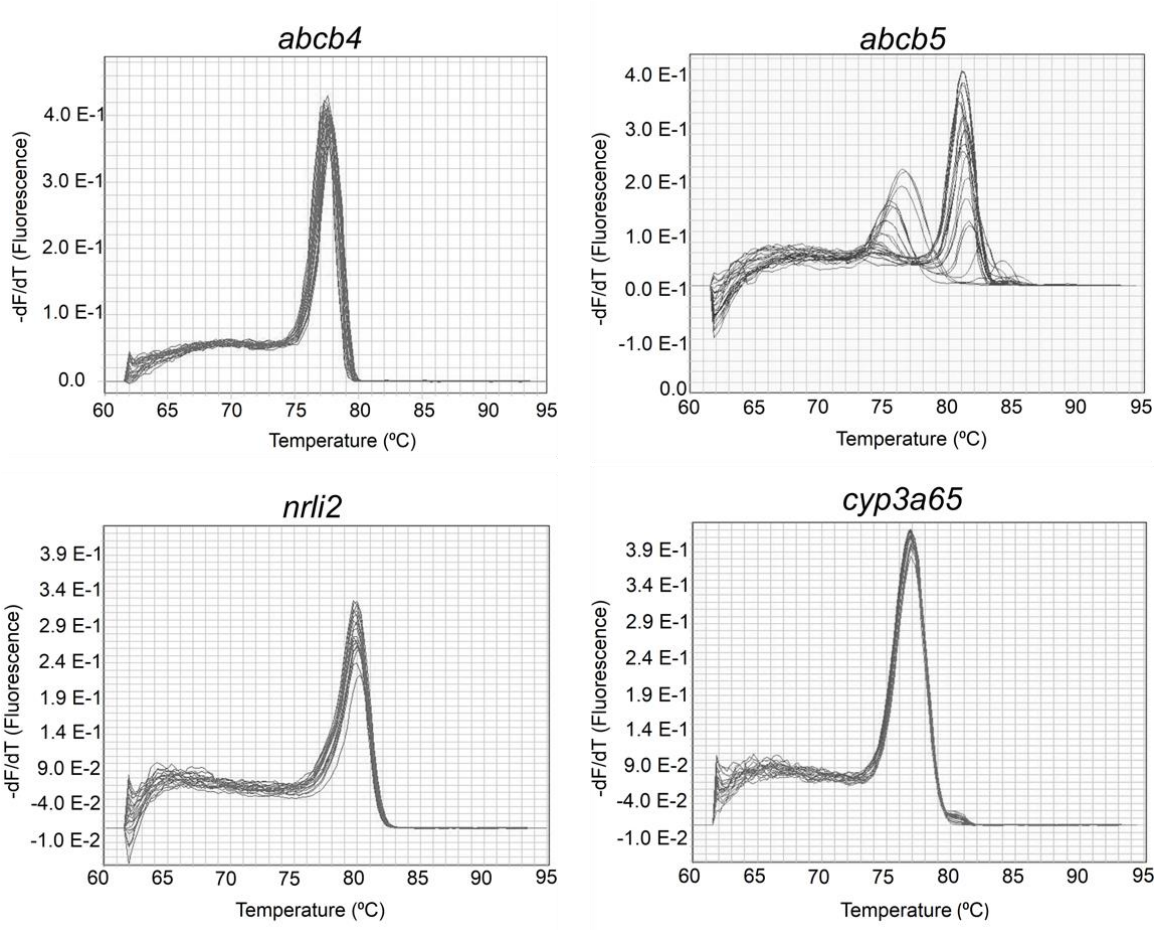

To test for qPCR amplification specificity, melting curve analysis for each target gene was performed from 60 - 95^0 C at a ramp rate of 2% (default setting for ABI 7900 HT). The melting curve for *abcb5* shows peaks at multiple temperatures, indicating non-specific amplification. All other target curves show peaks at a single temperature, indicating specific amplification.

Figure Q.1 (continued): qPCR melting curves

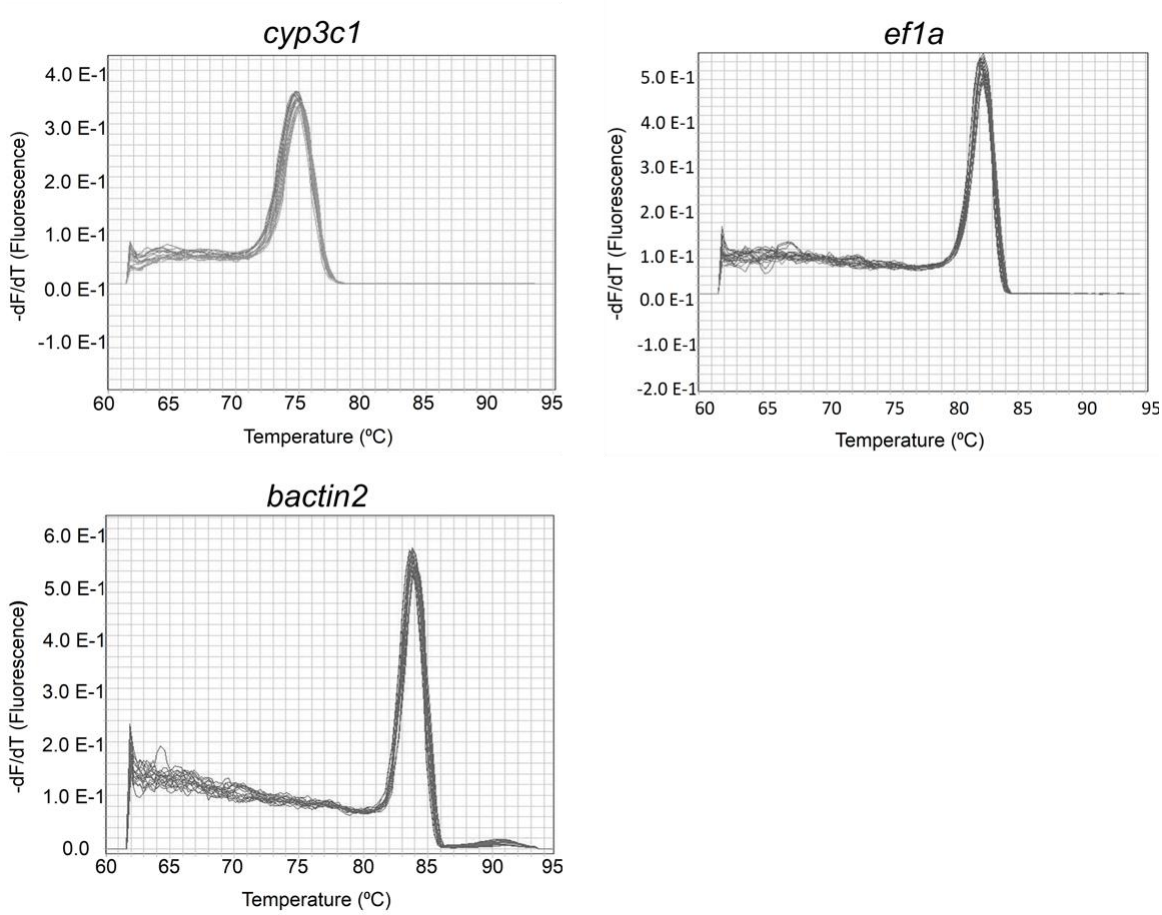

Melting curve analysis for cyp3c1 and the two endogenous reference genes, ef1a and bactin2, was performed as describe on previous page. Each curve shows a peak at a single temperature, indicating specifc amplification of these qPCR products.

Appendix R.

Figure R.1: Endogenous reference gene analysis

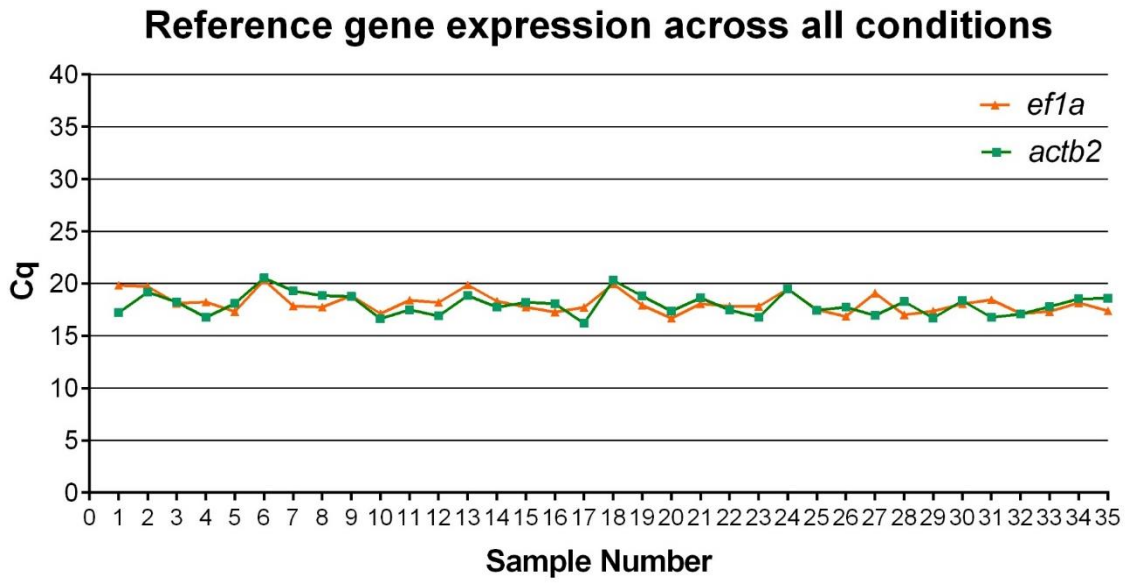

The Cq values for all samples (n = 35) show a relatively stable expression of actb2 and ef1a mRNA across experimental conditions (Samples: Control 1 – 12, PCN 13 – 23, KTC + PCN, 24 – 35). Incorporating the qPCR efficiencies, BestKeeper© (version 1) determined a pair-wise correlation coefficient (r) between ef1a and bactin2 to be r = 4.99 (p = 0.003).

Table R.1: Descriptive statistics of endogenous reference genes by BestKeeper©

Statistic	*bactin2*	*ef1a*
n	35	35
G. Mean [Cq]	17.97	18.12
A. Mean [Cq]	18.01	18.15
min [Cq]	16.20	16.68
max [Cq]	20.54	20.35
SD [± Cq]	0.88	0.76
CV [% Cq]	4.87	4.21
min [x-fold]	-3.13	-2.62
max [x-fold]	5.21	4.42
SD [± x-fold]	1.76	1.63

Values calculated from 35 samples (Control, n = 12; PCN, n = 11; KTC + PCN, n = 12). Genes with SD [± Cq] < 1 are considered stable by BestKeeper. The (min, max) [x-fold] values are the x-fold under- or over-expression of samples towards the geometric mean Cq according to the equations min [x-fold] = Emin [Ct]-GM [Ct] and max [x-fold] = Emax [Ct]-GM [Ct], respectively.

Mean [Cq] = arithmetic mean of Cq; G. Mean [Cq] = geometric mean of Cq; (min, max) [Cq] = the extreme values of Cq; SD [± Cq] = standard deviation of Cq; (min, max) [x-fold] = extreme values of expression levels expressed as an absolute x-fold over- or under-regulation coefficient where min [x-fold] = first value and max [x-fold] = last value; SD [± x-fold], standard deviation of the absolute regulation coefficients.

Appendix S.

Figure S.1: Restriction endonuclease digest of target amplicons

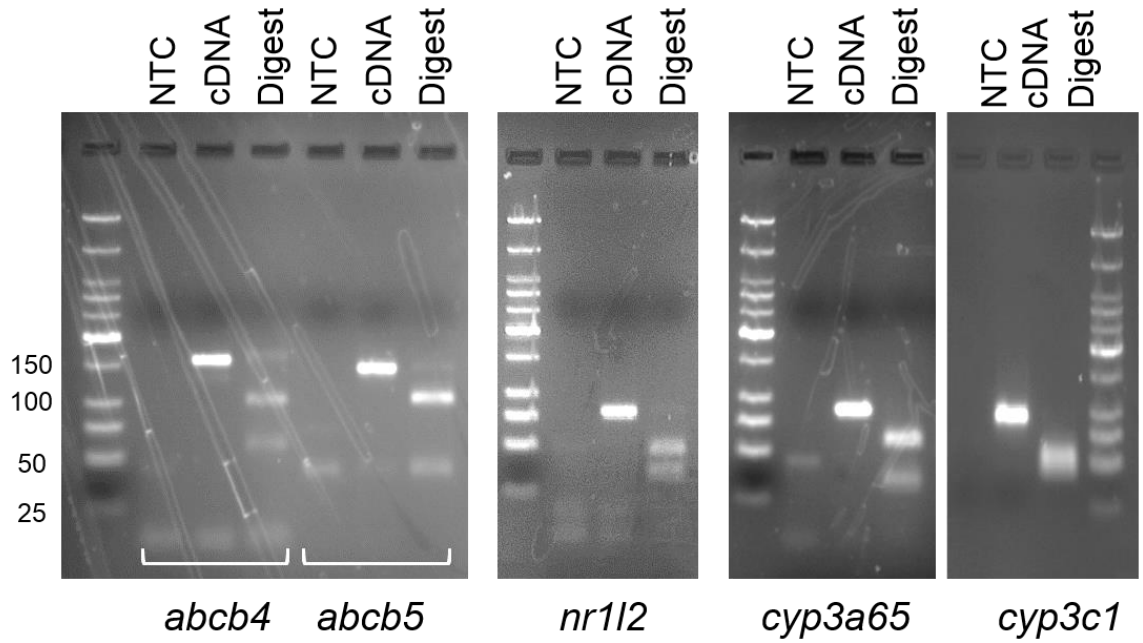

For each target gene, the no-template control (NTC), cDNA, and restriction digest were loaded into a 4% agarose gel. A low-molecular weight DNA ladder was used to help estimate the size of the small digest fragments. **Table 1 (below):** A list of the cDNA target, its amplicon size, the restriction enzyme used, and the sizes of the expected digest fragments.

Table S.1: Restriction endonucleases

Gene	Size of amplicon (bp)	Enzyme	Expected Fragments (bp)
abcb4	159	BtsCI	58, 101
abcb5	146	PleI	43, 103
nr1l2	81	PleI	34, 47
cyp3a65	86	BtsCI	31, 55
cyp3c1	81	Sau96I	35, 46